UNCLASSIFIED

AD NUMBER
AD518506

CLASSIFICATION CHANGES

TO: unclassified

FROM: confidential

LIMITATION CHANGES

TO:

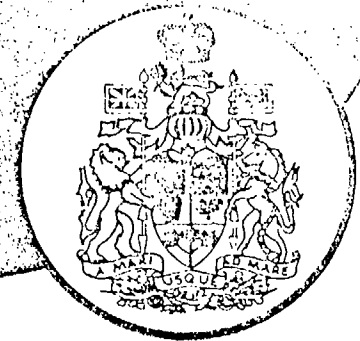Approved for public release, distribution unlimited
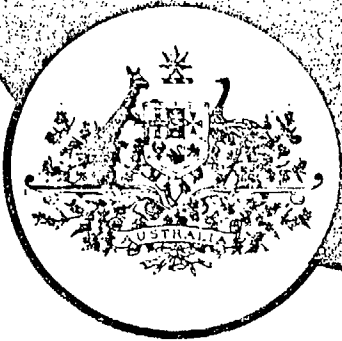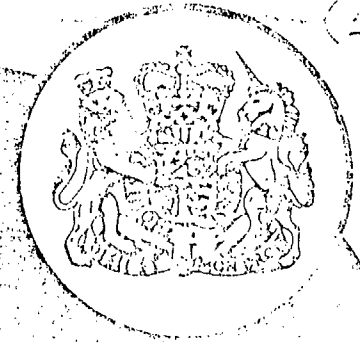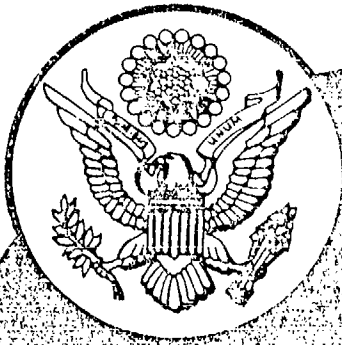
FROM:

AUTHORITY

DTRA ltr, 6 May 99; DTRA ltr, 6 May 99

THIS PAGE IS UNCLASSIFIED

DNA 2722T

(1)

AD-518 506

The
Technical
Cooperation Program

Panel N-2

EVENT DIAL PACK

SYMPOSIUM REPORT (U)

VOLUME III

Captain Kay
M. Ca...
Cdr. ...chter
Maj. Slezak
Major Kava
M. Little

November 1971

71578

RECEIVED

HEADQU...
LIBRA...

Col. Haidler
Col. Bun'y
Col. Akiyama
Cdr. Beech
Cdr. Chisholm
Mr. Diaz
Col. Fogarty
Mr. Gale
Col. Little
Col. Parlett

DNA 2722T

EVENT DIAL PACK
SYMPOSIUM REPORT (U)

VOLUME III

November 1971

Published by

General Electric Company—TEMPO
DNA Information and Analysis Center
Santa Barbara, California 93102

Copy No. 118

UNCLASSIFIED

TABLE OF CONTENTS

iii

UNCLASSIFIED

FOREWORD

(U) The DIAL PACK Symposium was held in Ottawa, Canada 30 March through 1 April 1971. The symposium was sponsored by the Defense Atomic Support Agency (DASA) and the Defence Research Board (DRB) of Canada to review the results of the 500-ton, high-explosive blast and shock trial carried out at the Canadian Defence Research Establishment Suffield (DRES) on 23 July 1970.

(U) The papers presented at the symposium are contained in Volumes I through III of this publication. This volume (Volume III) contains the U.S. Project Officer's papers that are either classified, or were selected to be published with the classified papers. These include the Project LN110, LN111, LN112, LN113, LN117, LN303, LN312, and LN314B papers.

(U) The other papers presented at the symposium (U.S., U.K., and Canadian) are contained in Volumes I and II, which are being published by the Defence Research Board of Canada.

v

LIST OF ATTENDEES

Mr. J. W. Adams	United States
Mr. J. H. B. Anderson	Canada
Mr. G. L. Arbuthnot, Jr.	United States
Mr. R. L. Averill	United States
Dr. M. J. Balcerzak	United States
Mr. R. A. Berry	Canada
MAJ R. T. Beurket	United States
Mr. G. D. Blake	Canada
Mr. L. R. Boyd	Canada
Mr. H. W. Brunton	Canada
SGT T. H. Burghard	United States
Dr. W. J. Byrne	United States
LTC J. W. Cable	United States
Mr. I. R. Cameron	Canada
COL W. E. Castellano	Canada
Mr. W. W. Chan	United States
Mr. R. S. Chapler	United States
LTC J. Choromokos, Jr.	United States
Mr. C. Clifford	Canada
Mr. W. R. Conley	United States
Mr. K. E. Conroy	Canada
LCDR J. W. Cook	United States
Dr. G. R. Cowper	Canada
Mr. W. M. Creelman	Canada
Mr. J. R. Crosnier	France
Mr. G. H. Custard	United States
Mr. F. G. Davey	Canada
Mr. W. D. Delaney	United Kingdom
Mr. M. M. Dembo	United States
Mr. W. L. Derksen	United States
Mr. M. J. Dudash	United States
Mr. G. Dupont	Canada
Mr. N. H. Ethridge	United States
CPT J. W. Fay	United States

Mr. J. M. Ferritto	United States
Dr. E. R. Fletcher	United States
Mr. A. Fluger	United States
Mr. V. A. Fratzke	United States
MAJ J. E. Frederick	United States
Mr. L. French	Canada
Mr. D. G. Gage	Canada
LTC D. C. Gavin	United States
Mr. R. P. Gaylard	Canada
Mr. L. Giglio-Tos	United States
MAJ W. Goshorn	United States
Mr. A. H. Grundy	Canada
Mr. J. F. Halsey	United States
Dr. M. C. Hamlin	Canada
Mr. W. D. Hart	United Kingdom
Col. H.-H. Heintzel	Germany
Mr. E. M. Hellberg	United States
Dr. L. B. Holmes	United States
Mr. M. E. Hughes	United States
Mr. D. S. Hyman	United States
Mr. C. R. Iverson	Canada
Mr. T. Jarvis	United States
Mr. A. Jenssen	Norway
Mr. W. A. Johnston	Canada
Mr. W. A. Jones	Canada
Maj. Ir. A. Kamphuis	Netherlands
Mr. R. E. Keeffe	United States
Mr. J. H. Keefer	United States
Mr. J. R. Kelso	United States
Mr. T. E. Kennedy	United States
Mr. E. C. Kenyon	Canada
LTC A. L. Knapper	United States
Dipl. Geophys. H. Koeppel	Germany
Mr. G. Lacasse	Canada
Mr. A. P. R. Lambert	Canada
Dr. D. Lane-Smith	Canada
CDR K. E. Lewis	Canada
Mr. A. K. Longair	Canada
Mr. E. W. Luedeking	United States
Mr. A. MacWaters	Canada
Dr. H. D. Madill	Canada
Dr. A. H. Makomaski	Canada
COL I. A. Marriott	Canada

Mr. E. J. A. Martinelli	United States
Mr. R. D. Mayerhofer	United States
Mr. R. W. Mayo	United States
Mr. J. J. Meszaros	United States
Mr. J. W. Meyer	United States
Mr. G. F. Miller	United States
Mr. J. B. G. Monzac	France
Mr. J. R. Morgan	Canada
Mr. B. E. Morris	United States
Mr. D. W. Murrell	United States
Mr. R. Naylor	Canada
Mr. C. E. Needham	United States
Mr. J. P. Neilsen	Canada
Mr. G. Nevrincean	United States
Mr. J. A. Norbutas	United States
Mr. R. J. Odello	United States
LT (N) D. G. Oke	Canada
COL W. J. Owens	Canada
Mr. C. R. Patterson	Canada
Mr. J. D. R. Pattman	Canada
Mr. J. Petes	United States
Dr. S. Pillai	Canada
Mr. C. A. Pope	Canada
Mr. R. R. Pope	United States
Dr. H. Reichenbach	Germany
Mr. R. E. Reisler	United States
Dr. D. R. Richmond	United States
Dr. D. J. Roddy	United States
CDR C. D. Roushorn	Canada
Mr. A. A. Rula	United States
Dr. G. Sachsse	Germany
Mr. F. M. Sauer	United States
Dr. L. Schindler	United States
Dr. D. Schofield	Canada
Mr. R. M. Schumacher	United States
LCDR P. H. Scilly	Canada
Mr. R. H. Seabold	United States
MAJ W. J. Shepard	United States
Mr. H. L. Solomonson	United States
Dr. W. Sommer	Germany
LTC H. F. Stolz	United States
Mr. E. Stroemsoe	Norway
MAJ R. E. Stroud	United States

Mr. S. K. Takahashi	United States
Dr. P. R. Ukrainetz	Canada
MAJ D. H. Thomas	United States
Mr. J. S. Toma	United States
Dr. D. S. Walkinshaw	Canada
Dr. H. S. Ward	Canada
Mr. J. Wareing	Canada
Mr. R. E. Warren	United States
CPT R. H. Waters	United States
Dr. M. B. Watson	United States
Mr. J. S. Watson	Canada
Mr. J. M. Watt, Jr.	United States
Dipl.-Ing. G. Weigel	Germany
Mr. S. N. White	Canada
Dr. N. J. B. Wiggin	Canada
CAPT (N) B. L. Wilkins	Canada
Mr. R. F. Wilkinson	Canada
Mr. L. G. Wilson	Canada
Mr. C. Wilton, Jr.	United States
MAJ D. R. Winchester	Canada
Mr. E. F. Witt	United States

R. Schumacher, Project Officer
Ballistic Research Laboratories

PROJECT LN110
BLAST SUSCEPTIBILITY OF TACTICAL
MISSILE SYSTEMS (LANCE) (U)

INTRODUCTION (U)

(U) The primary objective of this project was to determine the effects of blast on the internal and external components of a representative tactical missile system. This program is directly related to previous efforts of the Ballistic Research Laboratories with respect to blast susceptibility of missile systems. This includes paper studies and participation in large scale blast trials (see References 1, 2, 3, 4). The results of this test program will provide a basis for evaluating shock prediction capability of the various missile system manufacturers and give some insight into the factors which can be expected to significantly affect a systems response and its blast susceptibility.

(U) The missile system selected for this investigation was the Lance Missile System which is currently under development by the US Army. Two missiles were exposed during this test and represented two completely different configurations. The launch configuration (Figure 1) consisted of a missile with a conventional Warhead section (E 27) on a Launcher Zero Length (LZL) and elevated to 48°. The parked transport configuration (Figure 2) consisted of a missile with a nuclear warhead section (XM-234) on a Self Propelled Launcher (SPL) in the lowered tied-down position. In this configuration, the missile is hard mounted with respect to the vehicle body, but is shock and vibration isolated with respect to the ground through the normal undercarriage suspension system.
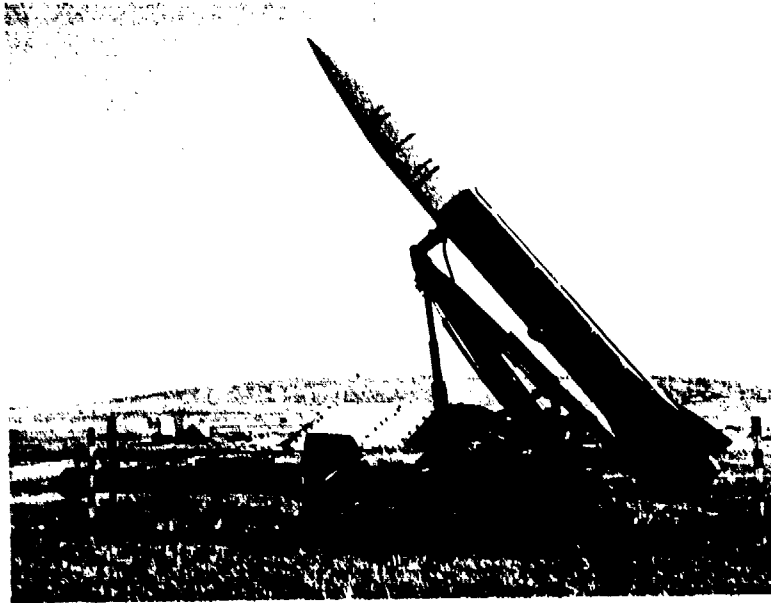
1

Figure 1 (U)   LZL test configuration (launch mode) (U).

Figure 2 (U)   SPL test configuration (parked-transport mode) (U).

2

EXPERIMENTAL PROCEDURE (U)

(U) Both missile configurations contained operable guidance and control (G&C) sections, operable Monitor Programmers and the nuclear warhead section of the SPL configuration utilized operable electrical components where practical. The only electrical components powered during blast encounter were the Monitor Programmer and the G&C section of the LZL configuration and they were in the launch ready mode of operation. Both missile systems were placed in a "Worst Case" orientation, i.e., side-on to the blast with the left side (viewed looking forward) facing the explosive charge. The predicted static overpressures at the SPL and LZL locations were 12 and 4 psi respectively. The rationale for selecting the overpressures was: to be assured that the missiles would not overturn or slide excessively (over 1 ft.) and that at least one system would not sustain structural damage. No attempt was made to evaluate design considerations for the simple reason that blast overpressure was not a design consideration for the Lance System (see Reference 5).

(U) Prior to shot day, all operable electrical components were checked for proper operation and after the test, the components were re-checked to see if they still operated properly.

INSTRUMENTATION (U)

(U) Both missiles were instrumented internally with accelerometers and pressure transducers and in addition, the LZL missile had strain gages on two of the four T-Bolts that join the warhead section to the propulsion section. Two moderate speed cameras (750 frames/sec) were used for each system (see Figure 3) to determine component reactions, overall displacement and to give indications of occurrences which might affect the instrumentation data.

(U) The Instrumentation for the SPL configuration (see Figure 4) consisted of 14 channels of accelerometer data and 5 channels of pressure data. All

R=2450'

INSTRUMENTATION
BUNKER

190°

-199°

LZ L

R= 350'

SPL

R=930'

GROUND ZERO

LEGEND

CAMERA LOCATION & DIRECTION

MISSLE LOCATIONS

INSTRUMENTATION BUNKER (MANNED)
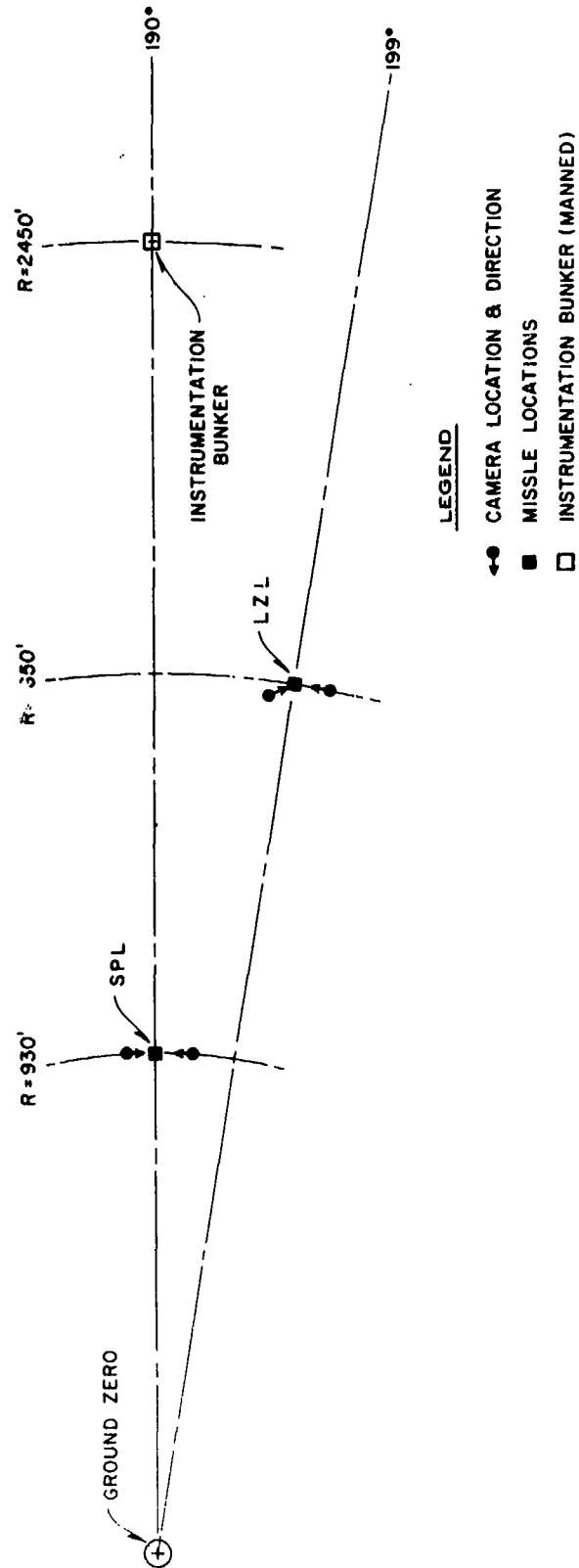
Figure 3 (U) General field arrangement (U).

4
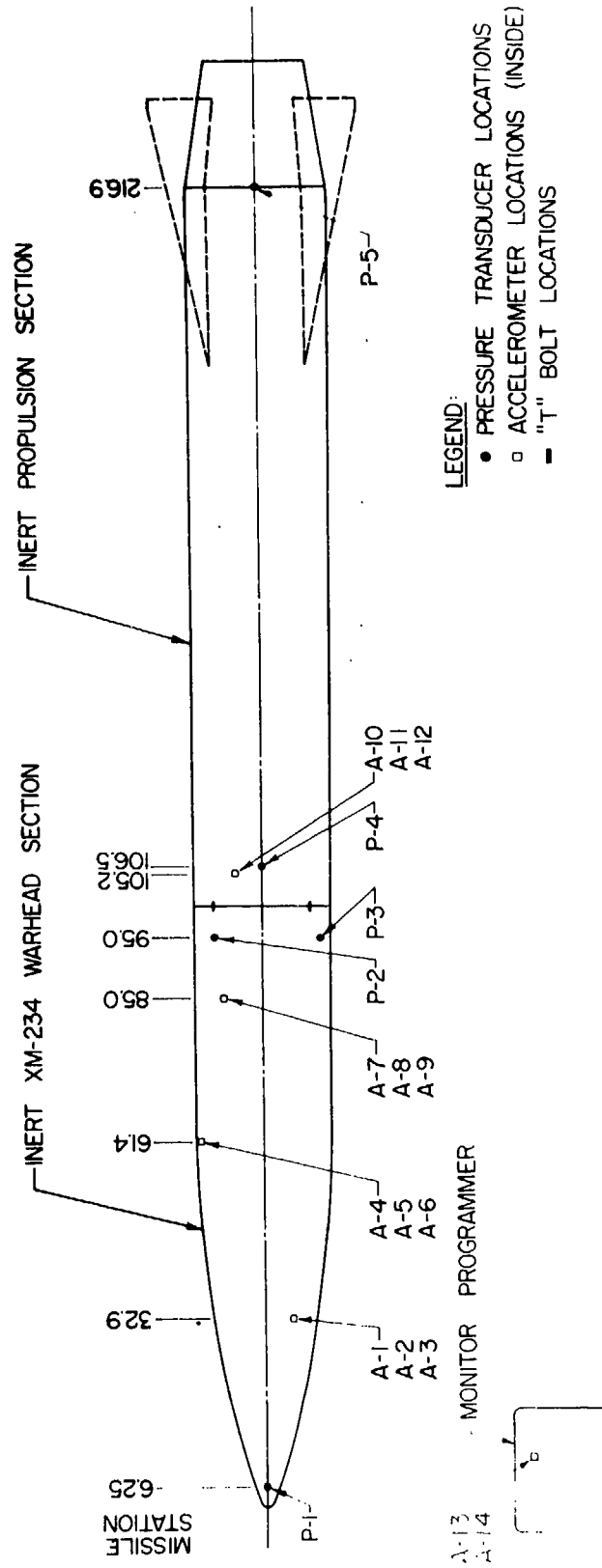
Figure 4 (U) Instrumentation locations on SFL configuration (U).

accelerometers were mounted on the most rigid structure available and as close to the missile outer skin as practical. With the exception of the Monitor Programmers, all accelerometer installations were of the triax configuration and had their axis parallel to the primary missile axes (which were not necessarily the same as ground reference coordinates). The LZL configuration instrumentation (see Figure 5) consisted of 8 channels of acceleration data, 3 channels of pressure data (one channel P-7 malfunctioned on the morning of the shot, could not be repaired or replaced and therefore was deleted) and two channels of strain gage data (T-Bolt tension loads).

(U) All instrumentation data was recorded on FM Magnetic Tape Recorders having a frequency response of DC to 20 KH_z* the pressure transducers and strain gages had frequency response in excess of the tape recorder, whereas the piezo-electric accelerometers, which were attached to charge amplifiers, had their low frequency response limited to about $3H_z$. The pressure transducers which were flush diaphragm types utilizing semi-conductor strain gages as the sensing elements were mounted within the missiles so that their diaphragms were flush with the missile outer skin.

RESULTS (U)

(C) All instrumentation data recording systems and moderate speed motion picture cameras functioned normally throughout the event. No malfunctions were observed and data were recorded on the 32 channels of instrumentation. Some of the accelerometer data indicated a zero offset or DC shift with subsequent decay to zero; however, it was concluded that this would not seriously affect the data over the frequency range of interest.

---

*The recording systems and associated support for this program was provided by Nuclear Effects Directorate Personnel from the White Sands Missile Range.
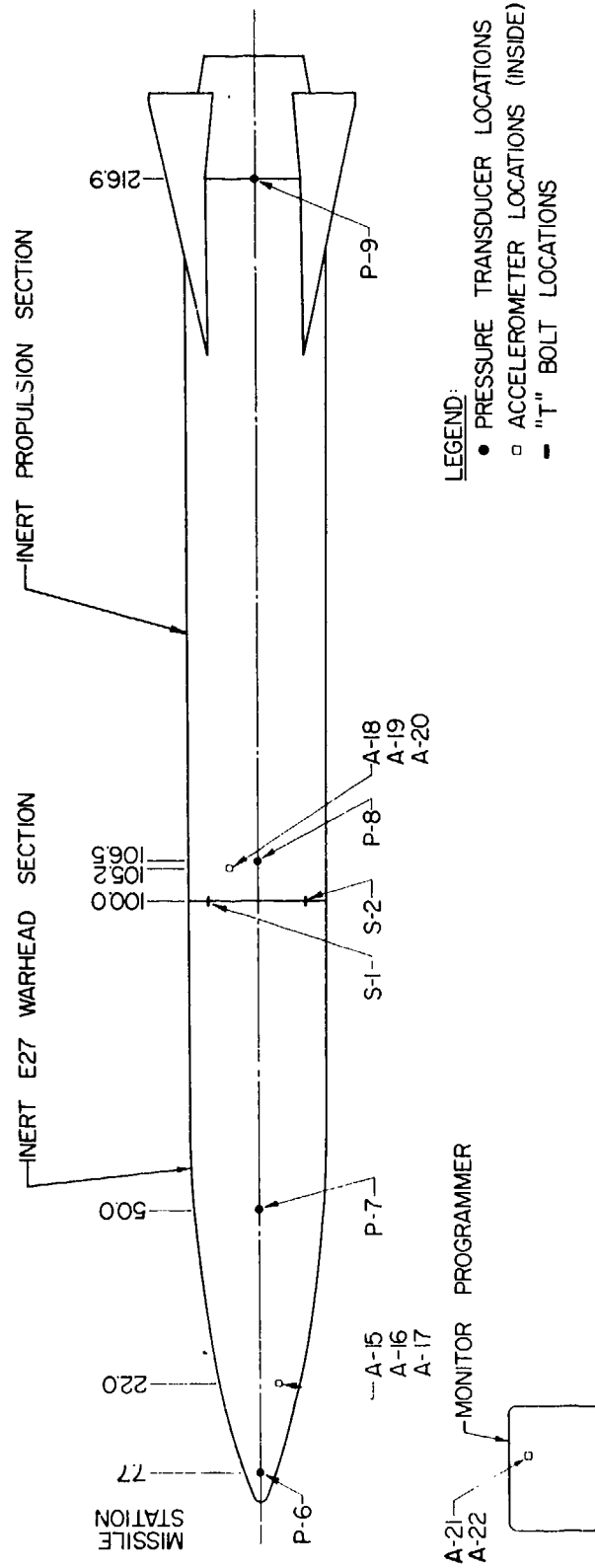
6

Figure 5 (U)   Instrumentation locations on LZL configuration (U).

(C) In Table I a comparison between the measured acceleration levels
and the specification requirement levels is made. No comparison is
made with respect to time duration because of the complexity of the test
data signal. All accelerometer data was shock spectrum analyzed using a
digital computer; however, for brevity, only a few accelerometer time
history plots and shock spectra will be discussed later.

(C) Tables II and III present the measured peak overpressures and the free
field blast parameters respectively. Table II indicates a considerable
variation in measured peak overpressures; this was to some extent expected
because of the location of the transducers in the missiles. Table III
indicates that the predicted overpressures were in general achieved
(within 5% of those expected).

(C) For brevity only 4 pressure-time histories are presented (2 for the
SPL configuration and 2 for the LZL configuration). Time history plots
for measurements P-2 and P-3 (SPL configuration) are presented in
Figure 6. These data indicate that for about the first 8 ms after shock
arrival, there is a significant difference in the pressure between P-2
and P-3 (P-2 being greater) this indicates a net downward force on the
missile tending to push it down into its support cradle. In Figure 7
two pressure time history plots for the LZL configuration are presented.
The expected classical type of pressure loading is indicated by measure-
ment P-8 while measurement P-9 (between missile fins) indicates an
unexpected decaying oscillation (about 91 H_z) superimposed on the
expected response. Post shot checks of the transducer indicate no
malfunctions or mechanical resonances at this frequency, therefore
it is concluded the oscillation is associated with the flow around the fins.

(C) The strain gage data for the LZL configuration indicated that the T-Bolt
loads were too small to be measured (or be of interest) and therefore, it
is concluded that the T-Bolts would not be susceptible structural attachments.

(C) Post shot evaluation of the major electrical systems and components
indicate there were no malfunctions or significant system degradation.

8

Table I (U)   Peak acceleration levels (U).

Measurements	Sensing Direction	Acceleration	
		Peak Specification Requirement (g)	Peak Measured Response (g)
SPL Configuration			
A-1	Vertical	47	100
A-2	Lateral	10	130
A-3	Axial	12	95
A-4	Vertical	40	440
A-5	Lateral	10	240
A-6	Axial	12	170
A-7	Vertical	34	80
A-8	Lateral	10	75
A-9	Axial	12	160
A-10	Vertical	100	110
A-11	Lateral	100	130
A-12	Axial	100	130
A-13	Vertical	30	230
A-14	Lateral	30	170
LZL Configuration			
A-15	Vertical	50	55
A-16	Lateral	10	75
A-17	Axial	12	35
A-18	Vertical	42	60
A-19	Lateral	42	80
A-20	Axial	60	50
A-21	Vertical	30	170
A-22	Lateral	30	210

Table II (U)   Peak pressure levels (U).

Measurements	Measured Peak Overpressures (psi)
SPL Configuration	
P-1	16.2
P-2	23.6
P-3	15.5
P-4	18.7
P-5	28.8
LZL Configuration	
P-6	6.2
P-7	-
P-8	8.9
P-9	10.4

Table III (U)   Measured air blast parameters (as interpolated from project LN101 line 1) (U).

Blast Parameters	SPL Location R= 930'	LZL Location R= 1650'
ΔP	11.4 psi	4.01 psi
I_p	0.818 psi-sec	0.476 psi-sec
t^+	0.214 sec	0.307 sec

ΔP = Peak Static Overpressure

I_p = Static Overpressure Impulse

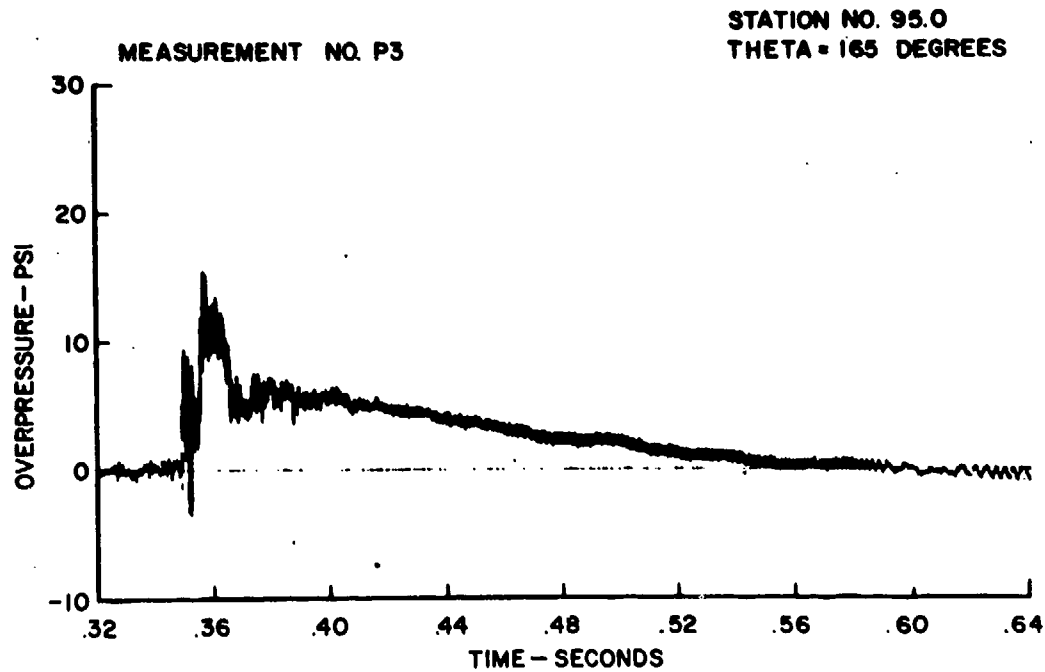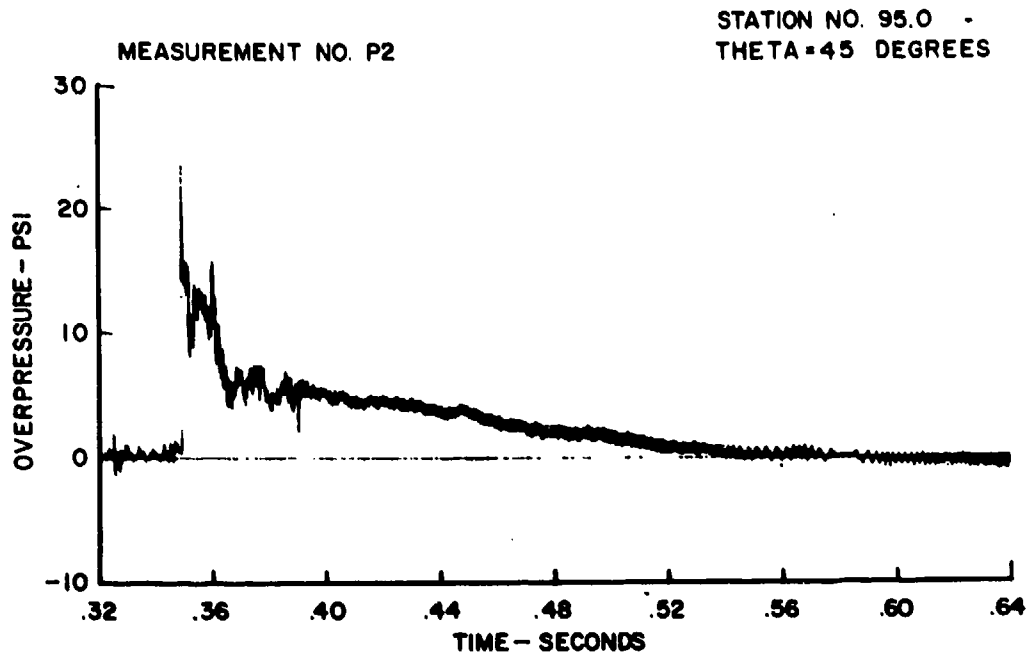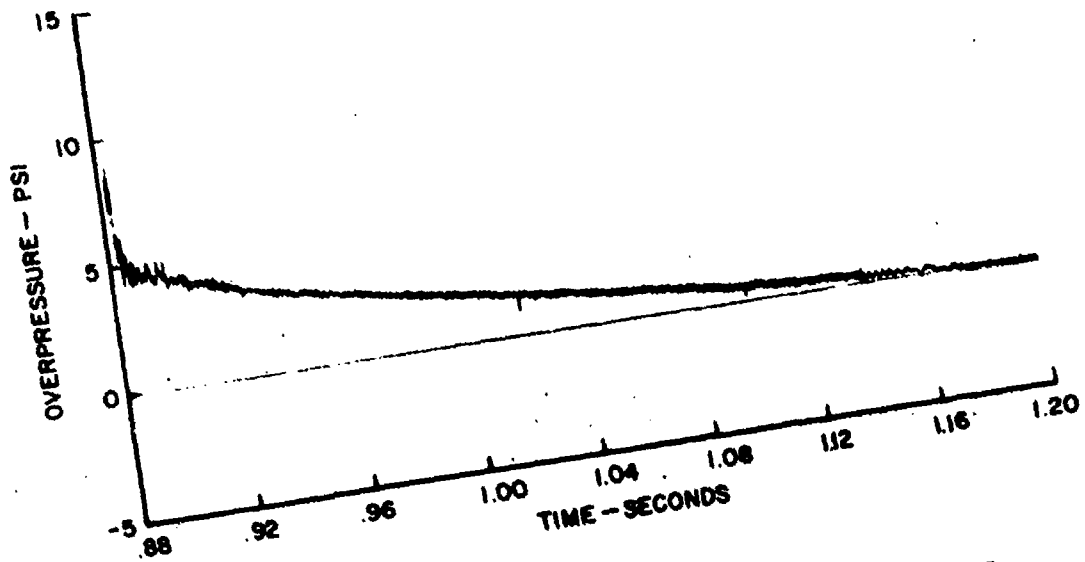t^+ = Positive Time Duration of Static Overpressure

R = Ground Range

Figure 6 (U) SPL configuration overpressure data (U).

11

STATION NO. 106.5
THETA = 90 DEGREES

MEASUREMENT NO. P8.
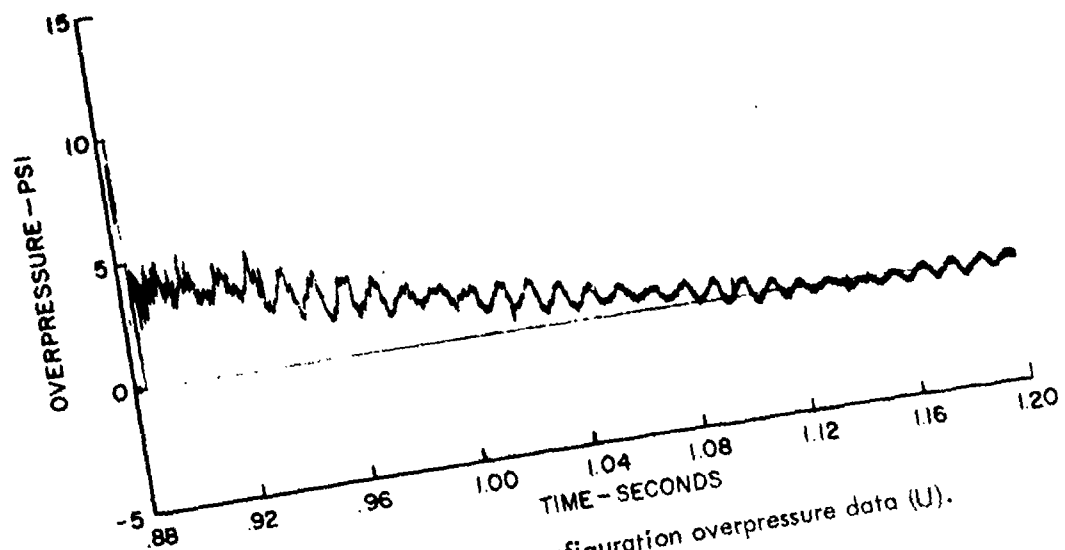

STATION NO. 216.9
THETA = 90 DEGREES

MEASUREMENT NO. P9

Figure 7 (U)   LZL configuration overpressure data (U).

12

other than damage to the propulsion section wiring harness on the SPL configuration. The LZL configuration sustained no damage except for a superficial bowing inward of the front of the sighting and laying case, this would generally be no worse than that expected from rough handling in the field. The SPL configuration sustained significant damage to the missile warhead section, propulsion section, sighting and laying case and the self propelled launcher.

(C) The XM-234 warhead section was structurally deformed (buckling and cracking) in the immediate vicinity of the forward cradle support. Examination of the inside of the warhead section indicated that the left side of the cradle support caused more damage (penetrated further) than the right side. The damage is shown in Figure 8. It appears this damage was primarily caused by the SPL translation and rotation forcing the front cradle support up and into the warhead section. The overpressure difference between P-2 and P-3 (as indicated earlier) probably was a contributing factor in causing this damage.

(C) The self-propelled launcher sustained considerable structural damage. The driver's compartment cab, which was in the lowered position was badly twisted and opened. The side of the vehicle facing the blast was bowed inward about 7 1/4 inches whereas the side opposite was bowed outward 2 3/8 inches. Figure 9 shows the damage to the side of the driver's compartment and the engine front access hatch.

(C) The missile propulsion section tankage (SPL) was not damaged, however, the cable harness fairing was blown completely off the propulsion section and the cable harness plug (at the aft end) was broken. Figure 10 shows the SPL left side damage and the damage to the propulsion section wiring harness. The plastic sighting and laying case (shown in Figure 10) was knocked out of its normal attachment and was severely cracked, however, this case is foam filled and fits the sighting and laying theodolite closely; therefore, it is not expected that the theodolite would have been damaged (the case was empty during the test).

Figure 8(U) SPL configuration warhead section and cab compartment damage (U).

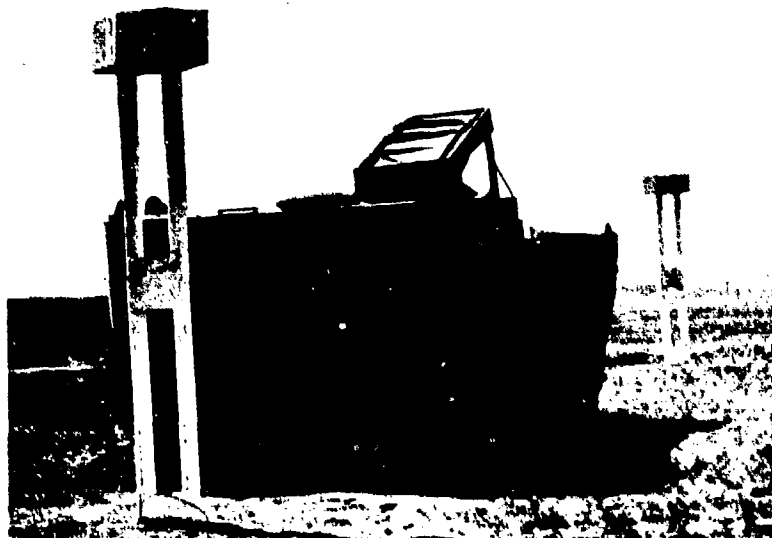Figure 9 (U) Damage to front and left side of SPL configuration (U).

14

Figure 10(U) Damage to propulsion section and left side of SPL configuration (U).

(C) No damage to the SPL power train or engine compartment components was observed even though the SPL had been translated 4 1/2 inches at the front and 6 1/2 inches at the rear in the direction of blast wave propagation. After the test, the vehicle was started and driven with no apparent difficulties.

(C) As indicated earlier, all accelerometer data were shock spectrum analyzed; however for brevity, only data from four accelerometers will be presented. The results are typical.

(C) For the SPL configuration, two measurements are presented (A-2 and A-5). The time history plots of the data that were analyzed are shown in Figure 11. Measurement A-2 has an indication of DC shift (as previously indicated) but shows the greatest activity at air blast shock arrival. Measurement A-5 indicates a second sharp shock at approximately 35ms after air shock arrival;this second shock appears to coincide with the observance of the warhead section upper quadrant buckle as seen in the moderate speed movies. This would indicate a secondary impact caused by the warhead (forward section) whipping upward and possibly the rear section hitting the structure. The shock spectra plots for measurements A-2 and A-5 are presented in Figure 12. It is readily apparent that the measured response is considerably greater than the shock specification (it should be remembered that air blast shock was not a design consideration). The low frequency effect (shift) is indicated in the spectra of measurement A-2, but appears to have little, if any, effect on the higher frequencies (above 10 H_z).

(C) For the LZL configuration, two acceleration channels were analyzed (see Figure 13). It is readily seen that the response is of the general type expected--a large positive acceleration at shock wave arrival followed by a subsequent damped decaying oscillation. Measurement A-16 is in the nose of the missile whereas A-19 is in the G&C section close to the missile forward support point. The shock spectra plots for these two measurements are presented in Figure 14. In general the shock spectra for the lateral
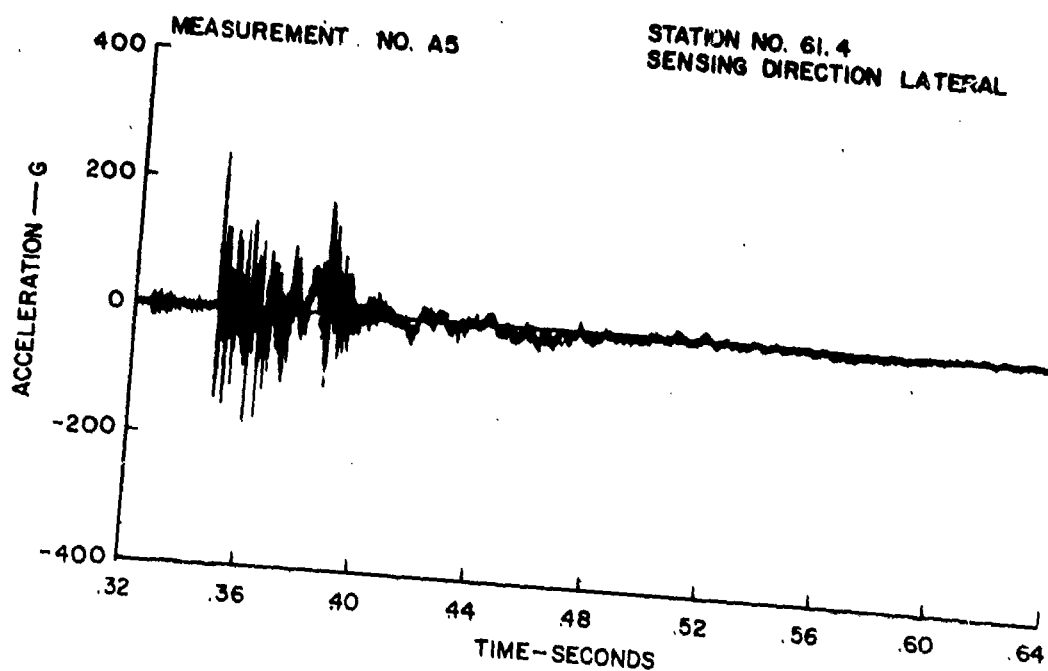
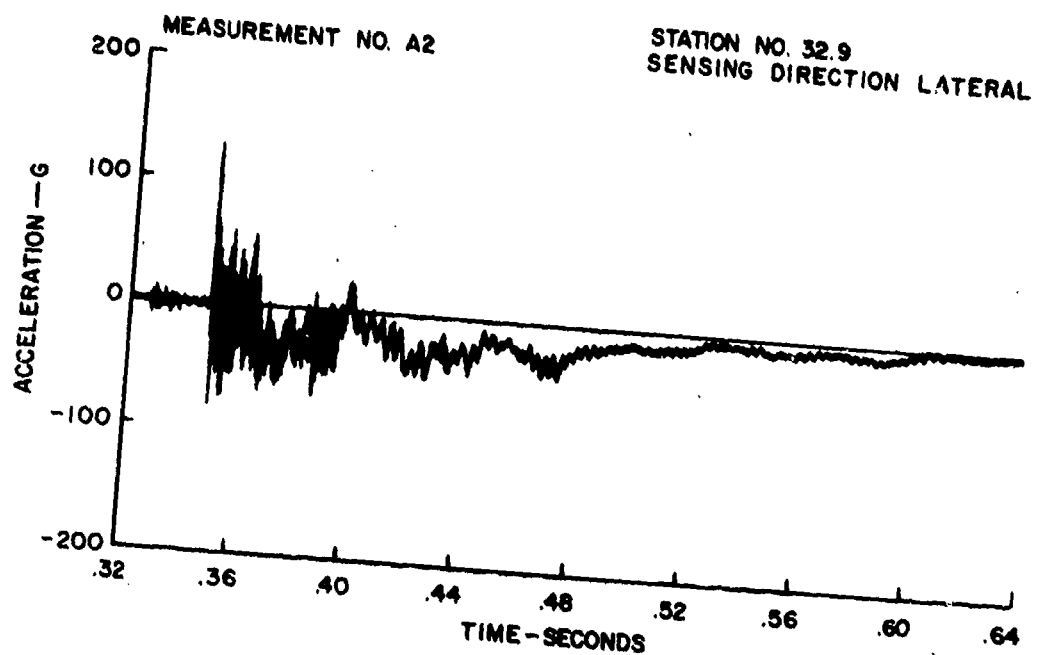Figure 11 (U) SPL configuration acceleration data (U).
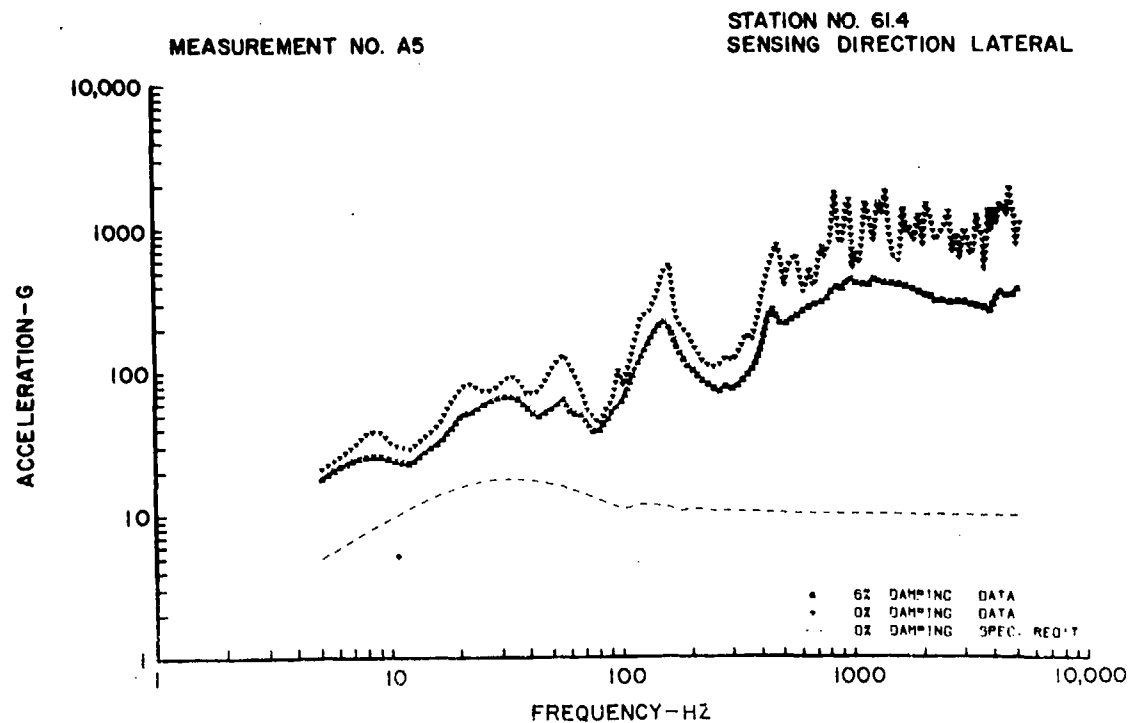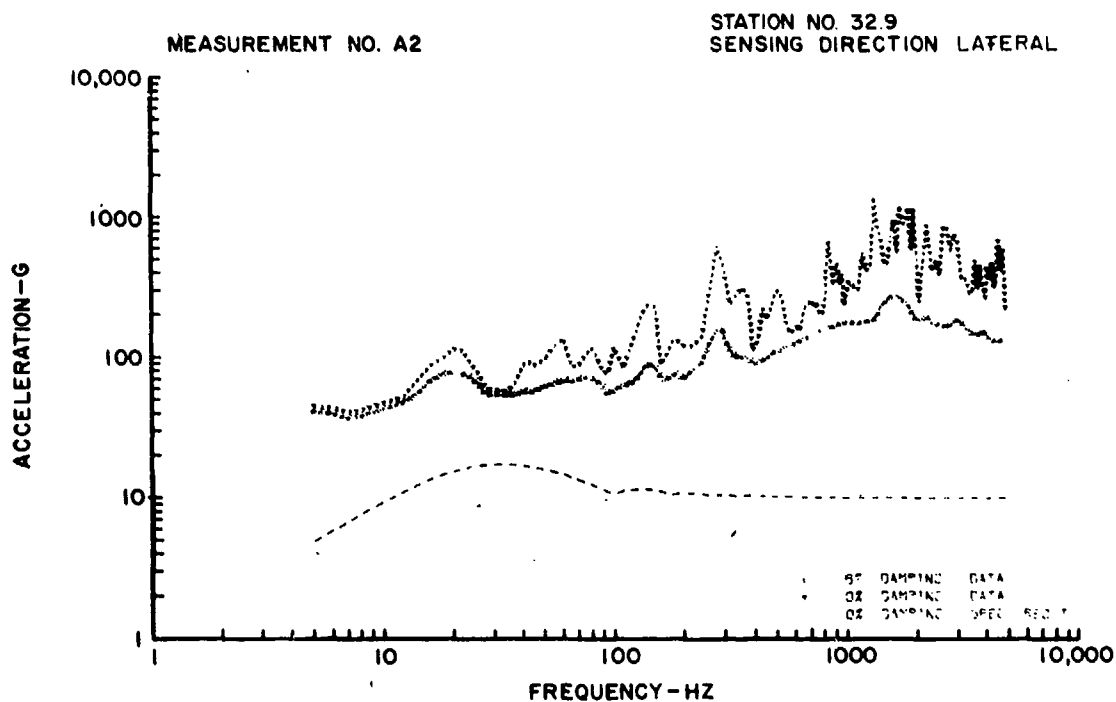
Figure 12 (U)   SPL configuration shock spectra (U).

18
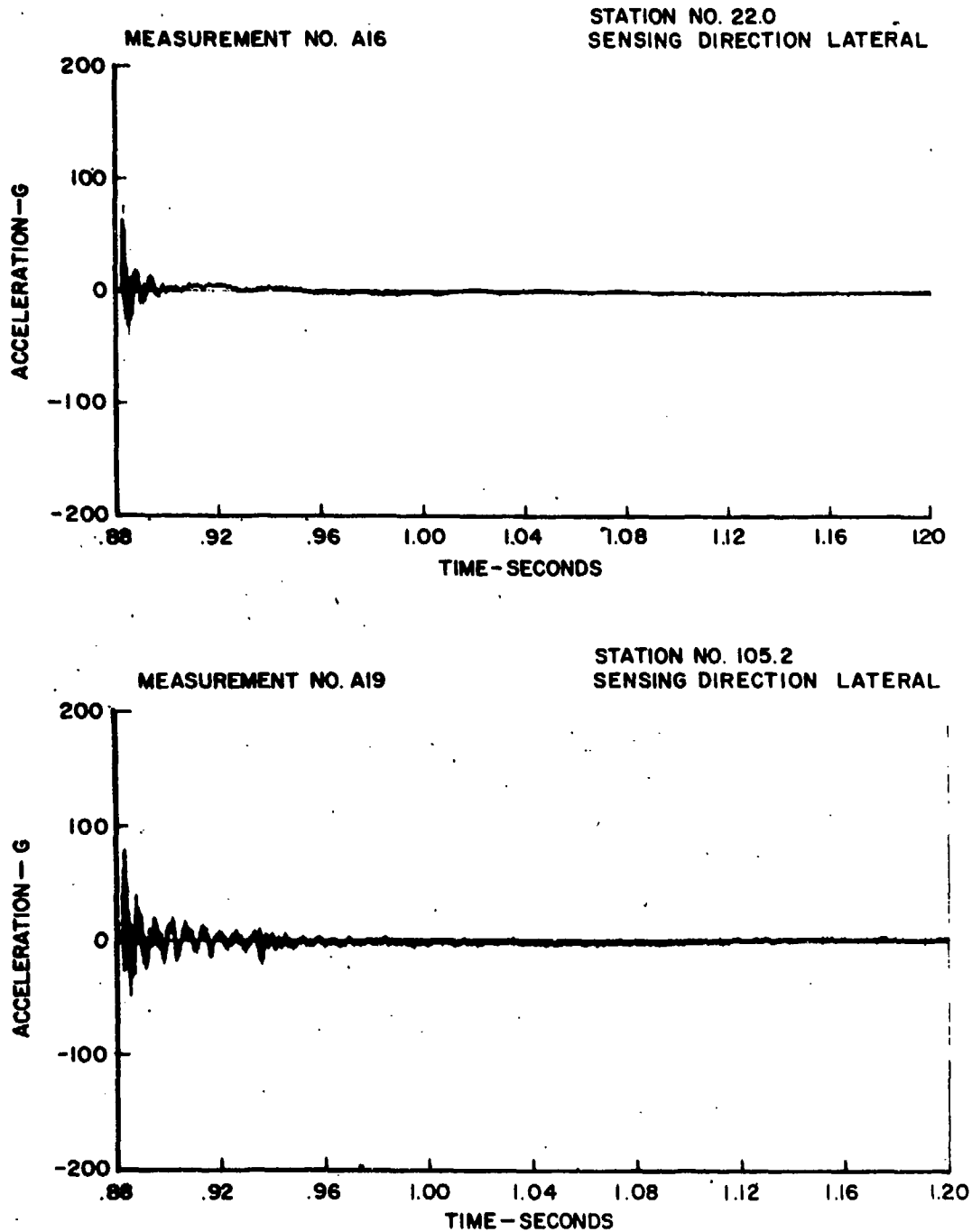
Figure 13 (U) LZL configuration acceleration data (U).

MEASUREMENT NO. A16.

STATION NO. 22.0
SENSING DIRECTION LATERAL

MEASUREMENT NO. A19

STATION NO. 105.2
SENSING DIRECTION LATERAL
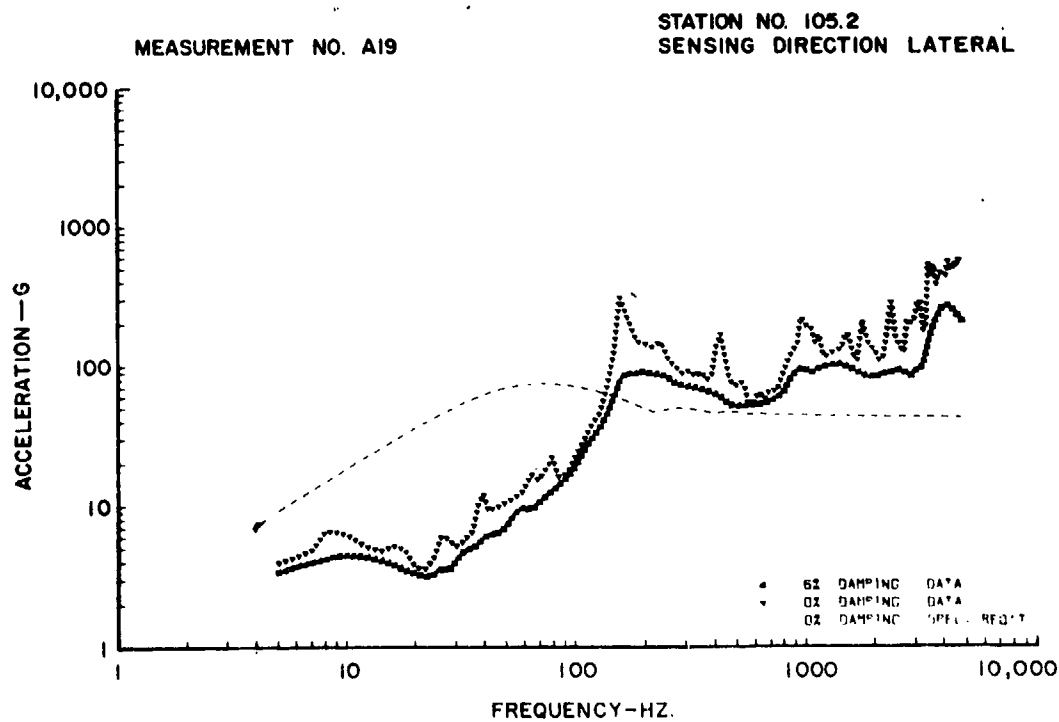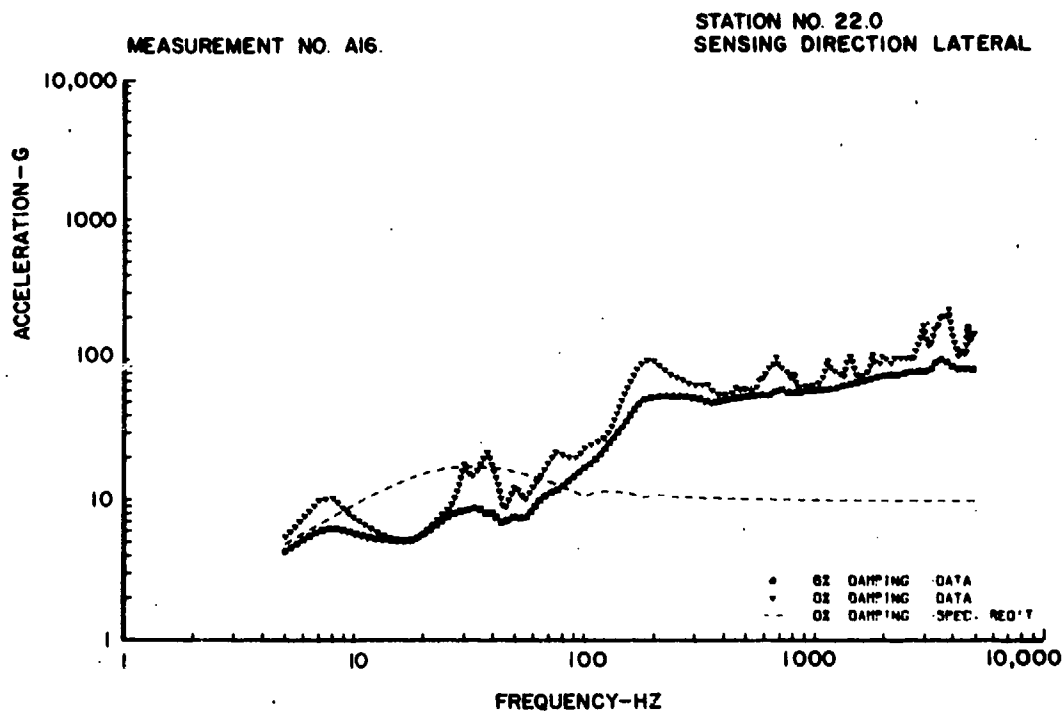

Figure 14 (U)   LZL configuration shock spectra (U).

20

direction are about the same for both the SPL and LZL configuration when
the differences in overpessure are taken into consideration. For the
vertical and axial directions (data not presented in this report) the SPL
shock spectra are significantly higher even when taking the differences
in overpressure into consideration. It should be noted that the two
damped shock spectra presented in Figure 14 (test data for measurements
A-16 and A-19) are essentially the same, whereas the shock spectra for the
specification requirements are considerably different.

CONCLUSIONS (U)

(U) The test results indicate the importance of establishing an air
blast criteria (if one is desired or expected to be required) early in
the design of a missile system. This test program clearly indicates that
the air blast environment is potentially the most severe shock environment
a missile system may be expected to survive (this is dependent upon the
values selected for the blast criteria) and that the premise "it's
inherently hard" is not necessarily true.

(U) The test results additionally indicate that a complete analysis of
combined air blast and structurally transmitted loading must be employed
to have any reasonable assurance of achieving a given level of blast
survivability. Although this test program indicated that electrical
components internal to the missile system did not fail prior to
structural damage, it should not be concluded this will always be the case.
If it can be argued that shock loading from handling or transportation
considerations are important in establishing performance specifications, then
it can also be argued that blast effects should also be considered.

(U) Equipment shelters, vans, etc., which are quite often associated with
tactical missile systems were not evaluated during this investigation because
the Lance system does not utilize them directly. However, a complete analysis
of other systems (new or existing) could possibly include these items. It
is therefore recommended that the results of project LN-112 "Blast Effects on
Electrical Equipment Shelters" be taken into consideration for a complete
system analysis or design evaluation.

21

REFERENCES

1. R. Mayerhofer and E. Rosicky, "Blast Damage to Missiles in Non-Flight Configurations (U)," U. S. Army Ballistic Research Laboratories Memorandum Report 1603, October 1964 (Confidential).

2. O. T. Johnson, R. Mayerhofer, and W. Schuman, "Effe ↸ of Blast Upon Simulated and Actual Missiles (Project 1.4 Operation Snow Ball) (U)," U. S. Army Ballistic Research Laboratories Memorandum Report 1655, May 1965 (Confidential).

3. K. Mikami and R. D'Amato, "Criteria for the Effect ⸗f Damage on the Operational Capabilities of U. S. Army Missiles S, ⸗⸗ems (U)," Kaman Avidyne Report TR-38 Vols I - V, Feb - Sep 1966 (Secret).

4. O. T. Johnson and R. D. Mayerhofer, "Susceptibility and Vulnerability of the Lance Missile System to Nuclear Effects (Blast) (U)," U. S. Army Ballistic Research Laboratories Memorandum Report 1862, August 1967 (Secret).

5. "Performance Specification for Warhead Section Compatibility, Lance Missile System (U)," LTV Aerospace Corp. Missiles and Space Division, Warren, Michigan, Report MSD-M5015a, 25 June 1969 (Confidential).

R. Mayerhofer, Project Officer
Ballistic Research Laboratories

PROJECT LN111
BLAST VULNERABILITY OF PARKED AIRCRAFT (U)

INTRODUCTION

Objectives

(U) The objective of this experiment was to determine the structural and component response of fixed and rotary wing aircraft, parked at various blast intensity levels, and to compare the results with predictions based upon current methodologies.

Background

(U) For many years, the aerial target vulnerability analysts have been striving to develop a methodology for determining the vulnerability of aircraft to conventional and nuclear blast. To date, the "cookbook" methodology does not exist; however, there are many "tools of the trade" that can be applied, such as, computer programs, experimental data, scaling laws, semi-empirical relationships established for scaled models of simple geometry, etc. The Vulnerability Laboratory methodology at present is a combination of the above.

(U) In the original planning of Project LN111, two obsolete U.S. aircraft were to be included as bonus targets in Project LN110, "Blast Susceptibility of Tactical Missile Systems (Lance)." However, late in the planning stages, four currently operational aircraft and one obsolete Canadian twin engine jet fighter aircraft* became

---

All efforts put forth in making this aircraft available for testing are acredited to DRES.

23

available for destructive testing. Because of the rare opportunity
to experiment with current aircraft, it became equally important as
an objective to obtain damage data as it was to evaluate the prediction
methodology. Within the time and funding constraints, extensive
instrumentation was not possible and camera coverage was the only
reasonable effort that could be made. Despite the problems of
trying to organize a meaningful project in the final stages of pre-
test planning, the objectives of the project were successfully
accomplished and the results have given new insight to future require-
ments.

PROCEDURE

Test Setup

(U) There were five aircraft used as targets in this experiment:
two OH-6 helicopters (Fig 1), one UH-1 helicopter (Fig 2), one YOV-1
fixed wing observation aircraft (Fig 3) and one CF-100 jet fighter
aircraft (Fig 4). All of the aircraft were in a parked configuration
and secured as they would normally be in a combat area; i.e. the
rotor blades of the helicopters were tethered to the fuselages, and
the YOV-1 was tethered to the ground. Due to the rainy weather the
aircraft had settled into the ground and the normally used wooden
chocks for the CF-100 were not needed. In addition, all of the
aircraft were positioned in the "worst case" orientation (side-on
to the blast or with the longitudinal axis of the aircraft normal to
the blast wave propagation). The YOV-1 aircraft was fully operable,
but all the others had been previously damaged; the pre-shot damage

24

Figure 1 (U)   The OH-6 helicopter (U).

Figure 2 (U)   The UH-1 helicopter (U).

25

Figure 3 (U)   The YOV-1 aircraft (U).

Figure 4 (U)   The CF-100 aircraft (U).

was documented to better assess the resultant damage. To minimize the dangers of fire and to simulate the weight of fuel, all fuel tanks were filled with water except for one of the OH-6 helicopters; sand bags were used because of leaking tanks. Each aircraft was photographed by two moderate speed movie cameras to determine aircraft and component response and displacements. Steel stakes were driven into ground and viewed by the cameras as reference points for measurements of aircraft displacements. Actual aircraft and camera locations are shown in Fig 5.

Cameras

(U) The cameras used were Redlake HyCam K2001R, 16mm full frame cameras. They were operated at 700-800 frames per second and the data was recorded on Kodak Ektachrome ER, type 7257 color film.

Prediction Methodology

(U) The prediction methodology consisted basically of determining the most susceptible critical structure of each aircraft, comparing that structure with similar aircraft structures for which experimental data existed, and then scaling by Johnson's relationship[1]* to predict the same damage for a yield of 1 KT. Difficulties were encountered with predictions for the CF-100 because little specification data was available; the aircraft is obsolete and the manuals are scarce. The YOV-1 simply could not be compared well with any aircraft in the damage data bank, and other methods had to be employed. The final prediction for the YOV-1 included a factor of conservatism in order to assure that resultant damage would not be greater than

---

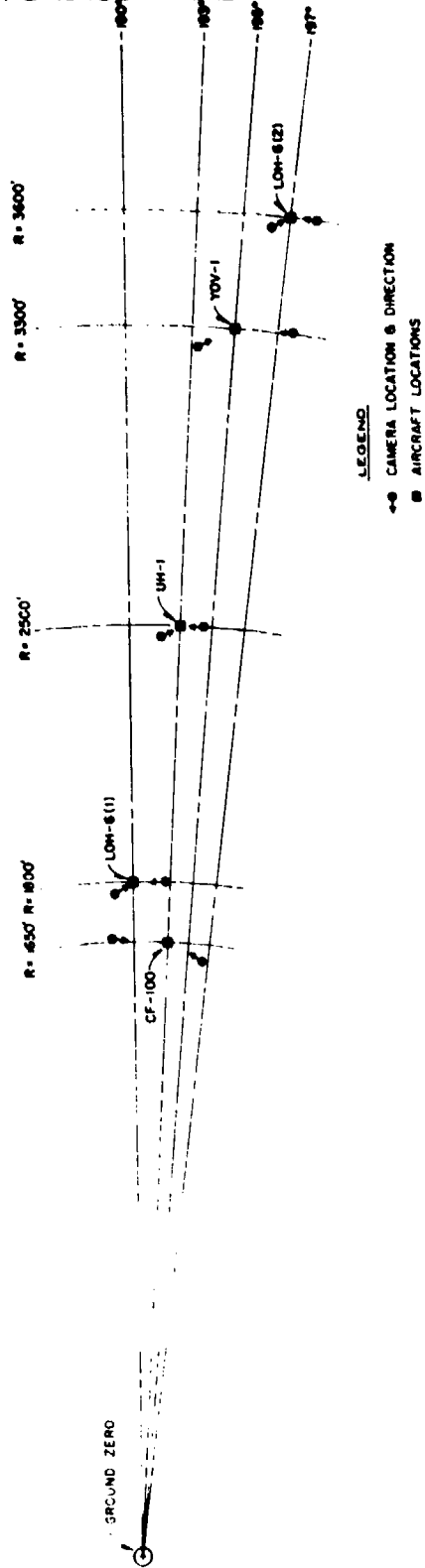*Superscripts refer to References at the end of this report.

27

Figure 5 (U)   Project LN111 test site layout (U).

28

predicted; procurement of this type aircraft for testing is very difficult and it was planned to use it again in follow-on programs.

RESULTS

(C) The tests results indicated that the methodology used for predicting aircraft blast damage was reasonably accurate for some of the aircraft and that modification will be required for others. A comparison between the predicted and actual damage (Table 1) based upon the general categories of Light, Medium, and Heavy damage, shows that the two OH-6 helicopters responded as predicted, the UH-1 helicopter was damaged slightly more than predicted, and the YOV-1 and CF-100 aircraft damage predictions were too conservative. When the resultant damage was evaluated based upon the more specific definitions of the damage categories, all of the predictions appeared to be more accurate. Examples of the kinds of damage that would be expected to satisfy the general damage categories are:

Light - Skin panel deformation, broken stringers, broken Plexiglas, loose or missing access panels, flat tires, leaking hydraulic and fuel lines, broken electrical wires, etc.

Medium - Broken main structural members (longerons, formers, spars, etc.), missing or badly deformed control surfaces or control linkages, misalignment beyond tolerances of major structural components (empenages, tail booms, wings, landing gear, etc.)

Heavy - Damage more severe than Medium damage or an excessive accumulation of Medium damage such that the aircraft is beyond reasonable repair.

29

Table I (C) Comparison of predicted and actual aircraft damage (U).

AIRCRAFT	DISTANCE (FT)	PREDICTED STATIC OVERPRESSURE (PSI)	DAMAGE DESCRIPTION	
			PREDICTED	ACTUAL
CF-100	1650	4.0	L	ND
OH-6(1)	1800	3.5	H	H
UH-1	2500	2.3	L	M
YOV-1	3300	1.5	L	ND
OH-6(2)	3600	1.3	L	L

H - Heavy: Not flyable and not reasonable to repair

M - Medium: Flyable after major repair

L - Light: Flyable with/without minor repair

30

(C) The following is a summary of the resultant damage:

CF-100 - The nose gear strut showed loss of hydraulic fluid and the nose gear door was blown loose at two attachment points (Figure 6). Several replacement screws used to attach the fairing between the right (blast side) outboard wing and engine nacelle were popped out. There was slight buckling of the center skin panels on the right engine nacelle just forward of the engine tail pipe (Figure 7). One small access cover was blown off the top center fuselage.

OH-6(1) - The helicopter was rotated such that the tail boom was approximately 8 feet from its original reference point. All of the Plexiglas except for one small window was blown out, and all the doors except the right (side opposite the blast) rear door were badly crushed or blown off (Figure 8). The cockpit framework was destroyed down to the floor line. The engine intake and exhaust housings were crushed, twisted, or blown off (Figure 9). The upper and lower tail boom fins were bent and broken (Figure 10). The most critical structural damage occurred on the blast side in the area where the fuselage and tail boom are joined (Figure 11). The joint was opened, indicating former deformation, and there was severe skin panel buckling.

UH-1 - The helicopter was rotated so that the tail boom was slightly more than 3 inches from its original reference point. All Plexiglas on the left side (blast side) of the aircraft and on the right rear door was blown out. The forward left door was badly buckled and the rear door was crushed inward about 3 inches, (Figure 12). Some of the

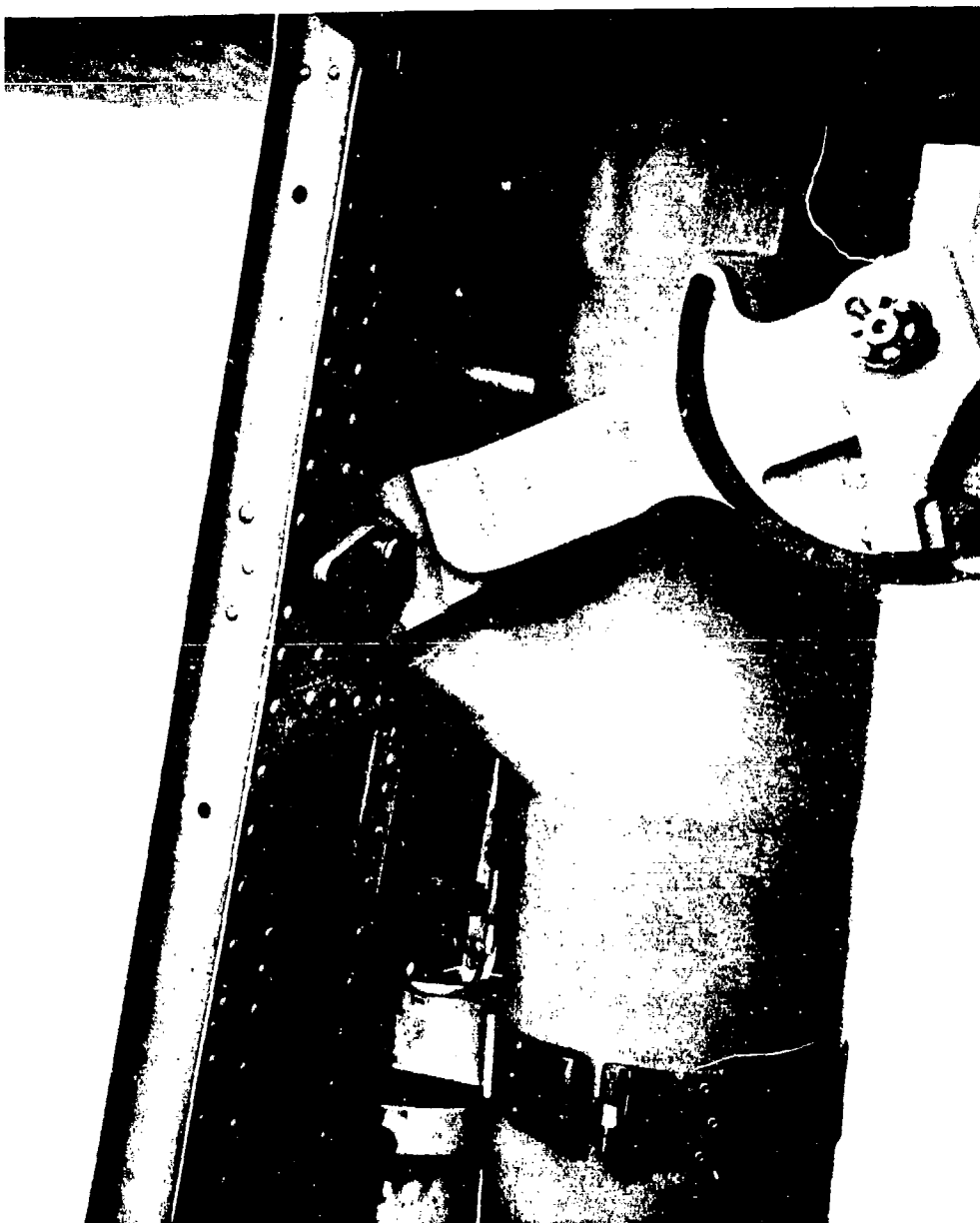Figure 6 (U)   The CF-100 nose gear door damage (U).

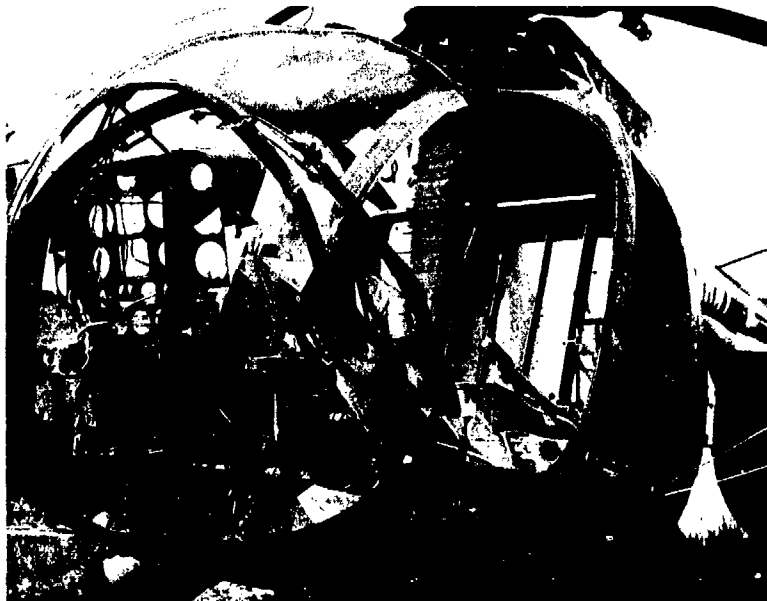Figure 7 (U)   Slight buckling of skin on the right engine nacelle (U).

33

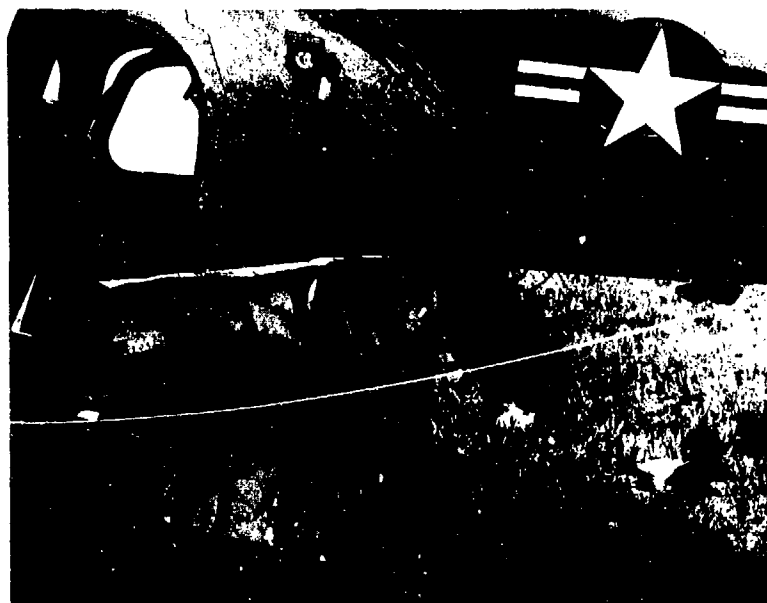Figure 8 (U)   Front and side fuselage damage to the OH-6(1) helicopter (U).

Figure 9 (U)   Damage to the intake and exhaust housings on
the OH-6(1) helicopter (U).

Figure 10 (U)   Damaged tail boom fins on the OH-6(1) helicopter (U).

Figure 11 (U)   Damaged tail boom—fuselage joint on the OH-6(1) helicopter (U).

Figure 12 (U) Front and side fuselage damage to the UH-1 helicopter (U).

36

frame work between these doors was twisted and buckeled. The upper
left side of the helicopter along the main fuselage length had significant
panel damage, which diminished over the topside. The engine covers were
blown open and three access panels on the left side of the aft fuselage
were popped open. The most severe damage occurred along the left side
of the tail boom (Figures 13-14); skin was torn and four formers were
broken loose from the longerons. The right side and underside of the
tail boom appeared to be undamaged.

YOV-1 - Essentially there was no damage, but the aircraft was
rotated such that the tail was slightly more than 1 inch from its
original reference point. The left side (blast side) canopy door,
one small access panel, and the foot step door were popped open.

OH-6(2) - The tail boom was shifted away from the blast about 3/4
inches from its original reference point. All Plexiglas on the left
side (blast side) was blown out or badly broken. There was some
broken Plexiglas on the opposite side, probably caused by secondary
fragments of Plexiglas. There was no apparent structural damage aft
of the rear doors. The left rear door was badly damaged (deformations
from 1 - 4 1/2 inches) and the left forward door was slightly buckled
(Figure 15).

DISCUSSION OF RESULTS

Camera Coverage

(C) The camera coverage was intended to provide measurements of
deflections and displacements of the aircraft and their structural
components. It was difficult to make exact measurements because of

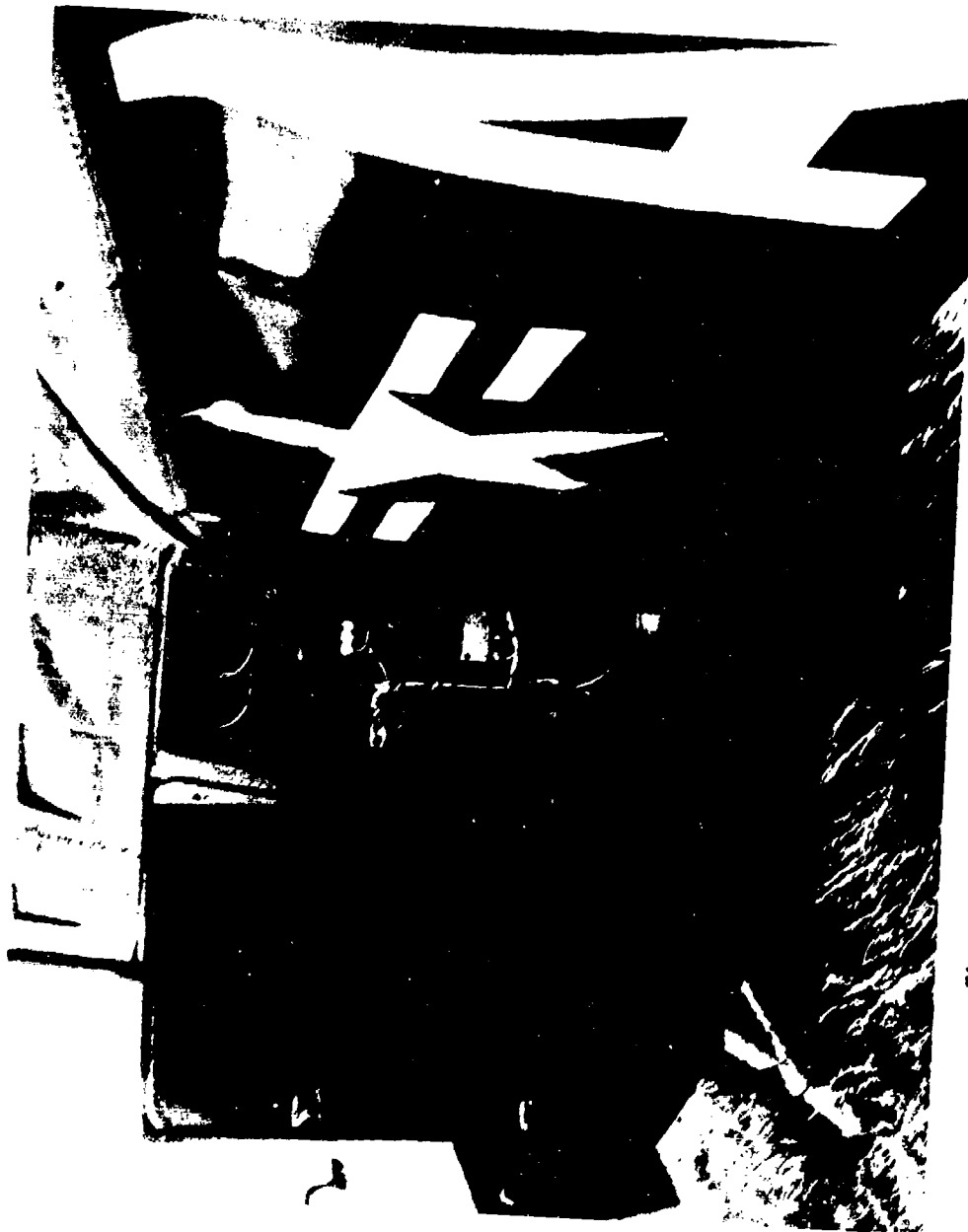Figure 13 (U) Tail boom damage on the UH-1 helicopter (U).

38
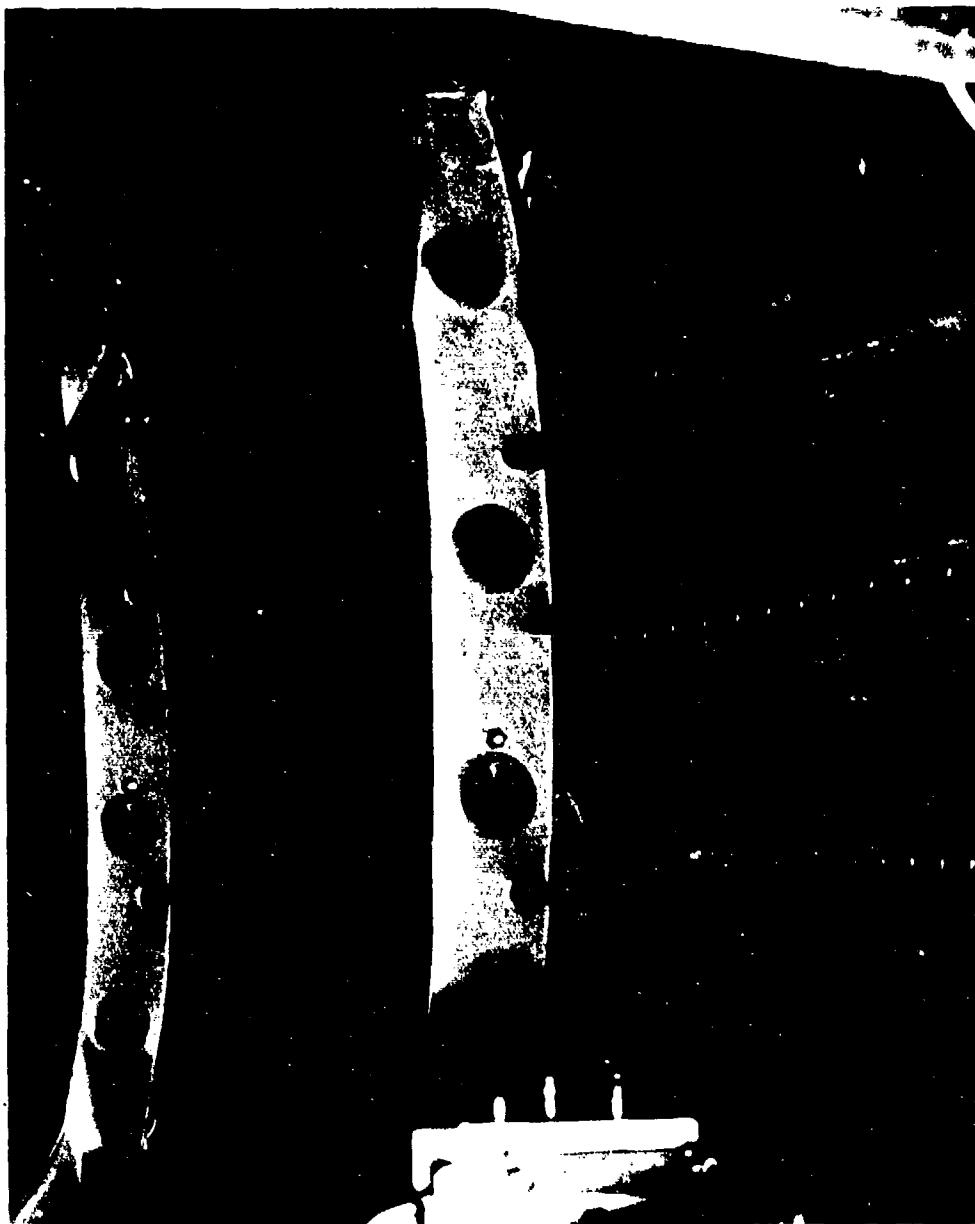
Figure 14 (U)   Internal view of tail boom damage on the UH-1 helicopter (U).

39

Figure 15 (U) Front and side fuselage damage to the OH-6(2) helicopter (U).

40

camera angles, the complex dynamics of motion (translation, rotation, and deflection), and picture size; however, some very interesting information and measurements were obtained. All aircraft were dynamically displaced greater than the measured static displacements. This appeared to result from the motion of the shock absorption systems in the landing gears. Films of the CF-100 showed the wing tip closest to the blast raised 8-10 in. and the horizontal stabilizer, on the same side of the aircraft, raised slightly more. This suggests that some deflection in the horizontal stabilizer or aft fuselage occurred. The films of the OH-6(1) showed the helicopter being prevented from overturning because of the two rotor blades on the side opposite of the blast striking the ground. In addition, the forward blast side rotor blade showed a 6-7 in. bow near the center-span; the loading appeared not to be from blast, but the inertia loading of the blade as the fuselage was rotated. The forward rotor blade tip of the UH-1 had risen approximately 18 in., which is not critical but information that could be used to support calculations of blast loading on a uniform airfoil cross-section near zero degree angle of attack to a blast wave. No measurements could be obtained from the camera coverage of the OV-1 but slight motion of the blast side wing tip and the empenage could be seen. For the OH-6(2), measurements were made of the rotor blade tip, tail boom, vertical fin and main rotor blade hub displacements.

Prediction Assessments

(C) Although the resultant damage to the CF-100 aircraft borders on satisfying the requirements for Light Damage, it was sufficiently insignificant to be classified as No Damage. It is estimated that the

41

pressure level of the environment should have been increased to 5-6 psi.

Except for the broken former damage to the tail boom on the UH-1

helicopter, the prediction was fairly accurate; probably a reduction of

0.5 psi would have given the desired damage. As with the C-100 aircraft,

the YOV-1 aircraft should have been at a pressure level 1-2 psi

higher. Although these two aircraft were not damaged, the data

are still valuable for establishing the threshold damage regions.

(C) The overpressures measured along the main blast lines indicated

that the actual overpressures were very close to the predicted values.

CONCLUSIONS

(U) The project as a whole was considered a success. The objectives

were accomplished; all cameras ran, measurements were made of the

aircraft displacements, detailed descriptions of the resultant

damage were obtained, and the extent to which the prediction methodology

must be corrected was clearly indicated. The results of this test have

also been used as new input data and to check other prediction method-

ologies.[2,3] In addition, considerable interest has been generated

in the Plexiglas breakup of windows in helicopters and what effects

it will have on humans and the balanced survivability criteria[4]. Future

plans for experimental tests will include studies of Plexiglas breakup

and the effects of blast on the aerodynamic stability of in-flight

helicopters.

42

REFERENCES

1. O. T. Johnson, "A Blast-Damage Relationship (U)," BRL Report No. 1389, September 1967, Confidential.

2. DASA 2048 Supplement, "Handbook of Computer Programs for Analysis of Nuclear Weapon Effects on Aircraft," Kaman AviDyne Report No. KA TR-50S, April 1970, Unclassified.

3. Institute of Nuclear Studies, "Vulnerability of Aircraft to the Effects of Nuclear Weapons (U)," USA Combat Developments Command Technical Report No. 1-70, July 1970, Secret.

4. Col. W. P. Schneider, Institute of Nuclear Studies, "Criteria for the Protection of Equipment Against Nuclear Weapons Effects (U)," USA Combat Developments Command Technical Report No. 2-68, December 1968, Confidential.

N.H. Ethridge, Project Officer
G.D. Teel
Ballistic Research Laboratories

PROJECT LN112
BLAST EFFECTS ON ELECTRICAL EQUIPMENT SHELTERS (U)

(U) INTRODUCTION

The objective of Project LN 112 of Event DIAL PACK was to determine the response of Electrical Equipment Shelters to blast.

The primary shelter of interest was the S-280 Electrical Equipment Shelter. This shelter is one of the components of major Army communications and electronic control systems which must function after exposure to blast. TACFIRE provided four of these shelters to the project. The shelters were new, empty, and unmodified in any way. It was not possible to obtain equipment to install in these shelters. However, two of these shelters were modified by USAECOM personnel at Ft. Monmouth, N. J., to include weighted racks and work benches to represent the strengthened conditions that might be produced by the installation of a system within the shelter.

At a very late stage in test planning two S-250/G Electrical Equipment Shelters, one S-335/TRC-113 shelter, and one S-390/TRC-145 shelter were supplied to the project. The latter two shelters are the basic S-250 shelter modified to include racks, work benches, and other equipment corresponding to the particular system installation. The shelters are similar in construction to the S-280 shelters, but are designed to be truck-mounted. Racks were in place in the S-335 and S-390 shelters, with block weights substituted for equipment.

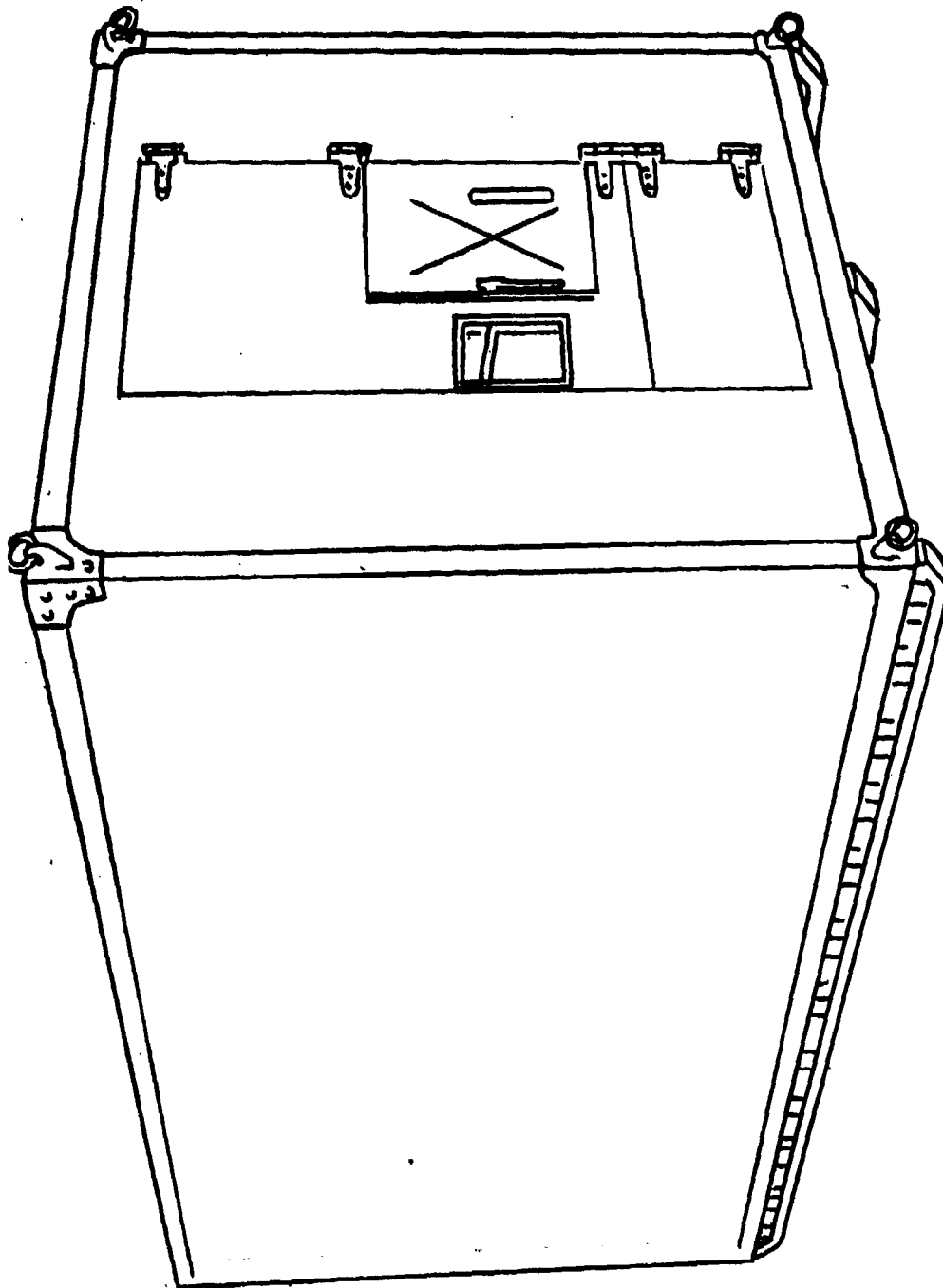Figures 1 and 2 show the outside configuration of the two types of

Figure 1 (U)   View of S-280/G electrical equipment shelter (U).

45
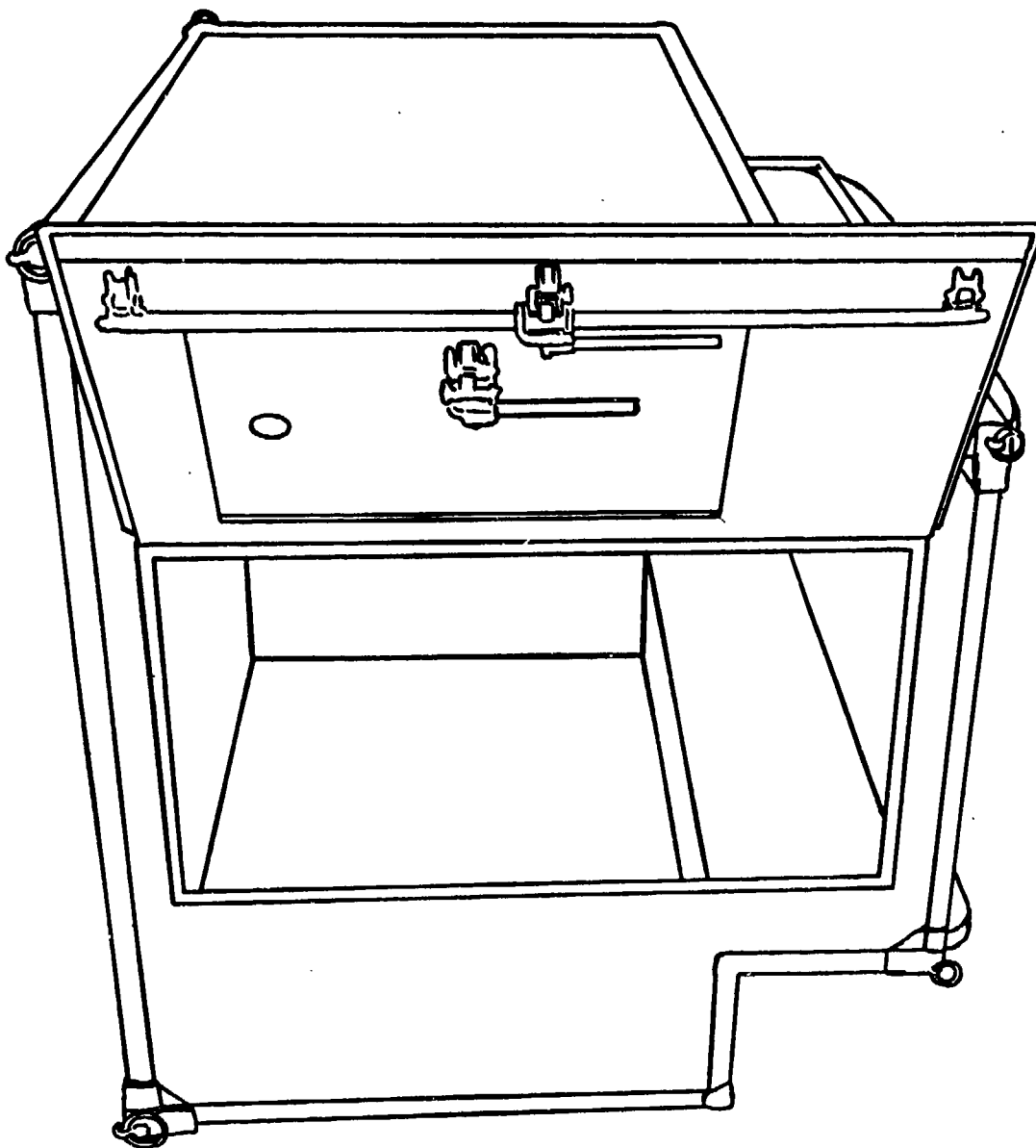
Figure 2 (U)   View of S-250/G electrical equipment shelter (U).

shelters. The walls are of sandwich construction, with stiffening members spaced at regular intervals. The inner and outer surfaces of the walls are 0.032-inch-thick aluminum sheets with plastic foam bonded in between the sheets. The stiffening members are aluminum rods with a hat cross-section. The walls of the S-280 shelter are two inches thick, and 1.5 inches thick in the smaller shelters.

(U) PROCEDURE

The most vulnerable orientation of the large shelter was expected to be that which placed the largest side parallel to the incident blast wave front. All shelters were placed so that the side wall to the left of the entrance was toward the charge.

Calculations indicated that the shelters might be displaced significantly by the blast. Such movement could be damaging to systems within the shelter, and therefore the shelters were tied down with guy wires attached to each corner. This is a relatively simple technique to increase resistance to blast, and should be operationally feasible for Army systems.

The placement of the shelters relative to the explosive charge was based on predictions of shelter wall response made using a single-degree-of-freedom model. An S-280 shelter with weighted equipment racks, the S-335/TRC-113 shelter and the S-390/TRC-145 shelter were exposed to an incident shock front overpressure of 4.8 psi. An S-280 shelter with weighted equipment racks and an S-250 shelter were exposed at 3.0 psi, a bare-walled S-280 shelter and an S-250 shelter were exposed at 1.7 psi, and one bare-walled S-280 shelter was placed at 0.9 psi.

47

The four S-280 shelters were instrumented with electronic pressure gages, accelerometers, and displacement-time gages. Very rigid mounts attached to the floor of the shelter provided the reference position for the displacement-time gages. The location of the electronic gages on the front wall of the S-280 shelter are shown in Figure 3. The wall sections were numbered, and these numbers are used with gage records to identify the locations of the gages. Recording was done with 20 KHz FM magnetic tape recorders. In addition to the active gages, passive mechanical gages which recorded peak wall and roof deflections were installed in all shelters.

High-speed cameras were used to photograph the interior of all S-280 shelters and the exterior of the shelters at 4.8 and 1.7 psi.

After the shelters were prepared for the test, sand bags were placed within them to increase the shelter weights to typical load levels. It was not necessary to add weight to the two S-280 shelters containing weighted racks.

All shelter doors and vent opening covers were latched for the test so that the shelters were essentially sealed.

Figure 4 shows an overall view of the shelters at the 4.8 psi station.

(C) RESULTS

After the explosion all shelters were intact and in position, but had sustained a range of structural damage. The tie-down system worked very well. There was no indication that any debris struck the shelters or that any significant amount landed in the vicinity of the shelters.
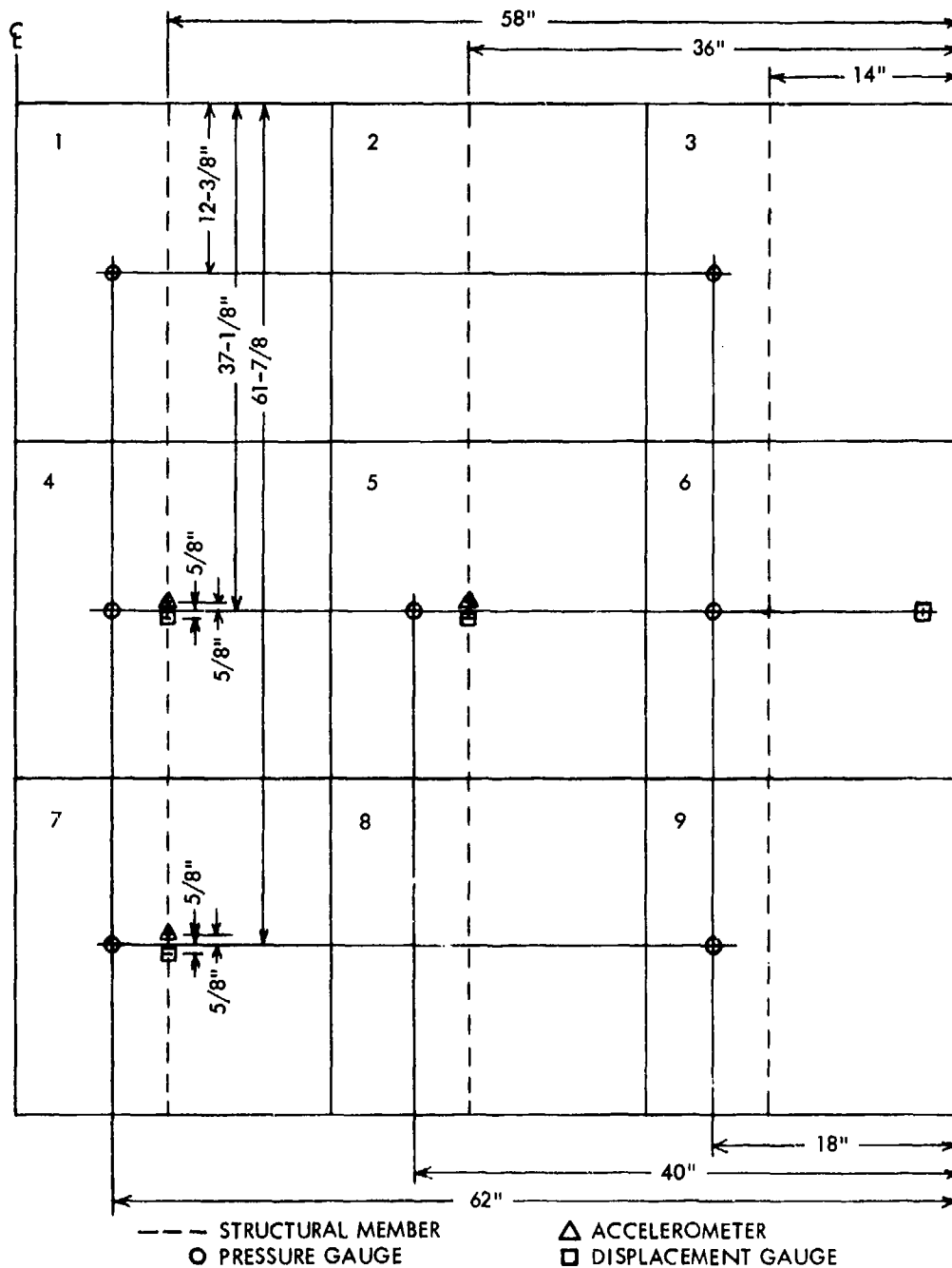
48 .

Figure 3 (U) Gage locations on the front wall of the S-280 shelter
viewed from inside the shelter (U).

Figure 4 (U) Overall view of 4.8 psi shelter station (U).

50

The S-280 shelter exposed at the lowest pressure level, 0.9 psi, had crinkled skin on the wall toward the blast. At stations closer to the charge, deformation occurred not only in the front wall but also on the door and end walls. At the closest station the door wall was sufficiently deformed to make door operation difficult. The vent cover on this shelter was also found open. The condition of the cover indicated that it remained intact during the positive pressure load, but opened when the pressure inside exceeded the pressure outside, probably during the negative pressure phase of the blast wave.

The S-250 type shelter showed no changes at 1.7 psi, crinkled skin on the wall toward the blast at 3.0 psi, and severe deformation with skin torn loose at corners on the front wall and top at 4.8 psi.

No damage was evident to the equipment racks in either the S-280 shelters or the S-335 or the S-390 shelters. However, in the S-335 and S-390 shelters fixtures were thrown violently from the walls and roofs. Figures 5 and 6 show the dangling light fixtures and debris on the floor of the S-390/TRC-145 shelter.

All instrumentation operated with the exception of one pressure gage channel which failed prior to the test and one camera. One of the acceleration records has rapid base line shifts and seems unusable. Six of the remaining 17 acceleration records saturated on the initial peaks. The pressure gages, although providing good records, seem to have been affected by the acceleration of the wall panels in which they were mounted.

Figure 7 shows the displacement-time records for Shelter 7, the S-280 shelter at 0.9 psi. The frequency of the oscillation is
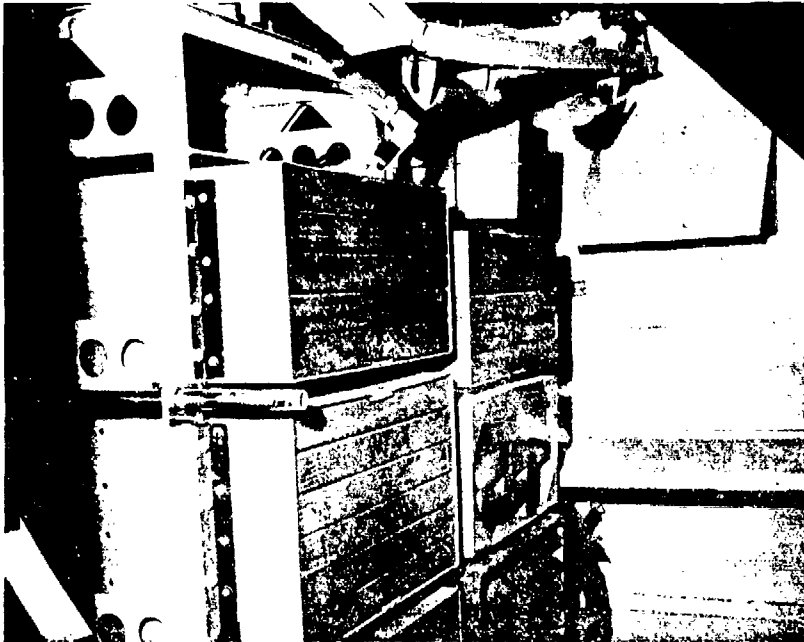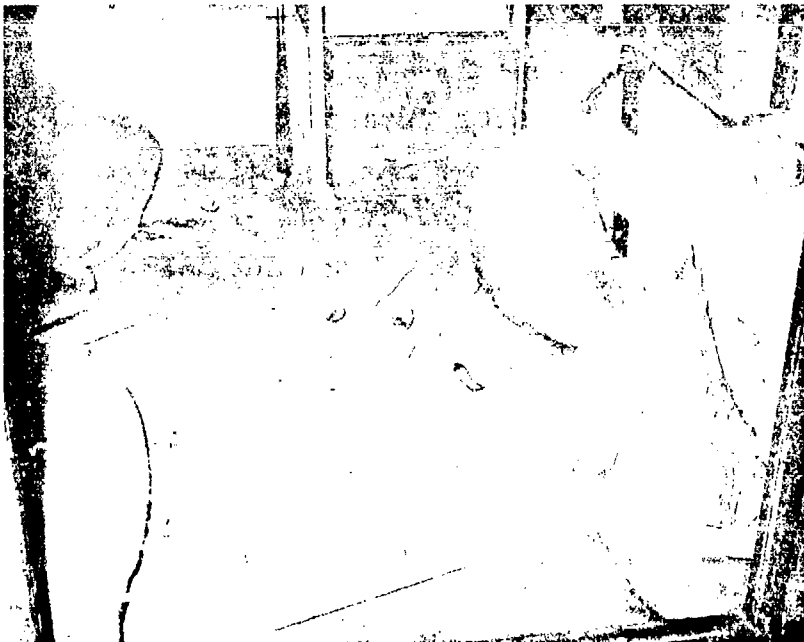
51

Figure 5 (U)   Interior damage to the S-390/TRC-145 shelter   (U).

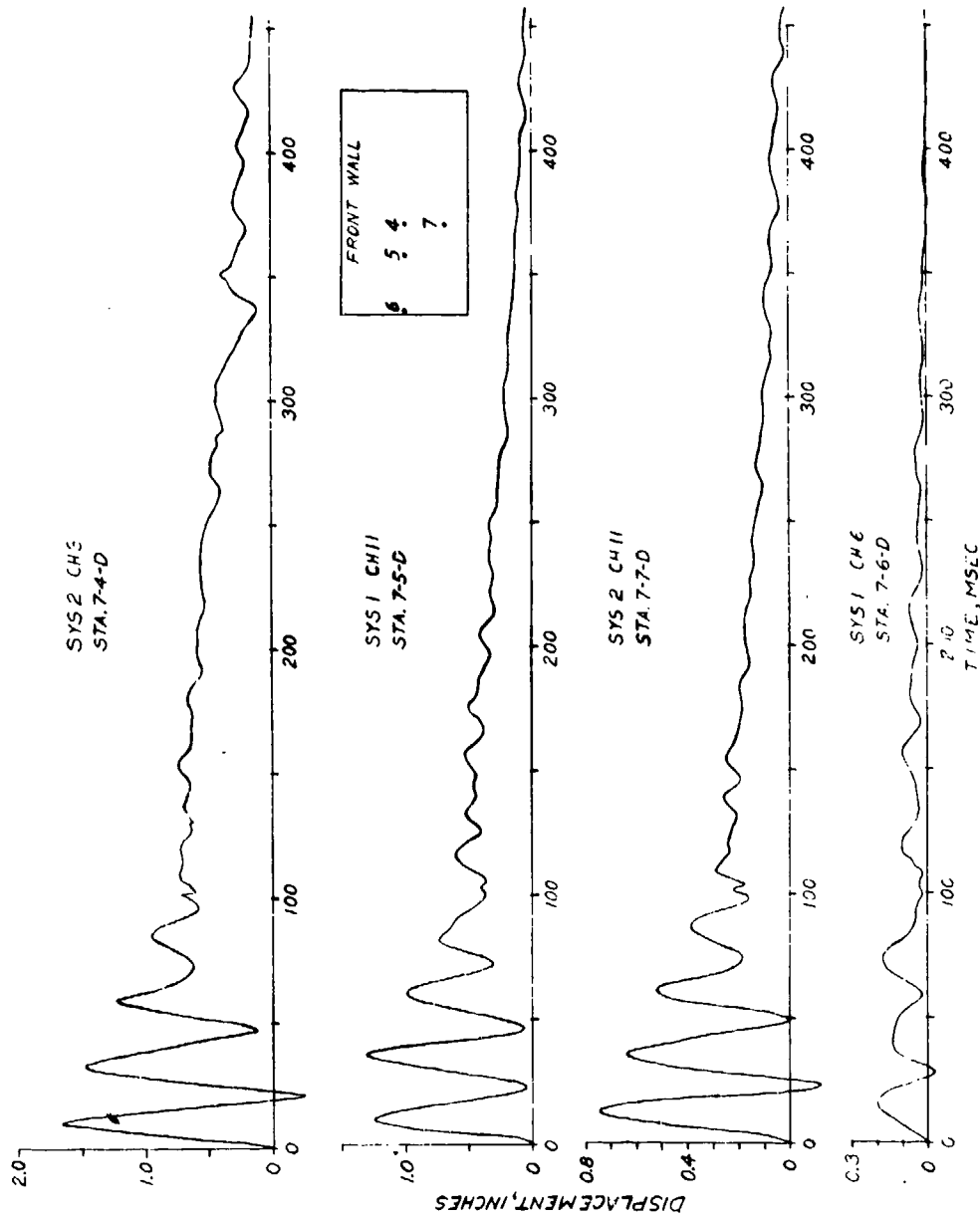Figure 6 (U)   Post shot debris in the S-390/TRC-145 shelter   (U).

Figure 7 (U)   Displacement-time records obtained in the bare-walled S-280 shelter at 0.9 psi (U).

about 40 Hz. The location of the gages can be determined by referring to Figure 3. The station nomenclature for System 2, Channel 3, is such that 7 refers to the shelter number, 4 refers to the wall section in which the gage was located, and D means displacement gage.

Figure 8 shows displacement-time records for Shelter 1, the S-280 shelter with weighted racks at 4.8 psi. The wall was made much stronger by the addition of the racks, and the deflection was about the same as for the bare-walled shelter at 0.9 psi. The frequency of oscillation was increased by the additional stiff ness to about 110 Hz.

Figure 9 shows acceleration records obtained on the S-280 shelter at 0.9 psi. Figure 10 shows the same records with an expanded time scale. Even at this low pressure level the wall experienced accelerations ranging from + 200 g's to - 200 g's.

Figure 11 shows an acceleration record obtained on the front wall of the S-280 shelter at 4.8 psi. The peak positive magnitude is considerably above 300 g's.

Figure 12 shows the record from an accelerometer which was mounted on the front of one of the racks in the S-280 shelter at 4.8 psi. The initial positive peak magnitude is about 70 g's.

Records obtained at other locations in the shelters show similar characteristics.

Figure 13 shows the maximum inward deflection of the S-280 shelters versus incident shock front overpressure as determined using both displacement-time gage results and data from the mechanical peak displacement gages. The curves are extrapolated

54
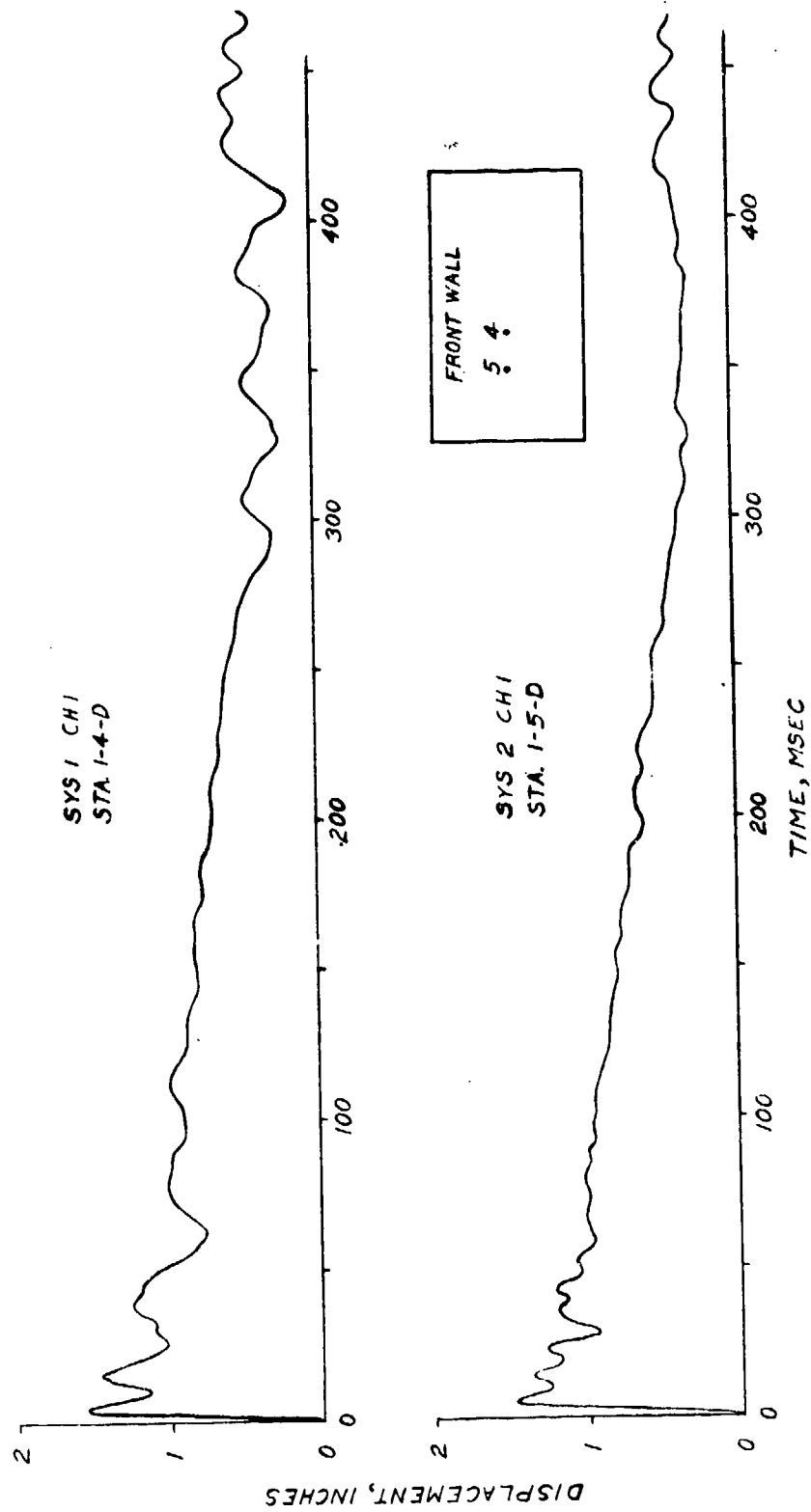
Figure 8 (U). Displacement-time records obtained in the S-280 shelter with weighted racks at 4.8 psi (U).

55
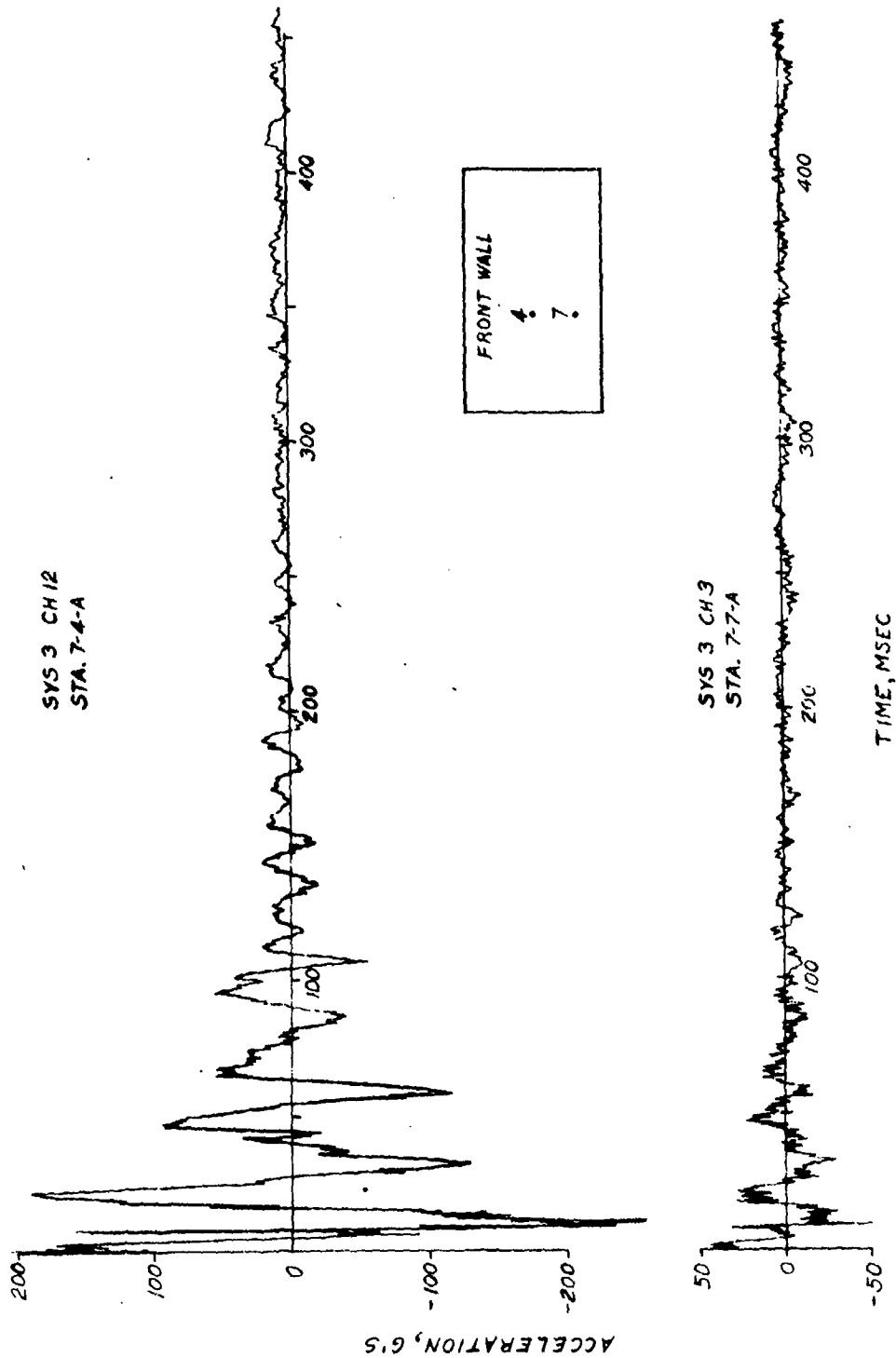
Figure 9 (U) Acceleration-time records obtained in the bore-walled
S-280 shelter at 0.9 psi (U).

Figure 10 (U)   Acceleration-time records with expanded time scale obtained
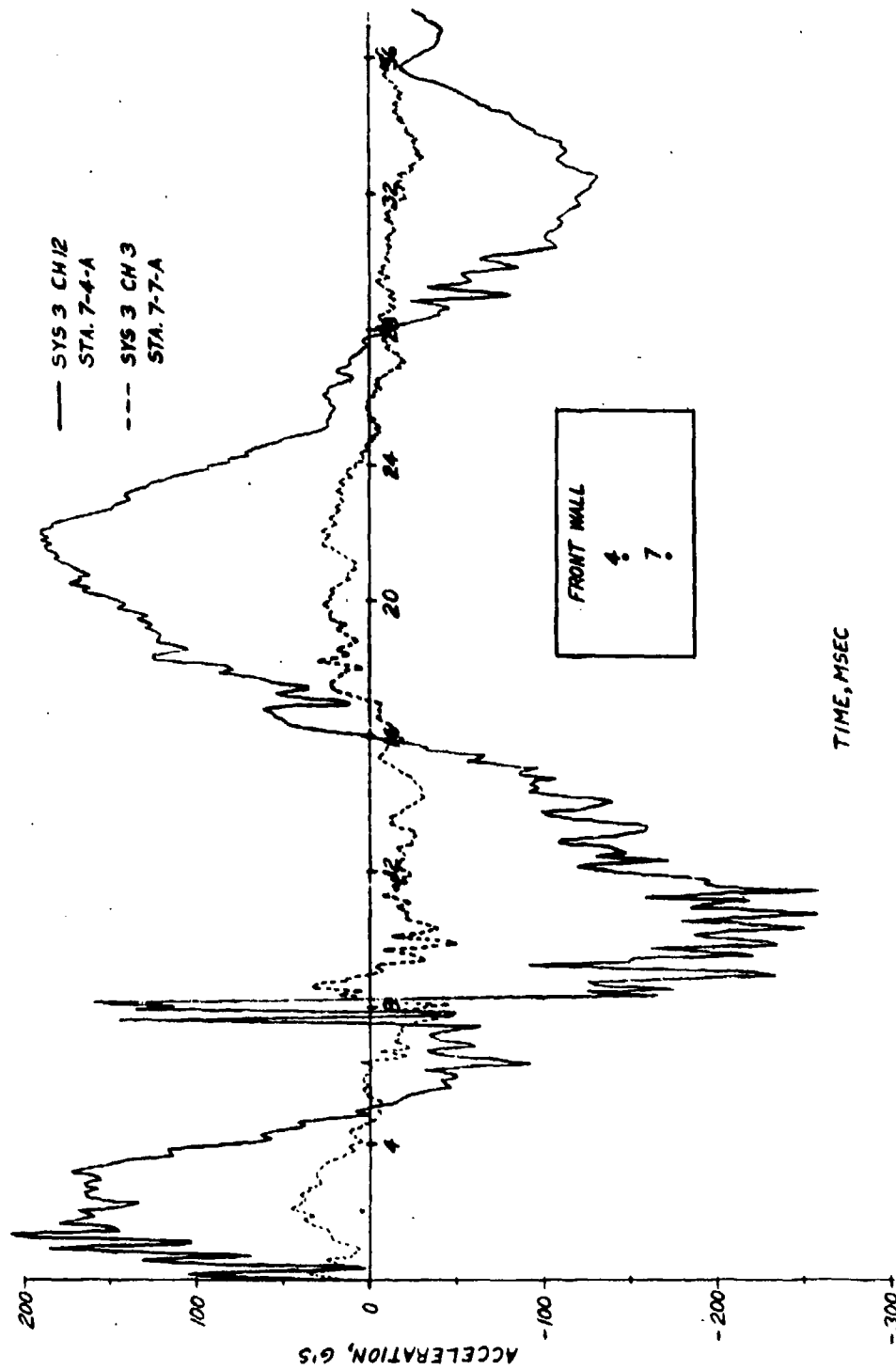in the bare-walled S-280 shelter at 0.9 psi (U).

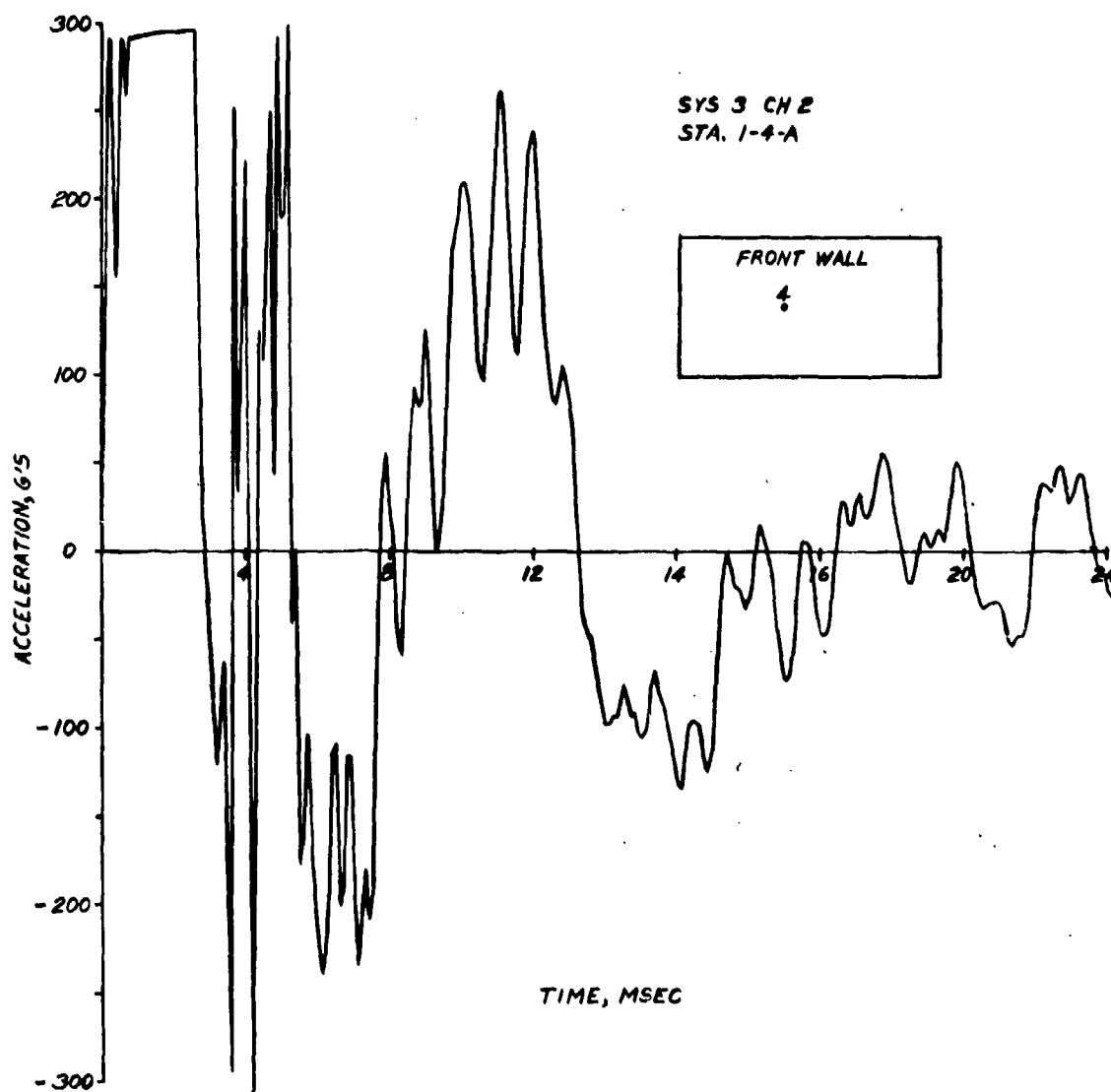Figure 11 (U)   Acceleration-time record obtained in the S-280 shelter with
weighted racks at 4.8 psi (U).

58
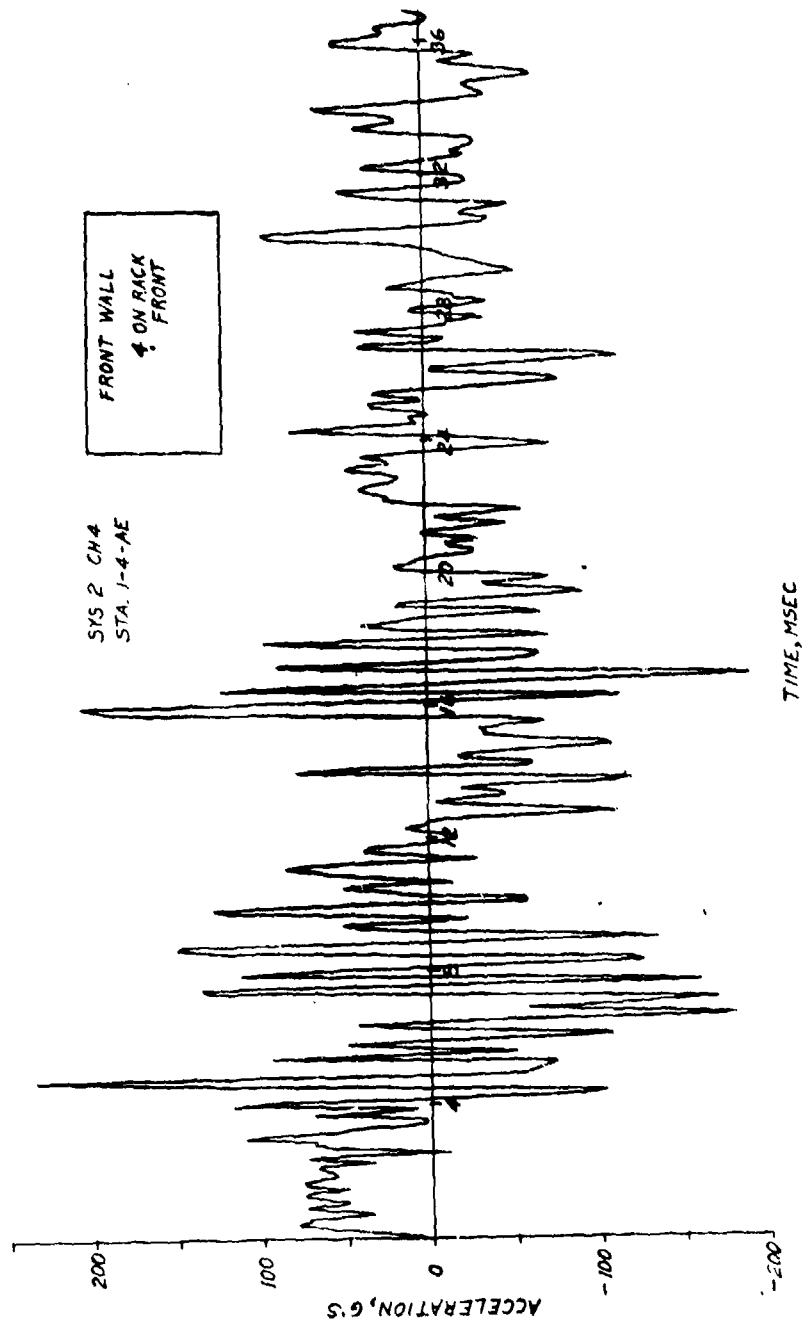
Figure 12 (U) Acceleration-time record measured on the front of an equipment rack in the S-280 shelter at 4.8 psi (U).

59

to the deflection which was observed to correspond to breaking of welds and tearing of the skin of the panels of both the S-280 and S-250 shelters. The curves apply only for a shelter tied down and oriented with the long wall perpendicular to the direction of shock front movement. If the front wall begins to break loose at 2.5 psi as shown in the figure, then catastrophic failure of the shelter seems likely at 4.8 psi. The addition of floor-to-ceiling racks on both front and rear walls greatly reduced the response of the front and top panels, and enabled the shelter to survive at 4.8 psi.

Figure 14 shows similar curves for panel deflection for a bare-walled S-250 shelter, also tied down and oriented as shown. The top and front wall were at the failure level at 4.8 psi, with rivets and welds broken and skin torn loose. The end is larger in area than the front wall and should experience greater damage than the front wall if oriented toward the blast. Thus it seems unlikely that the shelter will survive a shock wave of 4.8 psi with the shelter in its most vulnerable orientation.

(C) SYSTEM IMPLICATIONS

No electronic systems were exposed in the test, and thus no conclusive statements concerning the continuing functioning of particular systems after exposure to blast can be made. However, the acceleration levels measured in the S-280 shelters and probable in the smaller shelters were well above those which electronic equipment normally can survive. The basic S-250 shelter was at the failure level at 4.8 psi incident overpressure. The larger S-280 shelter was found to require reinforcement of all walls and the roof to survive at 4.8 psi for a blast wave striking at a random
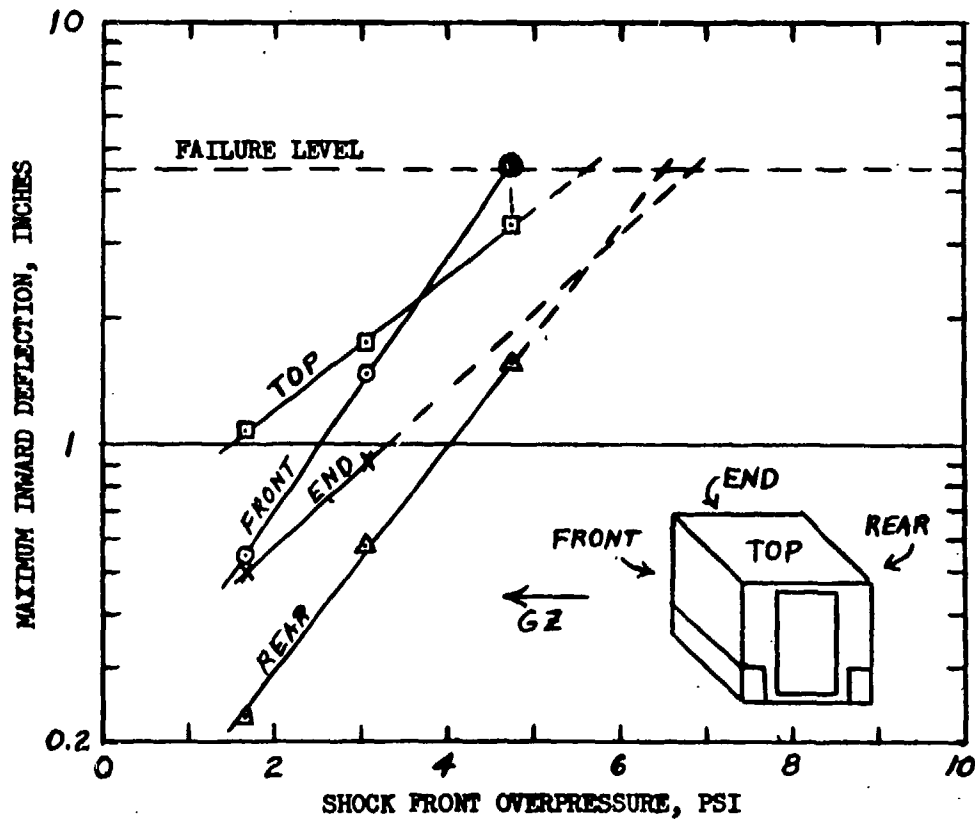
61

Figure 14 (C)   Maximum inward deflection of panels of the S-250 shelters versus incident shock front overpressure (U).

62

orientation.

The primary implication for shelter systems from these test results are that the placement and mounting of system components, the shock isolation characteristics of the systems, and the levels of shock and vibration which system components can stand will determine the continued operation of the shelter system after exposure to blast. Thus each shelter system and system configuration requires examination to determine its susceptibility to blast.

(C) CONCLUSIONS AND RECOMMENDATIONS

The bare-walled S-280 shelter will not survive at 4.8 psi overpressure. No wall panel will survive in the S-280 shelter at 4.8 psi incident overpressure without being strengthened, if the most vulnerable orientation of the wall is assumed.

The bare-walled S-250 shelter is at the failure level at 4.8 psi incident overpressure for the orientation used in this test, both for the front wall and top. For an orientation where the wall opposite the door is toward the charge, failure is expected at less than 4.8 psi because of the larger panel area.

The statements above for levels of overpressure for failure assume the explosion is equal to or larger than the explosion of 500 tons of TNT.

Systems designers must carefully examine placement and mounting of racks and equipment within a shelter to insure structural survival of the shelter to blast. They must also carefully evaluate the shock resistance of their system components, and by selection of components and by shock isolation techniques protect the system from the acceleration levels generated by blast loading.

63

Further testing of shelter systems to blast should include actual system components which are activated and instrumented.

To improve resistance to blast, shelters used by the Army should be tied down securely where this is feasible.

Consideration should be given to the design of a special shelter to provide blast protection to electronic and electrical systems.

.

64

W. R. Conley, Project Officer
Naval Ship Research and
Development Center

PROJECT LN113
RESPONSE OF NAVAL TEST STRUCTURES
TO AIR BLAST (U)

INTRODUCTION

(U) The primary objective of project LN 113 was to obtain air blast loading

and structural response data for several examples of topside shipboard equip-

ment and structures. Specific objectives were as follows:

1. To determine the magnitude and character of shock motions induced by air

blast on two model deckhouses.

2. To obtain experimental structural response of several communication

antennas.

3. To determine the adequacy of the design of the communication antennas

tested.

4. To determine the air blast loading on a radar antenna reflector.

EQUIPMENT TESTED

One-Third Scale Model Deckhouses

(U) In a cooperative effort between the Naval Construction Research Establishment

(NCRE), Dunfermline, Fife, Scotland, and NSRDC, shock motion measurements were

made by NSRDC on the NCRE deckhouses. Two deckhouses were tested at 10 psi

overpressure. One deckhouse was fabricated from aluminum (yield strength 27.8

ksi) and the other from steel (yield strength 33.6 ksi). The deckhouses were

prototypes of a design used by the British which incorporates vertical framing

65

as opposed to longitudinal framing used in U. S. Navy ships (See Figure 1). Each deckhouse was fixed to a concrete foundation by a number of one inch diameter steel bolts.

Whip Antennas

(U) Two types of 35 ft whip antennas, the NT 66047 made of aluminum and the AT 1022/SR made of glass reinforced plastic (GRP) were tested. One aluminum and one GRP antenna were installed at the predicted 8 psi range. A single GRP antenna was installed at the predicted 15 psi range. Each antenna was mounted on a steel support box on a concrete foundation.

(U) The NT-66047 is a 35-ft aluminum whip antenna composed of five equal lengths of 6061-T6 aluminum tube. The lengths are joined together by fitting the adaptor sleeve at the bottom of the upper pieces into the larger diameter lower pieces and securing the joint with a threaded cap and lock nut. The NT-66047 was standardly mounted on the IL-18/U insulator feedthrough.

(U) The AT-1022/SR is a 35-ft GRP whip antenna composed of two sections approximately equal in length. The antenna is uniformly tapered from an outside diameter at the base of 5-1/2 inch into an outside diameter at the top of 1-1/2 in.

(U) Figure 2 shows the NT-66047 aluminum whip antenna and the AT-1022/SR GRP antenna installed at the predicted 8 psi range.
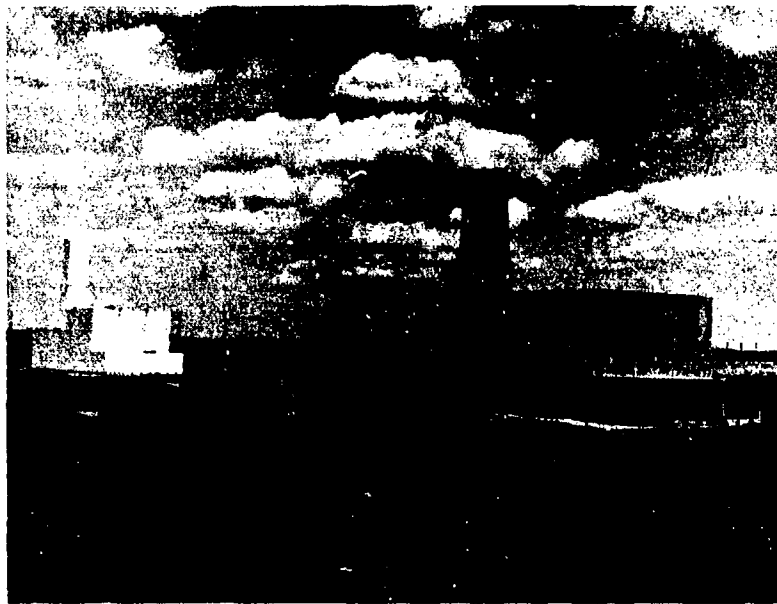
66

Figure 1 (U)   NCRE deckhouses at the predicted 10-psi range (U).

Figure 2 (U)   The AT 1022/SR glass-reinforced plastic whip antenna
(right) and the NT 66047 aluminum whip antenna (left)
at the predicted 8-psi range (U).

67

Wire Rope Antennas

(U) Two #2-3 dual twin fan wire rope transmitting/receiving antennas were tested. This antenna is constructed of 5/16 in. type C (6x19) phosphor bronze wire rope. It was attached to the support columns using standard connectors and fittings at each end. The length of the transmitting wire is approximately 57 feet. With insulators, turnbuckles, safety links, and various other components installed the overall length is approximately 66 ft. These antennas were placed at right angles to the direction of propagation of the blast front at the predicted 10 and 15 psi ranges. Steel columns set in concrete served as end supports. (See Figure 3).

AN/SPS/10E Radar Antenna Reflector

(U) The air blast loading on an AN/SPS-10E radar reflector due to diffraction and drag was measured by suspending the reflector in a pendulum type configuration (See Figure 4) and recording its motion during the blast using two accelerometers and a high speed camera. Applied load can be calculated using the measured acceleration and the known mass of the reflector.

INSTRUMENTATION

Transducers

(U) The target structures were instrumented with a total of 35 transducers for the measurement of strain, acceleration, and velocity. Three pressure transducers were located at the predicted 8, 10 and 15 psi overpressure range to record the actual overpressure. The signal from each transducer (except velocity meters), was transmitted by an eight-conductor shielded cable

68

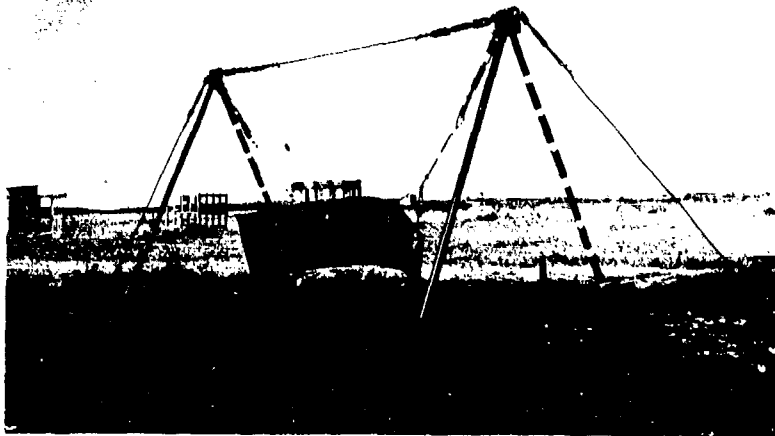Figure 3 (U)   The 2-3 wire rope antenna installation at the
predicted 15-psi range (U).

Figure 4 (U)   The AN/SPS-10E radar antenna reflector installed
at the 10-psi range (U).

69

running from the target to the instrumentation trailer. The velocity meter cabling consisted of two-conductor shielded cables. Average cable runs from the target structure to the blast resistant bunker housing the instrumentation trailer were approximately 1900 feet. All cables were laid in trenches and covered with soil before the test. The instrumentation trailer was equipped with three tape recorders. Each recorder was a 14-channel frequency-modulation machine, having a frequency response of 0 to 20,000 Hz. Input voltages from the transducers were, in general, amplified to 0.7 volt before being fed into the tape recorders. One channel on each recorder recorded a time code signal compatible with digitizing playback equipment at NSRDC. One other channel on one recorder recorded the time of detonation. The recorders were started manually two minutes before detonation, Z-2 minutes.

(U) Calibration was accomplished by recording a step pulse (Cal-step) representing a known transducer output value on each channel prior to and following the event. Accelerometers and velocity meters were calibrated at NSRDC to determine the relationship between motion input and signal output.

(U) The instrumentation effort consisted primarily of velocity meters for the deckhouses, strain gages for the whip antennas, load cells for the wire rope antennas, and accelerometers for the AN/SPS-10E radar reflector. A summary of this information follows:

(U) NCRE Deckhouses - Seventeen DTMB type velocity meters were used to monitor air blast induced shock motions in the aluminum deckhouse. Five DTMB type velocity meters were used in the steel deckhouse. Gage positions are indicated in Figure 5.
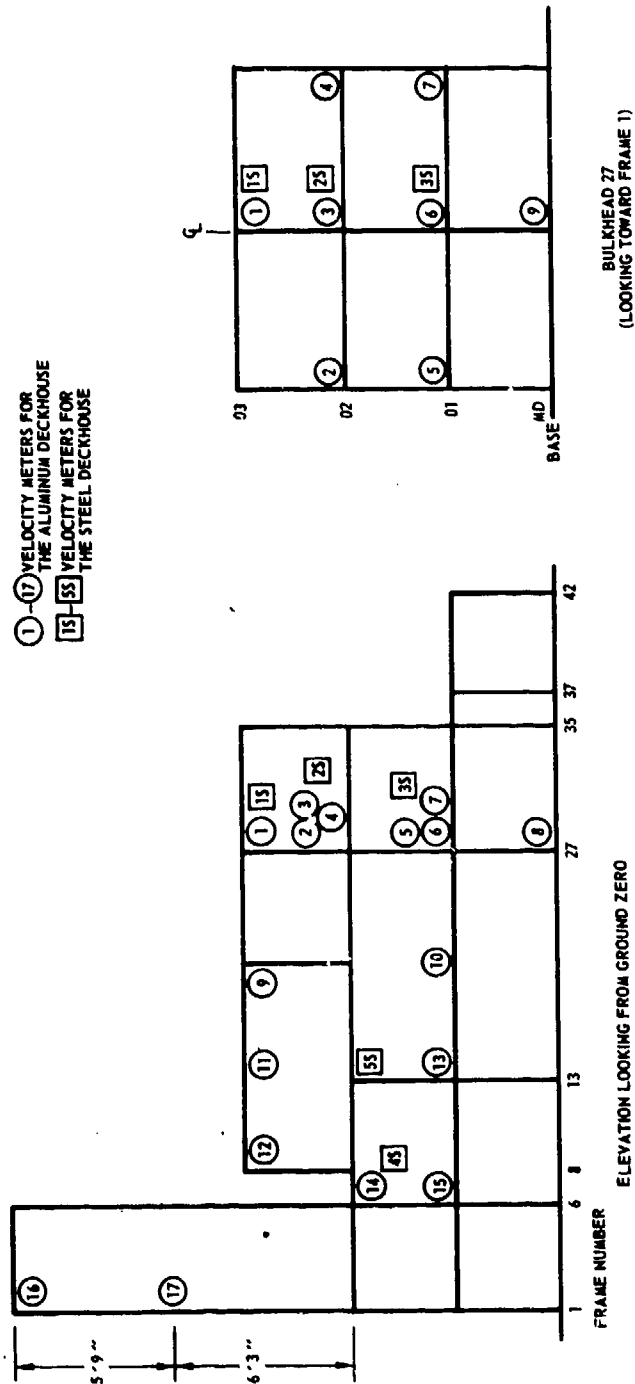
Figure 5 (U)   Velocity meter gage positions on the NCRE deckhouses for Event DIAL PACK (U).

71

(U) <u>Whip Antennas</u> - Three strain gage channels per antenna were used to measure structural response of the NSRDC whips. Gage positions are as in Figures 6 and 7.

(U) <u>Wire Rope Antennas</u> - One load cell per antenna was used to measure tension in the antenna due to the blast loading. Gage positions are shown in Figure 8.

(U) <u>AN/SPS-10E Reflector</u> - Two accelerometers were used to measure motion of the suspended antenna reflector. Gage positions are shown in Figure 9.

(U) Three tape recorders and associated signal conditioning equipment were located in the NSRDC concrete bunker inside the instrumentation trailer. With 38 data channels, one det zero (time of detonation) channel, and three time code channels (one per recorder), the total instrumentation effort was 42 channels.

<u>PHOTOGRAPHY</u>

(U) Six high-speed cameras running at approximately 1000 frames per second were used for photographic coverage during the test. These cameras were enclosed in blast resistant housings attached to wooden poles averaging about 4 feet high. Five of these cameras were positioned to record the response motions of the targets. One high speed camera was located at a range of approximately 1250 ft looking toward GZ to photograph the entire NSRDC sector and the fireball. A timing signal at Z-1-1/2 seconds remotely started the cameras which ran for approximately 4-1/2 seconds stopping at Z + 3 seconds. The photographic coverage also included over 200 still photos taken both pre-and postshot.

72
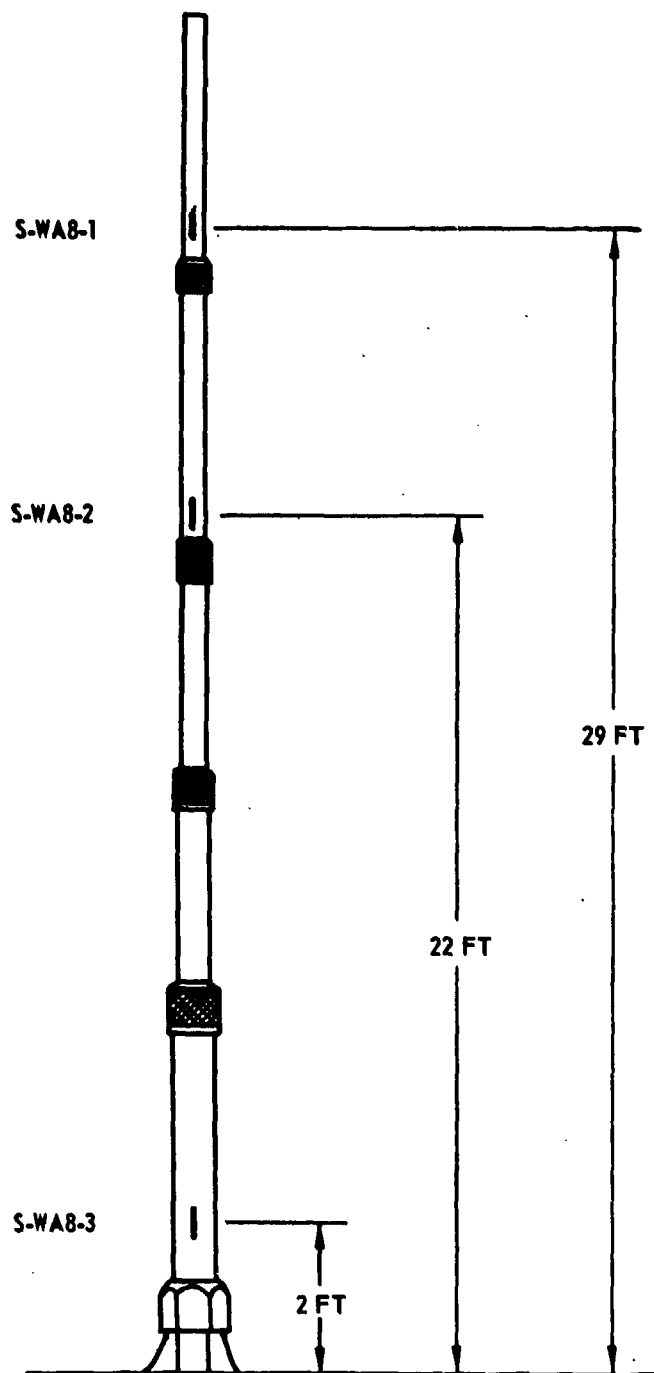
Figure 6 (U)   Strain gage locations, aluminum whip antenna (NT 66047), 8-psi range (U).

73

S-WF8-1 OR
S-WF5-1

S-WF8-2 OR
S-WF5-2

32 FT

24 FT

S-WF8-3 OR
S-WF5-3

2 FT
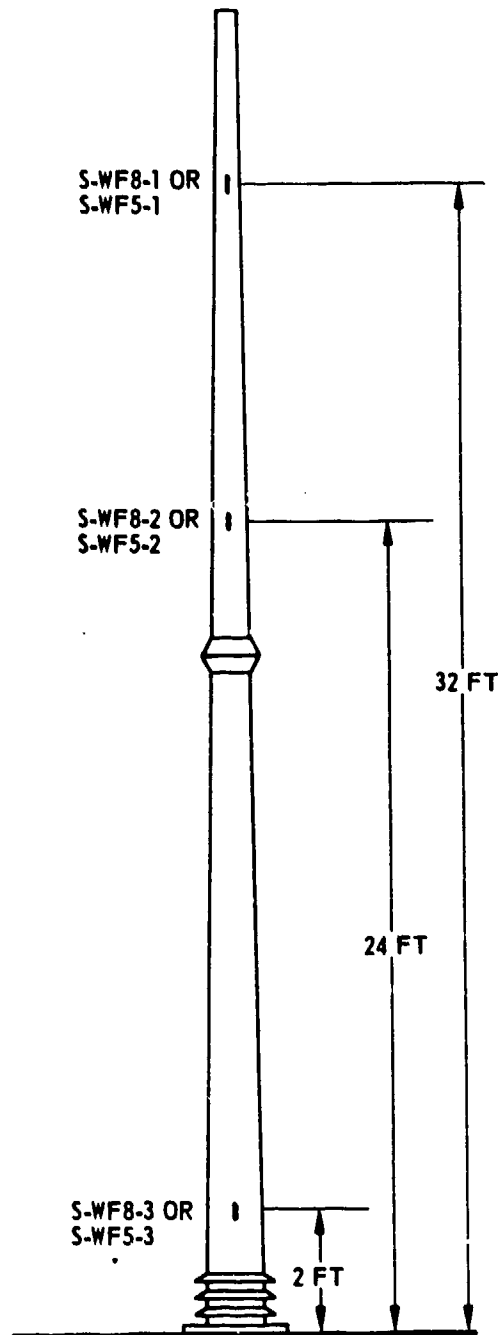
Figure 7 (U)   Strain gage locations, glass-reinforced plastic whip
antenna (AT 1022), 8- and 15-psi ranges (U).

74
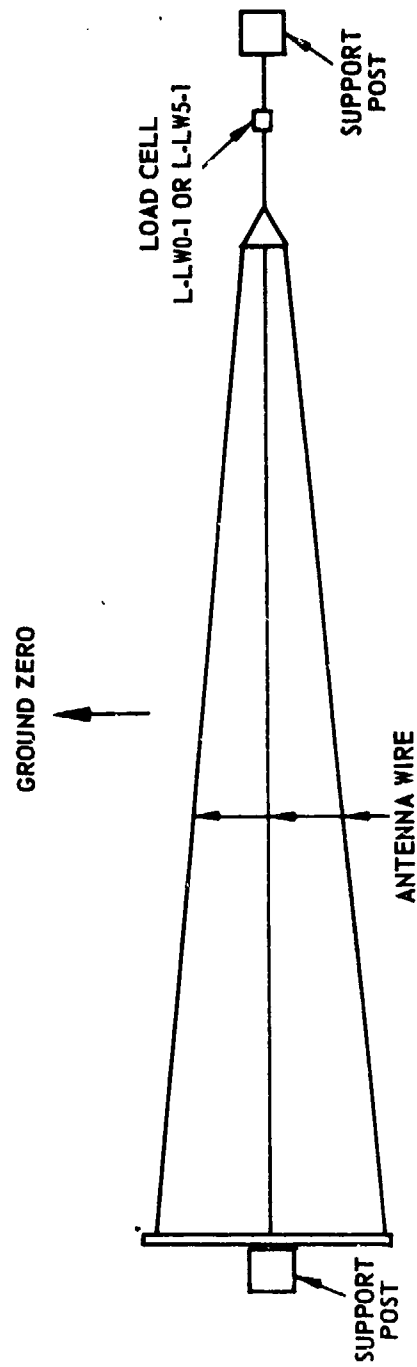
Figure 8 (U) Wire rope antenna installation (plan view), 8- and 15psi ranges (U).

Figure 9 (U)   AN/SPS-10E radar antenna, reflector truss (U).

RESULTS

Transducer Instrumentation

(U) All 42 data channels were successfully recorded with signals comparable to the calibration steps recorded before the shot. No channels were over-loaded and no extremely low level signals were received. Noise on all channels was within expected tolerances. One strain gage channel ceased recording 500 msec after the initial gage response but did post-calibrate adequately. The significant p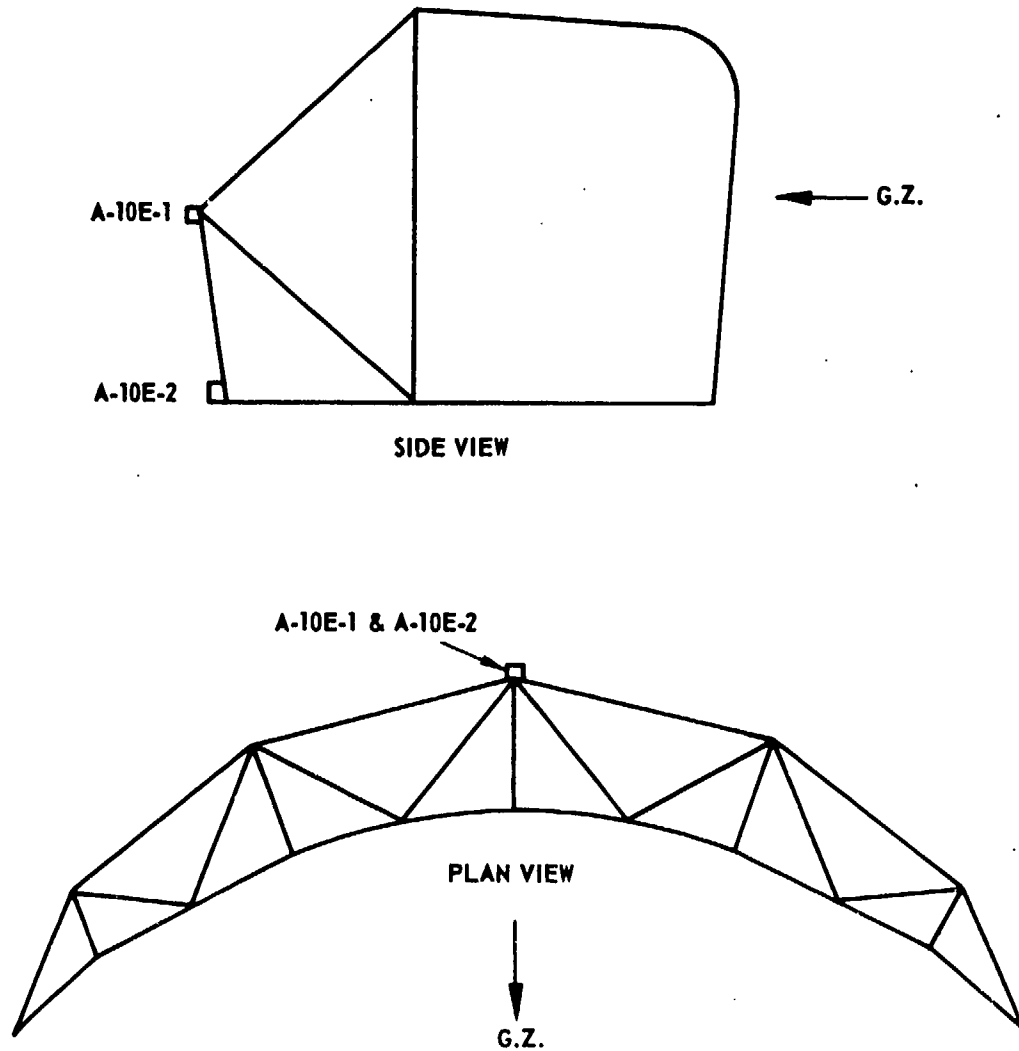art of this record was obtained in the first 300 msec. At Z + 5.448 seconds, a momentary power failure occurred in the instrumentation trailer. Recorders were immediately restarted manually and recording of the post-calibrations was completed. All significant data was obtained before power was lost and therefore the power failure was of no consequence to the success of the recording effort.

(U) Seventeen velocity meters were installed in the aluminum deckhouse to monitor air blast induced shock. Five velocity meters were installed in the steel deckhouse. All meters were epoxied in place. Eighteen of the twenty-two velocity meters dislodged from the deck at different points in time following the arrival of the blast. These times were determined by studying the processed digital record and noting the time at which the velocity meter ceased picking up high frequency structural vibrations. All records are valid for the initial peak velocity and a great majority remained intact for enough time to obtain the maximum displacement. Hence, much useful data was obtained before the separation occurred between the velocity meter and deck plating.

77

(U) Peak values of velocity from the NCRE deckhouses are presented in Tables 1 and 2. The values generally represent the magnitude of the first significant peak in the record. However, selection of a single peak from an oscillating record is subjective. Due to the large quantity of data obtained, it is not practical to present plots from all transducers. All plots are, however, available at NSRDC. A sample uncorrected velocity record is presented in Figure 10. A sample corrected velocity record is shown in Figure 11. Peak displacements obtained from numerically integrating the velocity records are presented in Tables 1 and 2. A sample plot of displacement from a velocity meter record is presented in Figure 12.

(C) Peak values of strain on the whip antennas are presented in Table 3. A sample strain record is shown in Figure 13.

(C) A sample acceleration record from the radar antenna reflector is shown in Figure 14. Peak values are presented in Table 4. The records were integrated twice to obtain velocity and displacement as a function of time. A sample velocity and displacement record, respectively, is shown in Figures 15 and 16.

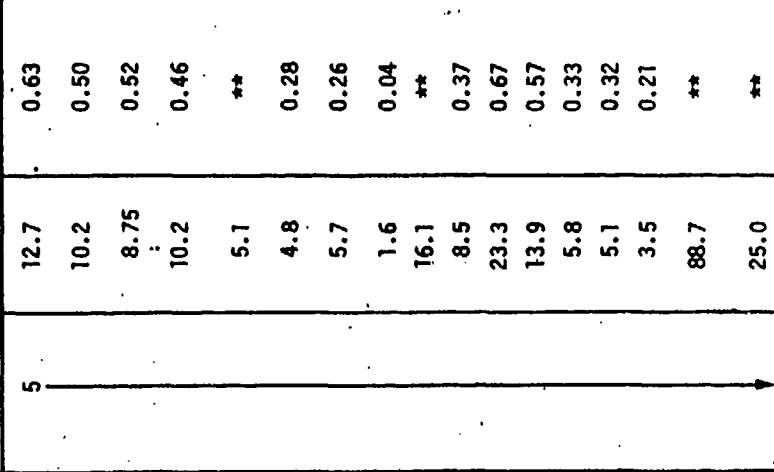(C) Peak forces measured in the wire rope antennas are given in Table 5. A sample record is shown in Figure 17.

(U) Peak overpressures are presented in Table 6. Figures 18, 19 and 20 present the free field overpressure records.

Photography

(U) All six high speed cameras started and ran during the test as planned. All film was processed and exposure was found to be acceptable.

Table 1 (U)   Aluminum deckhouse velocity meter results   (U).

Transducer Number	Transducer Location			Reference Figure No.	Peak Velocity ft/sec	Peak* Displacement in.
	Deck Level	Frame	Transverse Position			
V-AL- 1	03	27	Centerline	5	12.7	0.63
- 2	02	27	6 in. from Blast Side		10.2	0.50
- 3	02	27	Centerline		8.75	0.52
- 4	02	27	6 in. from Lee-ward Side		10.2	0.46
- 5	01	27	6 in. from Blast Side		5.1	**
- 6	01	27	Centerline		4.8	0.28
- 7	01	27	6 in. from Lee-ward Side		5.7	0.26
- 8	Base	27	Centerline		1.6	0.04
- 9	03	21			16.1	**
-10	01	21			8.5	0.37
-11	03	13			23.3	0.67
-12	03	8			13.9	0.57
-13	01	13			5.8	0.33
-14	02	1			5.1	0.32
-15	01	1	Centerline		3.5	0.21
-16	℄ Stack	1	12 ft above 02 Deck Level		88.7	**
-17	℄ Stack	1	6 ft 3 in. above 02 Deck Level		25.0	**

*Calculated by integrating the corrected velocity meter record.
**Not determinable from calculated displacement record.

79

Table 2 (U) Steel deckhouse velocity meter results (U).

| Transducer Number | Transducer Location | | | Reference Figure No. | Peak Velocity ft/sec | Peak Displacement in. |
	Deck Level	Frame	Transverse Position			
V-ST-1	03	27	Centerline	5 ⟶	4.5	0.27
-2	02	27	Centerline		4.4	0.26
-3	01	27	Centerline		2.1	0.17
-4	02	1	Centerline		4.4	0.30
-5	02	13	Centerline		3.8	0.13

80

Table 3 (C) A summary of strain gage data obtained during Event DIAL PACK (U).

| Gage Number	Target Structure and Gage Location	Measurement	Reference Figure No.	Peak Strain µin./in.
	Whip Antenna NT66047 8 psi range			
S-WA8-1	29 ft above base	Bending Strain	6 ⟶	4550.
S-WA8-2	22 ft above base	Bending Strain		4400.
S-WA8-3	2 ft above base	Bending Strain		3900.
	Whip Antenna AT1022/SR 8 psi range			
S-WF8-1	32 ft above base	Bending Strain	7 ⟶	1750.
S-WF8-2	24 ft above base	Bending Strain		2410.
S-WF8-3	2 ft above base	Bending Strain		2250.
	Whip Antenna AT1022/SR 15 psi range			
S-WF5-1	32 ft above base	Bending Strain	7 ⟶	3200.
S-WF5-2	24 ft above base	Bending Strain		4400.
S-WF5-3	2 ft above base	Bending Strain		4350.
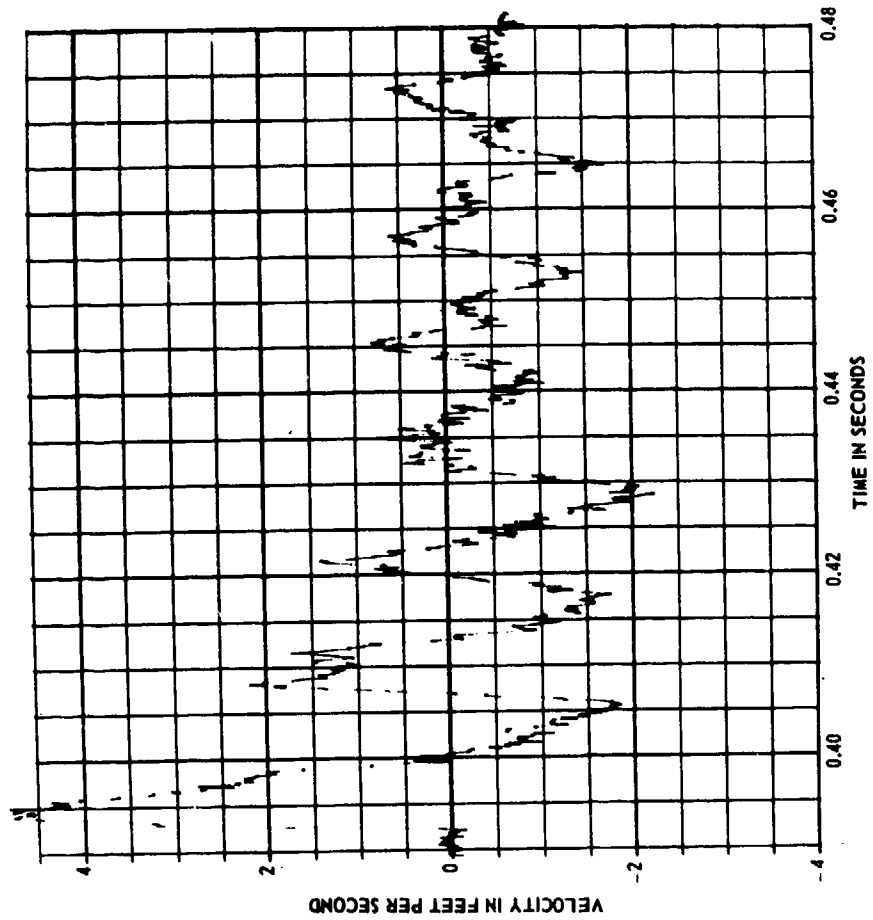
Figure 10 (U) Sample velocity meter record, uncorrected (transducer V-AL-6) (U).

82
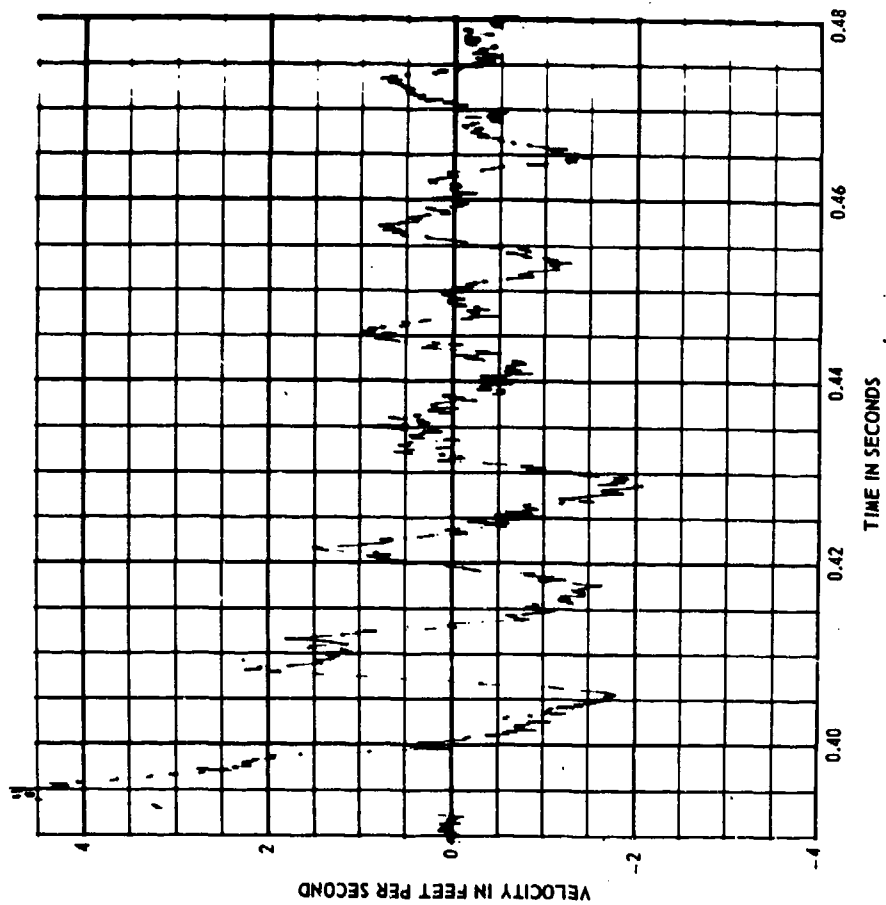
Figure 11 (U) Sample velocity meter record, corrected (transducer V-AL-6) (U).

83
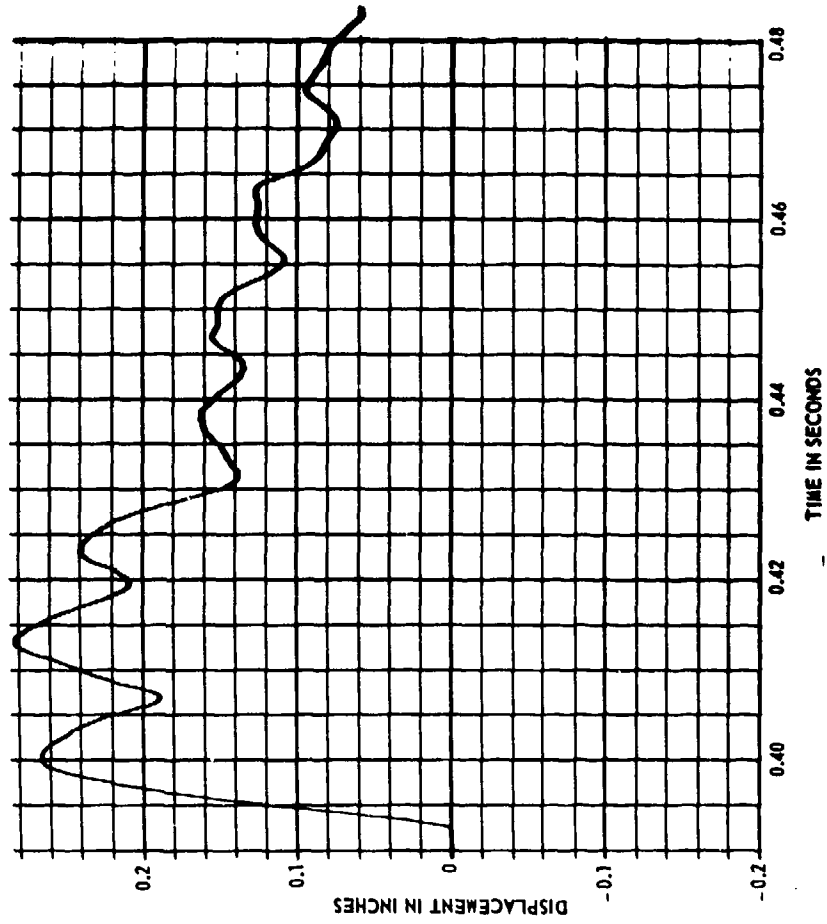
Figure 12 (U)   Sample displacement record computed from velocity meter record (transducer V–AL–6) (U).

84
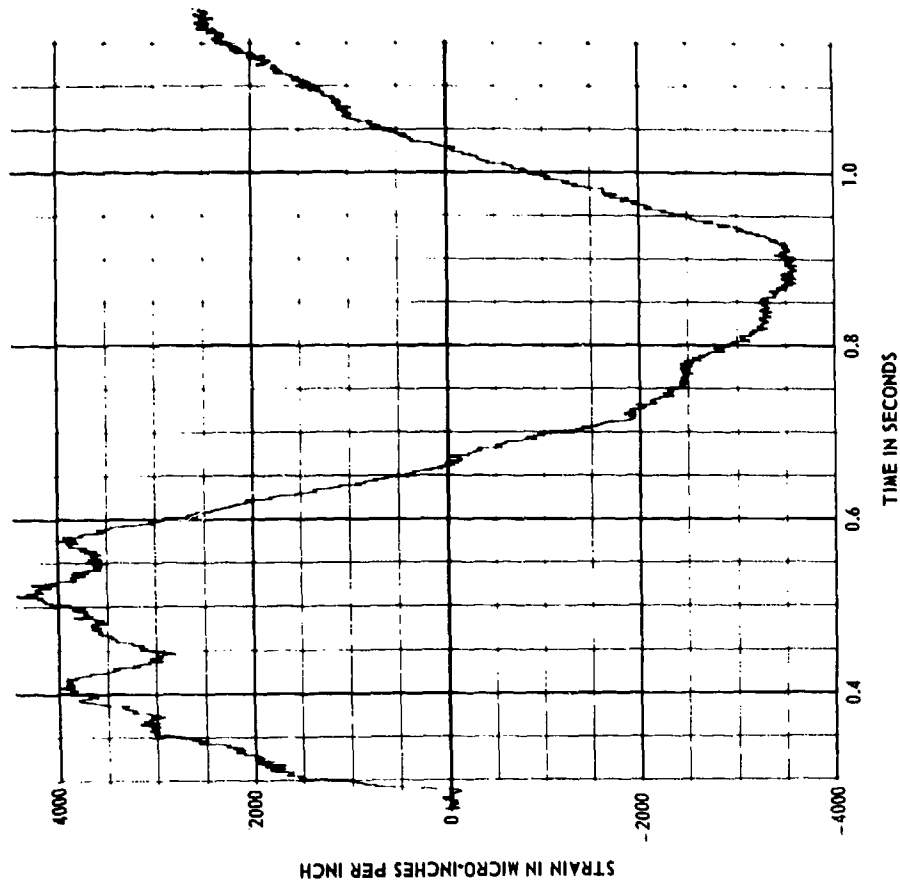
Figure 13 (C) Sample strain gage record (transducer S-WF5-3) (U).

85

Table 4 (C) Accelerometer results from the AN/SPS-10E radar antenna reflector (U).

Transducer	Location	Reference Figure No.	Peak Acceleration (g's)
A-10E-1	Top Rear Reflector Truss at Center	9	112
A-10E-2	Bottom Rear Reflector Truss at Center	9	118

Table 5 (C) Wire rope antenna load cell results (U).

Transducer	Predicted Pressure Range (psi)	Reference Figure No.	Peak Load (pounds)
L-LW0-1	10	8	3880
L-LW5-1	15	8	5000

86
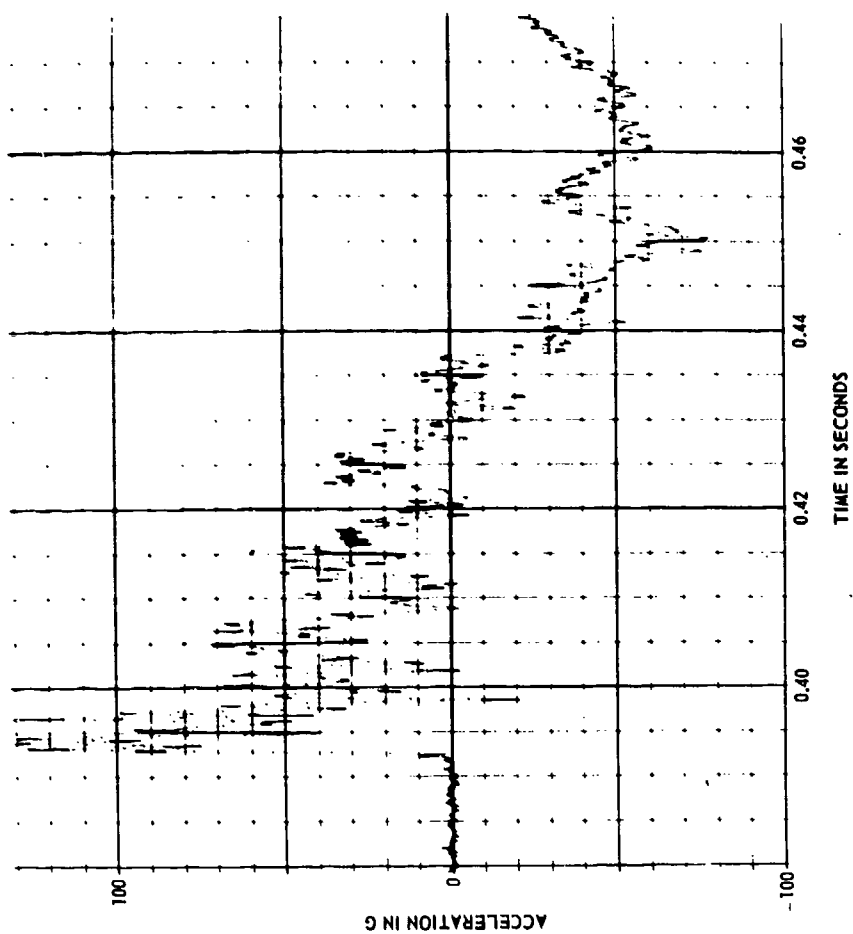
Figure 14 (C) Sample accelerometer record (transducer A–10E–1) (U).

87
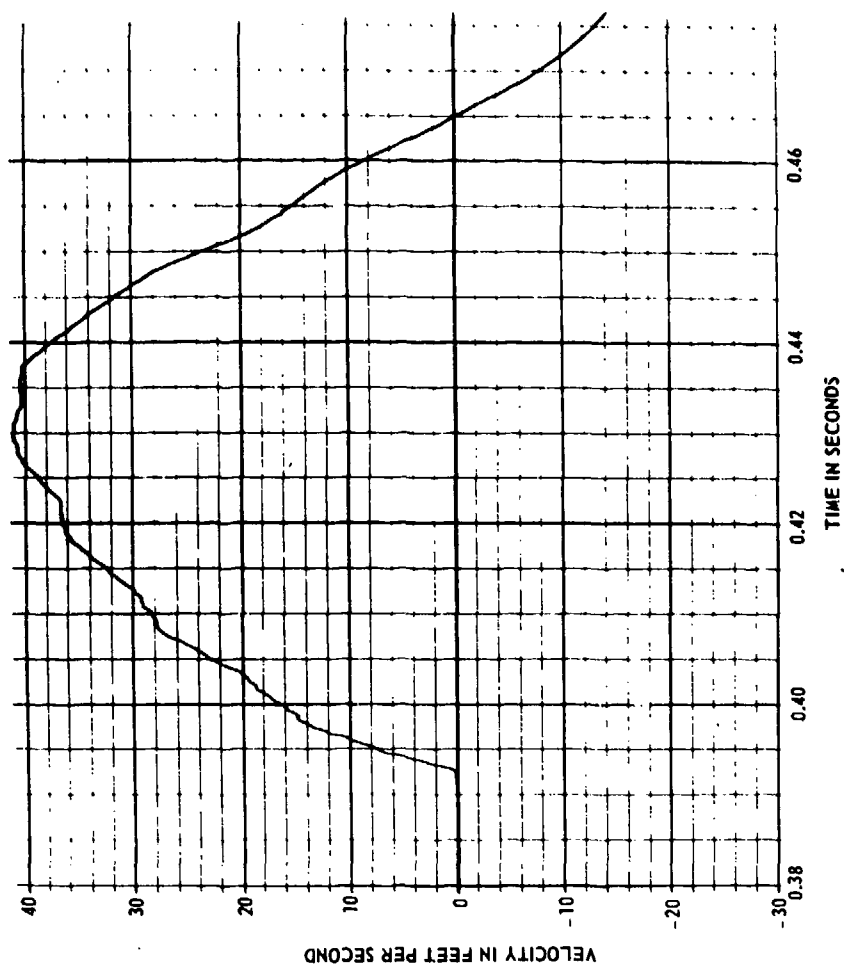
Figure 15 (C) Sample velocity record computed from acceleration record (transducer A–10E–1) (U).
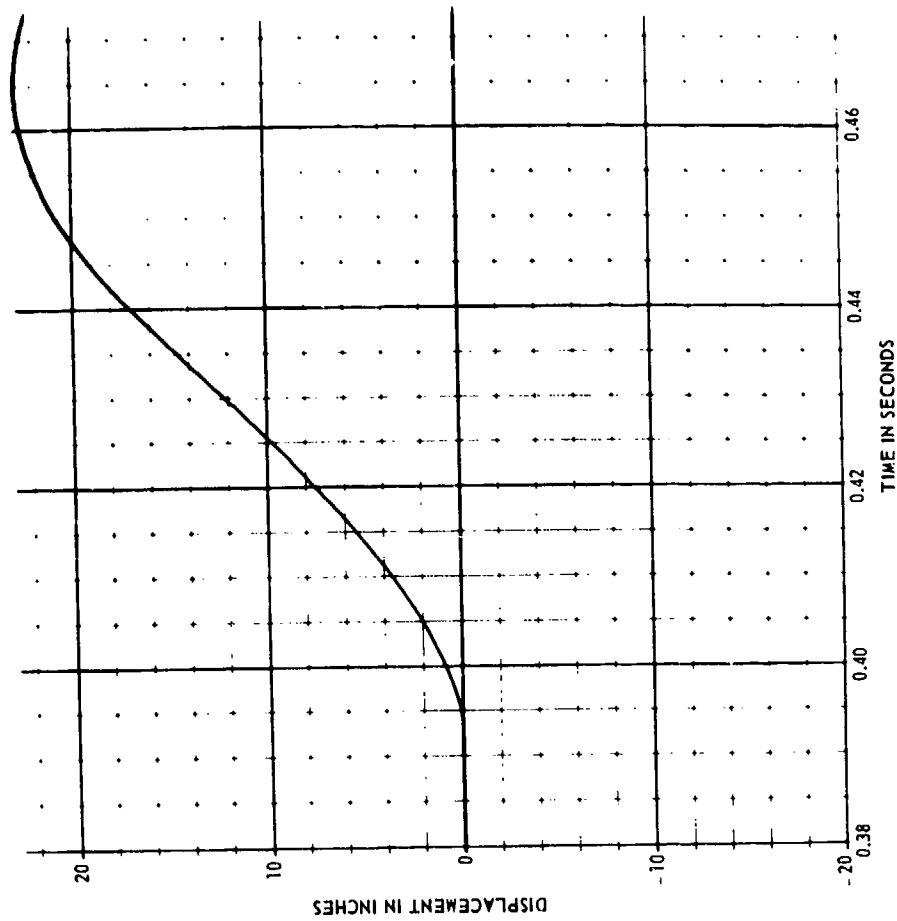
Figure 16 (C)   Sample displacement record computed from acceleration record (transducer A–10E–1) (U).

89
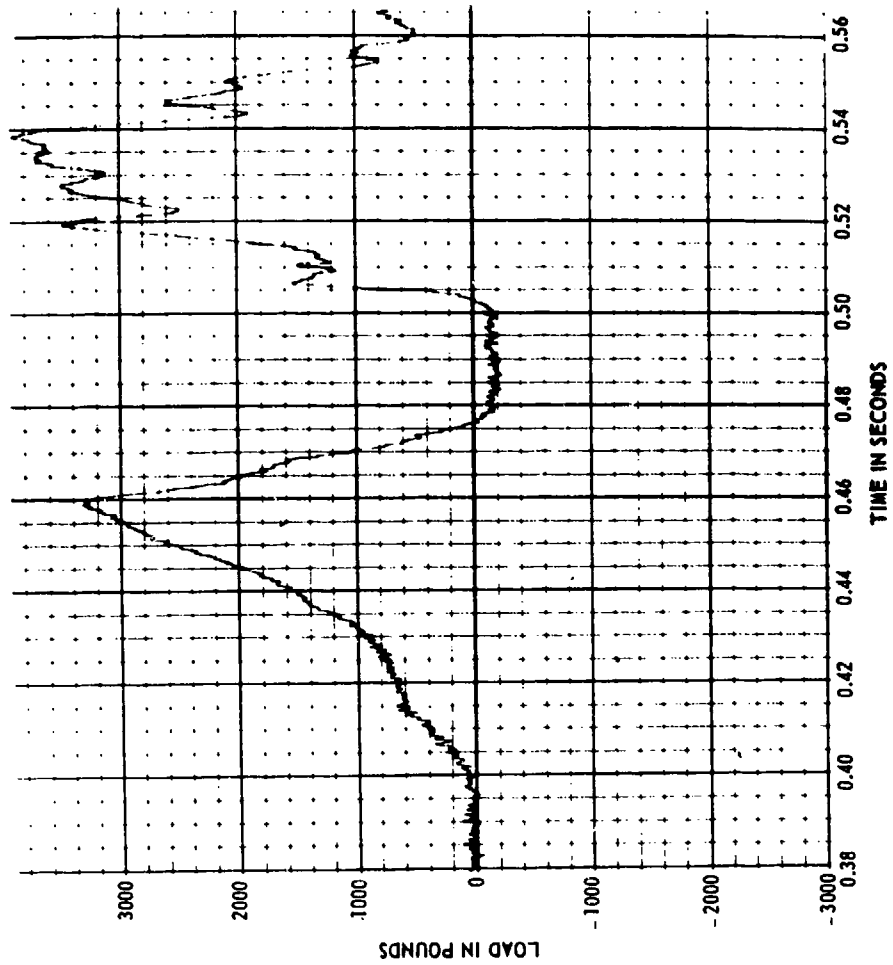
Figure 17 (C)   Sample load cell record (transducer L-LWO-01) (U)

90

Table 6 (U) A summary of pressure transducer results from Event DIAL PACK (U).

Gage	Transducer Location	Distance from G-Z (ft)	Azimuth	Predicted Peak Overpressure (psi)	Measured Peak Overpressure (psi)	Positive Phase Duration (ms)	Arrival Time (ms)	Maximum Impulse (psi-sec)
P-08-1	Wooden Pole	1110.	76°	8.0	7.70	232.	468.	0.656
P-10-1	Wooden Pole	1000.	70°	10.0	9.50	228.	392.	0.738
P-15-1	Wire Rope Antenna Pole	840.	80°	15.0	13.60	195.	285.	0.890

91
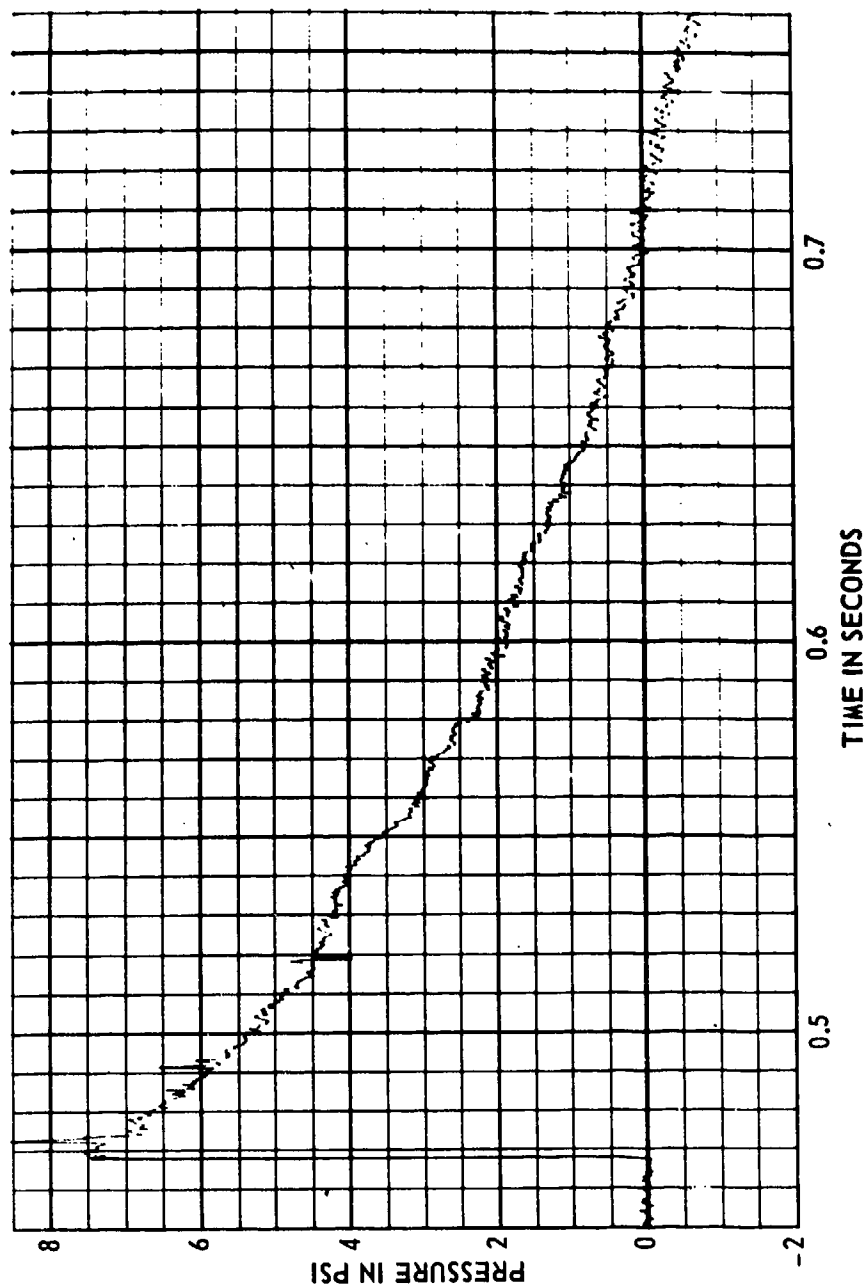
Figure 18 (U) Pressure gage record, 1110-foot range (transducer P-08-1) (U).
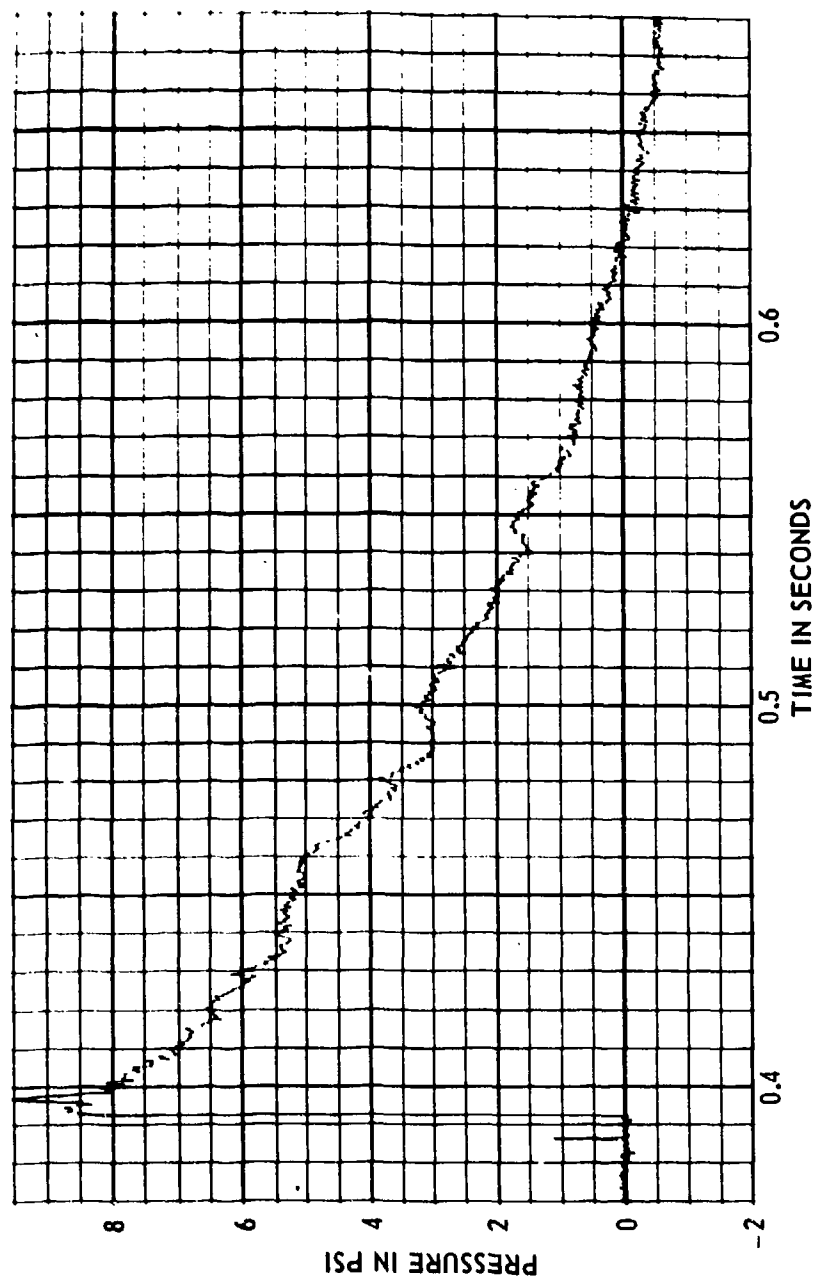
Figure 19 (U)   Pressure gage record, 1000–foot range (transducer P–10–1) (U).
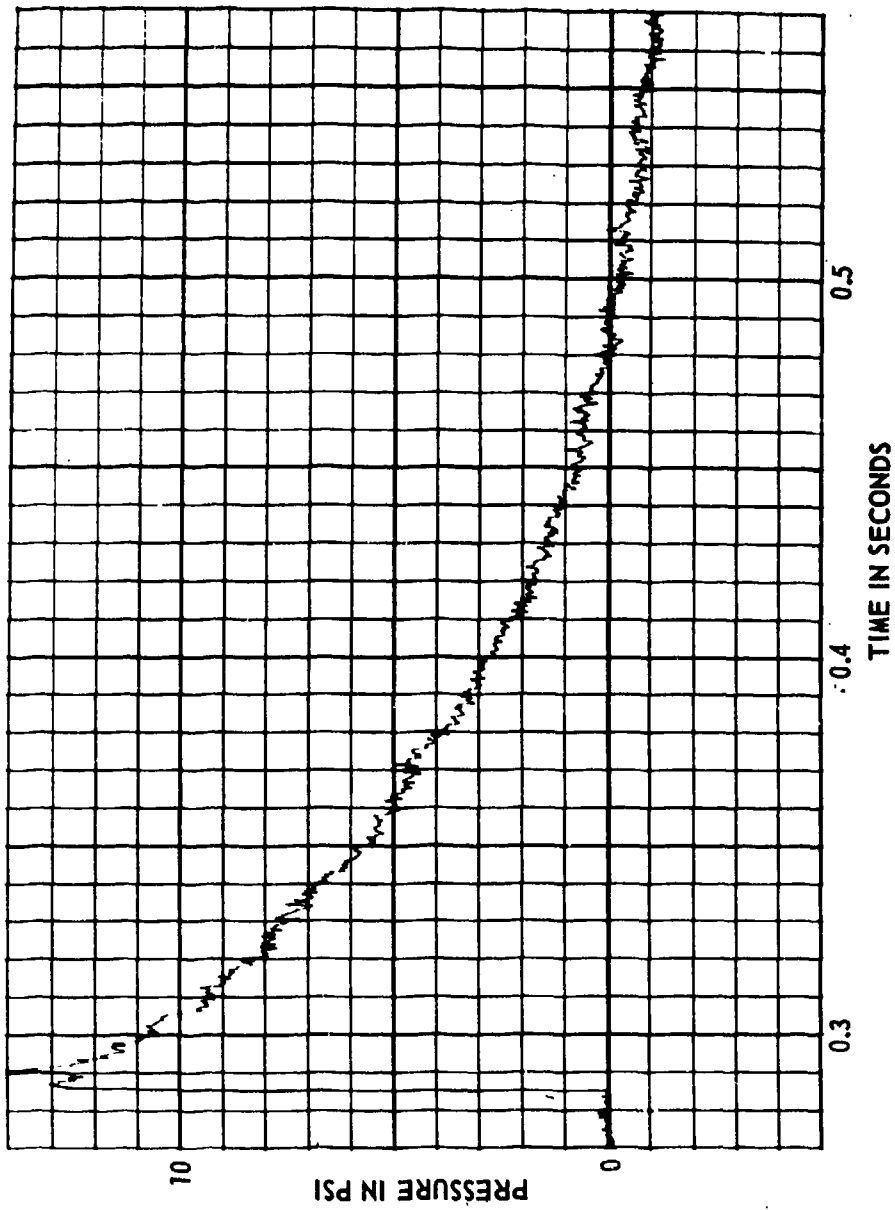
Figure 20 (U) Pressure gage record, 840-foot range (transducer P-15-1) (U).

94

The cameras covering the whip antennas and antenna reflector obtained excellent coverage of target response. The overall camera view was also good. However, the two cameras covering the wire rope antennas were hit by debris during the initial target response. The camera at the 15 psi range was partially tilted downwards and complete target response was not obtained. Some significant data was obtained, however, in this condition. The camera at the 10 psi range rendered some useful data also, but, due to its close proximity with the ground surface, dust obstructed the view of the complete target response. Adequate documentary movie and still photo coverage was obtained.

Damage to Target Structures

One-Third Scale Model Deckhouses

(U) No visible damage was noted on the aluminum and steel deckhouses except for a slight amount of dishing of the plating on the blast side of each deckhouse. Permanent deformations were determined by NCRE using surveying techniques and will be reported by them. NSRDC's primary interest in the deckhouses was to make measurements of air blast induced shock motion within the structures. Assessment of the damage to the deckhouses themselves will be made by NCRE.

Whip Antennas

(C) The 35 foot fiberglass antennas at predicted 8 psi and 15 psi survived the blast with no visible damage. Strain measurements indicate the antennas responses were well within the elastic range. The 35 foot aluminum antenna reached the onset of structural failure. Evidence of plastic yielding could be seen in sections fourteen feet above the base (See Figure 21). Measured

Aluminum
Whip Antenna
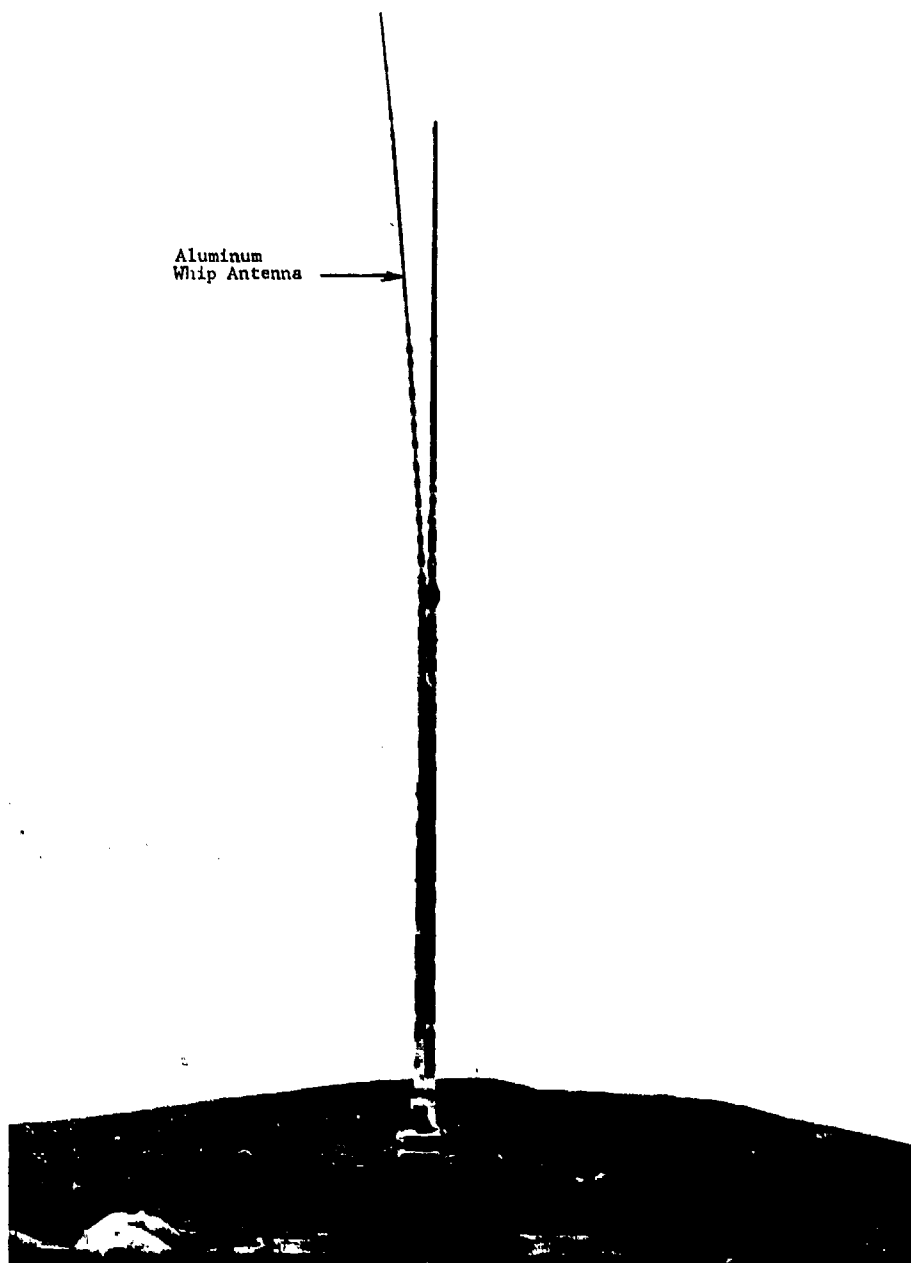
Figure 21 (C)   The 35-foot aluminum whip antenna (post shot) (U).

strains indicate the yield point of the aluminum had been reached. The antenna could still be considered operable but very close to the point of ultimate structural failure.

Wire Rope Antennas

(C) The #2-3 long wire rope antenna at predicted 10 psi suffered a slight degradation due to failure of the safety links (see Figure 22). This condition would not impair the antenna electrically and therefore it would remain operable. The identical antenna at 15 psi failed catastrophically approximately 80 milliseconds after the shock wave arrived; see Figure 23. The middle wire failed in the cable composing the safety link and would have been grounded or shortened out further transmissions had the antenna been operating. The vulnerability of the long wire rope antennas to a one megaton weapon has been determined by extrapolation to be between 5.0 and 7.5 psi overpressure.

AN/SPS-10-E Radar Reflector

(C) The reflector was not tested for its vulnerability to air blast but rather to obtain loading data which would be used in antenna design and analysis. The reflector was undamaged during the test.

DISCUSSION

Overpressures

(U) Free field overpressures were monitored at the three ranges at which NSRDC had test structures. As can be seen from Figures 18, 19, and 20, the pressure time histories are non-classical during the first 5-6 milliseconds.

Figure 22 (C)   The 2-3 wire rope antenna at the predicted
10-psi range (post shot) (U).
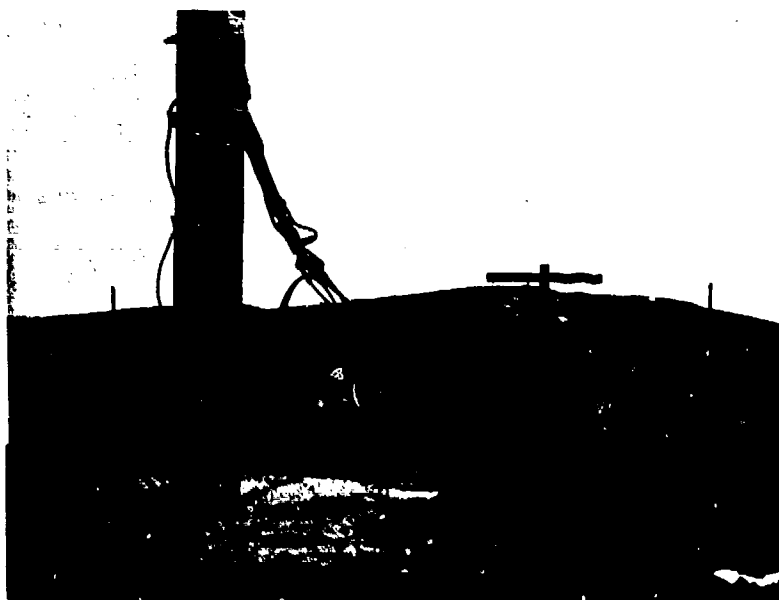
Figure 23 (C)   The 2-3 wire rope antenna at the predicted
15-psi range (post shot) (U).

98

A double peak occurred on all records indicating the presence of a multiple shock. Selection of a peak value for each overpressure range is subjective due to the fact that normally, the first peak is the greatest in magnitude. In these records the second peak is the larger of the two but dies off rather quickly to a value comparable to the first one. The peak values presented in Table 6 are the ones the author feels would be the peak overpressures for a classical shock wave of this sort. The structures tested by NSRDC were primarily drag type targets; i.e., they were much more sensitive to the dynamic pressure than the overpressure.

Significance of Data

(U) The data obtained from this test satisfied the first specific objective; that is, the magnitude and character of shock motions induced by air blast on the two NCRE deckhouses were determined. The length of record which is valid is not as long as one might wish but most records are long enough to obtain useful information concerning the magnitude and character of the shock motions.

(U) The second stated objective was met very well. Experimental structural response for the whip antennas and wire rope antenna were determined. The third objective, determining the adequacy of the design of these antennas was also met.

(U) The fourth objective, to determine the air blast loading on a radar antenna reflector, was also accomplished successfully.

CORRELATION WITH PREDICTIONS

One-Third Scale Model Deckhouse

(U) Predictions of the structural response of the aluminum and steel deckhouses to the blast were made by the use of an NSRDC computer program in which the deckhouses were modeled as multi-degree of freedom systems.

99

(U)   Output from the program included accelerations, velocities and displacements of various positions within the deckhouses.

(U)   The average measured peak velocities for the meters installed in the aluminum deckhouse were approximately 86 percent of the average predicted peak velocities. The average measured peak velocities in the steel deckhouse were approximately 36 percent of the predicted peak velocities.

(U)   The assumption that the foundations of the deckhouses were fixed; that is, would not move during the test was not verified. A velocity meter located on the base of the aluminum deckhouse indicated a peak horizontal velocity of 1.65 feet/second.,

(U)   The data obtained during Event DIAL PACK on the NCRE deckhouses is currently being analyzed and compared with the theoretical predictions of the deckhouse response.

Whip Antennas

(C) Predictions of the maximum strain for the GRP whip antenna at the 8 psi predicted range, after being adjusted for the measured 7.7 psi, are an average of about 10 percent lower than the measured peak strains. At the 15 psi predicted range, after being adjusted for the measured 13.6 psi, the predicted strains for the GRP whip are approximately 20 percent higher than the measured values. In the high speed movies, the 8 psi GRP antenna is seen to deflect horizontally 9.2 feet as compared to the predicted 8.1 feet. The 15 psi whip was predicted to deflect 17.9 feet; the measured-deflection obtained in the movie was 16.7 feet. Strain records indicate natural frequencies in the fundamental and higher modes which correlate very well with predicted modal frequencies. Peak measured strains indicate that the antenna material remained well within the acceptable stress levels.

(C) The 8 psi (predicted) aluminum whip antenna was predicted to go into the plastic range and fail. Records indicate yield strains occurred where expected. Predicted natural frequencies were of the same order as those obtained from the strain records. The 8 psi aluminum antenna was predicted to deflect 16.5 feet; the measured deflection from the high speed movies was 18.7 feet. The antenna reached the onset of structural failure as can be seen from the strain records and yielding of the material.

(C) Interestingly enough, the high speed movies gave insight into the effect of higher modal frequencies which are induced in the antenna due to the blast. These higher frequencies can be seen quite readily and their effect contributed significantly in the overall response pattern.

Wire Rope Antenna

(C) Predictions of the maximum tensile load in the (predicted) end components of the wire rope antenna at the 10 psi level were approximately 13 percent higher than the peak measured load. The safety links failed as predicted.

(C) The wire rope antenna at the 15 psi (predicted) range was predicted to fail. The strain insulator in the end components was suspected to be the weakest link. The antenna did fail catastrophically after failure of the safety links but not in the expected component. The wire composing the safety link in the middle wire failed approximately 80 milliseconds after the arrival of the shock front. Unfortunately, yielding of the cross brace supporting the wire rope antenna (see Figure 24) occurred, relieving the tension in the remaining two cables and therefore relieving the tension in the end components which were suspect. The maximum tensile

Figure 24 (C)   The deformed cross brace on the 15-psi (predicted) wire rope antenna support (U).

102

force in the two remaining cables after failure of the middle one was about 5000 pounds or 2500 pounds per cable. This was not enough tension to break the strain insulator.

An/SPS-10E Radar Reflector

(C) Predictions of the maximum loading on the reflector were 35 percent lower than the value calculated from the measured accelerations. The peak loading on the antenna was calculated to be in the order of 7500 pounds (using the relationship, $force = mass \times acceleration$). Further studies will be made to refine the method of predicting the loading.

EVALUATION OF TEST PROCEDURES

(U) The procedures followed in the preparation and execution of this test were, for the most part, successful. Dislodgement of the velocity meters from their bases was the most serious problem encountered. Although the effect was undesirable, its results were not catastrophic. No failures of the transducers or recording equipment occurred. All data channels are usable and the records are considered valid within three percent. The high-speed photography was successful. All cameras ran, although two of the six were hit by debris and were tilted partially downward. However, useful data could still be obtained from the films. All data has been re-covered, put into usable form, and is currently being analyzed.

Conclusions

(U) Continued large air blast trials such as Event DIAL PACK are required. Equipment not suitable for testing in shock tubes should be tested during field trials. Many areas of air blast remain experimentally uninvestigated such as the response of aircraft carriers and associated components, not to

mention a variety of exposed shipboard equipment. Tests such as these, of course, should be paralleled by theoretical studies to determine areas where technological gaps remain and empirical data is required.

(U) The specific objectives of Event DIAL PACK Project LN113 were successfully accomplished as follows:

1. The magnitude and character of air blast induced shock motions on two 1/3 scale model deckhouses were successfully measured.

2. Structural response to air blast of two types of shipboard communications antennas were monitored.

3. The air blast vulnerability of the communications antennas tested was determined allowing evaluation of the adequacy of the present design.

4. The air blast loading on space frame type radar antenna reflector was determined by recording acceleration of the suspended reflector.

104

UNCLASSIFIED

D.J. Roddy
U.S. Geological Survey

PROJECT LN303
U.S. GEOLOGICAL SURVEY ACTIVITIES

Introduction

The 500-ton TNT Dial Pack sphere was detonated in July 1970, tangent to a ground surface underlain by poorly consolidated alluvium at the Defence Research Establishment Suffield, Alberta, Canada. The U.S. Geological Survey participated in this trial to study the structural deformation and cratering processes and make morphological and structural comparisons between this crater, earlier explosion craters, and large terrestrial and lunar impact craters. Field and laboratory studies, and high speed airblast and aerial stereographic photography were completed to assist in this study. The crater and surrounding ejecta blanket were also used as a field test site for thirteen of the astronauts as part of the U.S. Geological Survey/National Aeronautics and Space Administration Apollo training program. A brief summary is given in this paper of A) Geologic and structural studies of the Dial Pack Crater, and B) Lunar applications.

A) Geologic and Structural Studies of the Dial Pack Crater
Aerial and Ground Photography

The U.S. Geological Survey flew oblique, stereo and high

UNCLASSIFIED

speed airblast photography using a Cessna 170 with high/low altitude capabilities. The high speed airblast photography was completed with a set of four Milliken cameras mounted on a moveable platform in the side of the aircraft (figs. 1, 2, 3). At shot time the aircraft was flown at approximately 18,000 feet in a

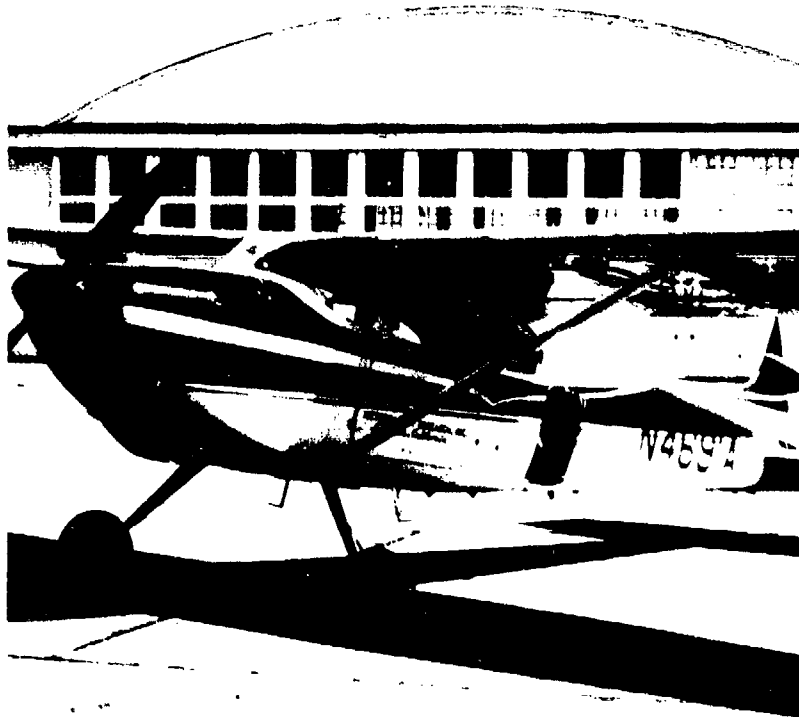Figure 1　U.S. Geological Survey Cessna 170 with four Milliken high-speed cameras mounted on moveable platform with baggage access door removed.
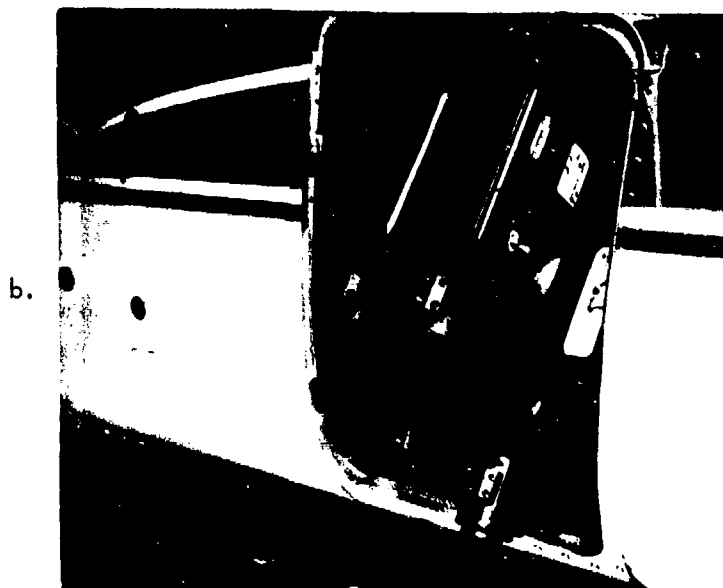
106

Figure 2   Four Milliken high-speed cameras mounted on
moveable platform in Cessna 170 with baggage
access door removed. (Platform supported by
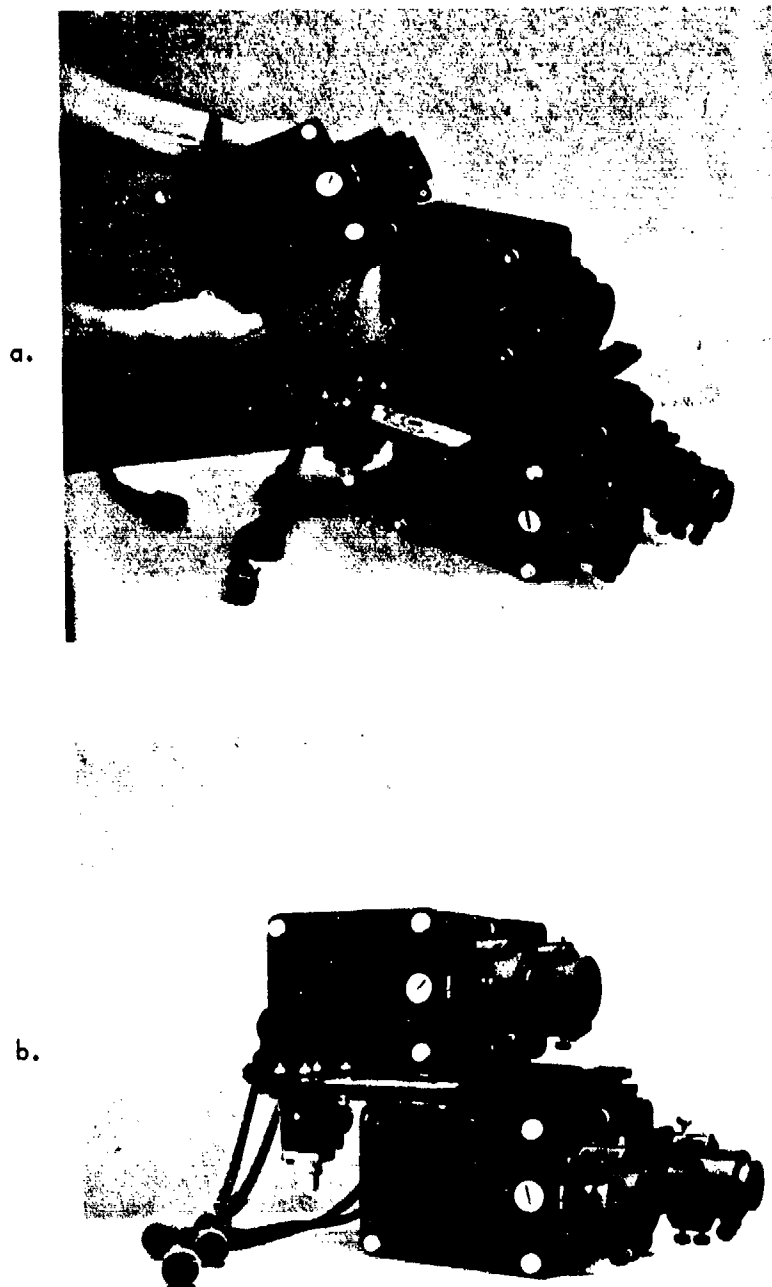free-swinging cable and aimed by operator.)

107

a.

b.

Figure 3   Four Milliken high-speed cameras on moveable platform.

circular orbit around ground zero. A predetermined bank angle was maintained during the orbiting and the cameras were continuously pointed by this writer at the explosion and expanding shock wave. The equipment configuration allowed the full 20 seconds of film time to be directed at the explosion, shock wave, and cloud rise (fig. 4); longer explosion tracking times are easily possible with this equipment mounting and flight technique.

The high speed aerial photographs of the explosion show that the major luminous jets and the minor fireball extensions developed early in the expanding fireball and continued to move outward until the fireball stopped horizontal expansion. The dust jets also developed early in the explosion and moved outward behind the expanding air shock wave. The outward movement of these two types of jets was completed between 300 and 400 milliseconds after detonation.

The oblique (figs. 5a, 5b, 5c) and stereo (figs. 6a, 6b, 6c, 6d) low-altitude photography were both completed successfully. A high-resolution T-12 aerial stereo camera was used for black and white and color photography at several different altitudes that ranged from 2500 feet down to 150 feet. The aerial photography was taken periodically during each day through a range of sun angles from one hour after shot time to three days later to insure adequate definition of the ejecta and to observe crater modifications. Resolution is extremely good, allowing particles as small as one inch across to be identified in the low-altitude flights (fig. 6c, 6d).

109
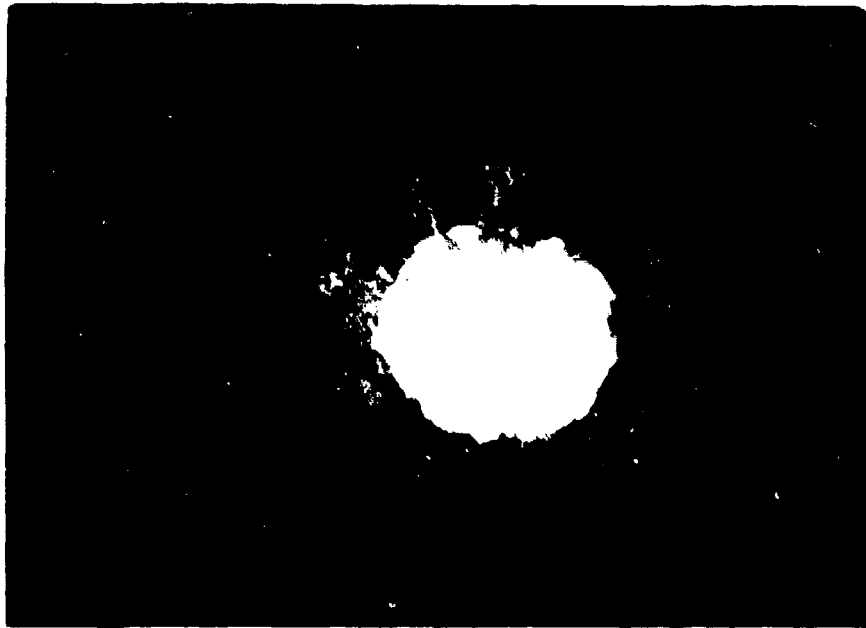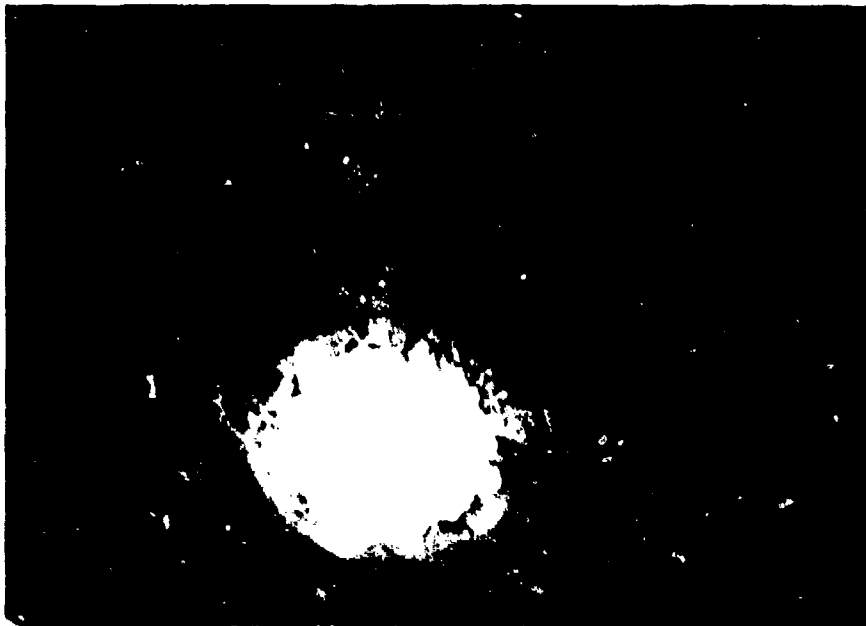
a. (~0.1 sec)

b. (~0.5 sec)

Figure 4   Representative high-speed frames of the explosion and cloud rise taken from orbiting U.S. Geological Survey Cessna 170 using Milliken cameras mounted on moveable platform. (Approximate frame times after detonation are noted under photographs.)

110

d. (~20 sec)

c. (~2 sec)

N
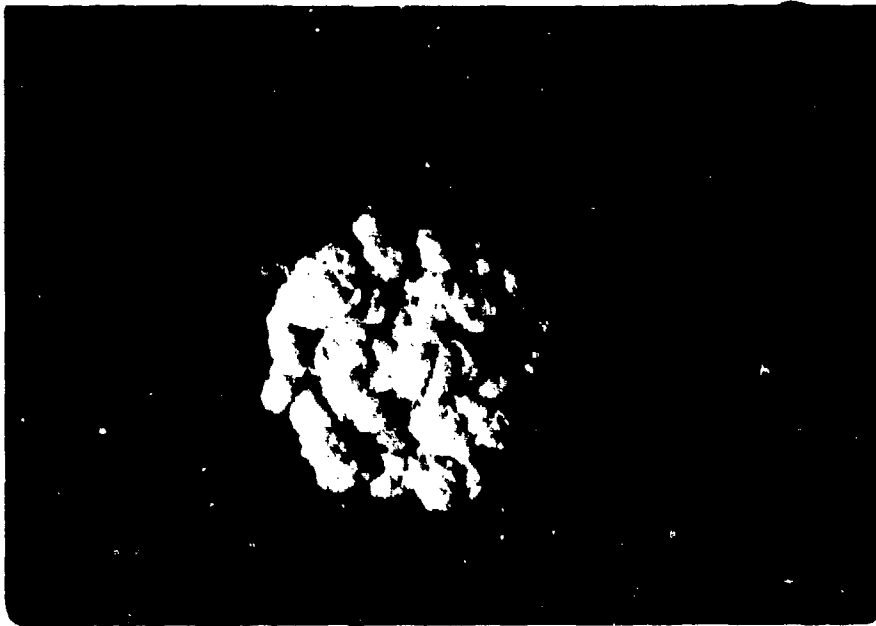
Figure 4   Representative high-speed frames of the explosion and cloud rise taken from orbiting U.S. Geological Survey Cessna 170 using Milliken cameras mounted on moveable platform. (Approximate frame times after detonation are noted under photographs.) (continued)

Figure 5a Aerial oblique photograph by USAF(AAVS), Norton AFB, California of DIAL PACK crater about 30 minutes after detonation. (Water beginning to flow from fractures in central uplift. Dark patches on crater rim are wet clay blocks from deepest alluvium cratered. Note Apollo astronauts in crater.)

112

b.

c.
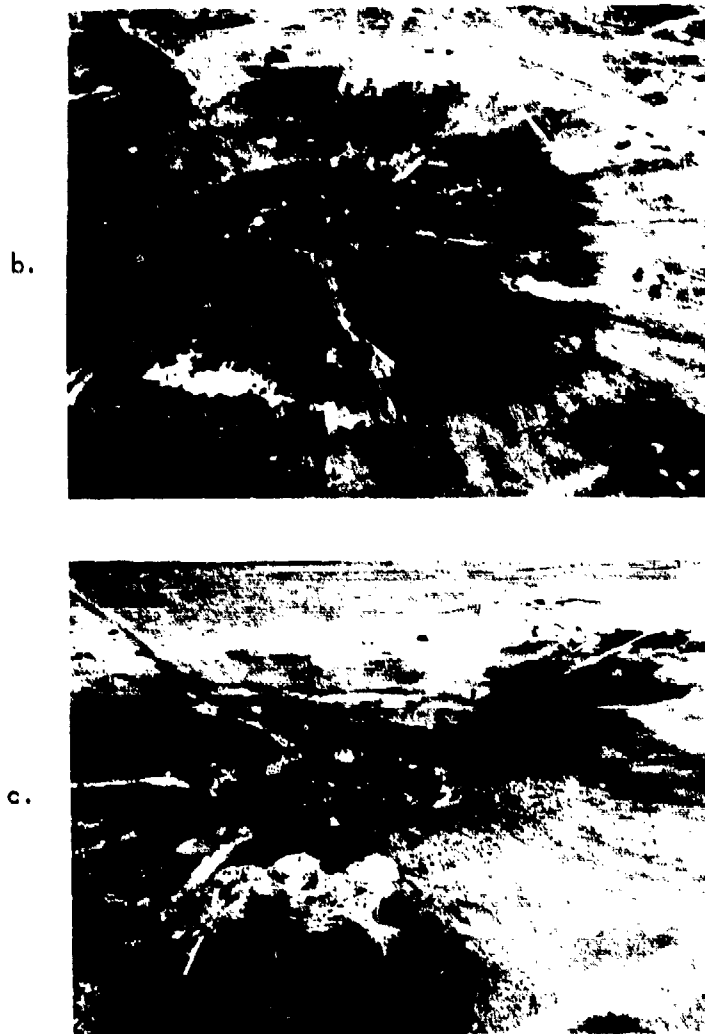
Figure 5b,c   Aerial oblique photograph by U.S. Geological Survey of DIAL
PACK crater two days after detonation. (Central uplift and radial
ridges on crater floor are surrounded by lake that formed from
water flow from fractures in crater floor. White patches on crater
walls are deformed alluvium exposed by slump of fallback. Blocky
unit surrounding crater is mainly deeper clay beds that broke up
during overturning of flap. Very bright, long, irregular patches
in outer rim are water and deposits of alluvium brought to surface
by water along fracture. Excavations were completed in outer rim
to recover buried equipment.)
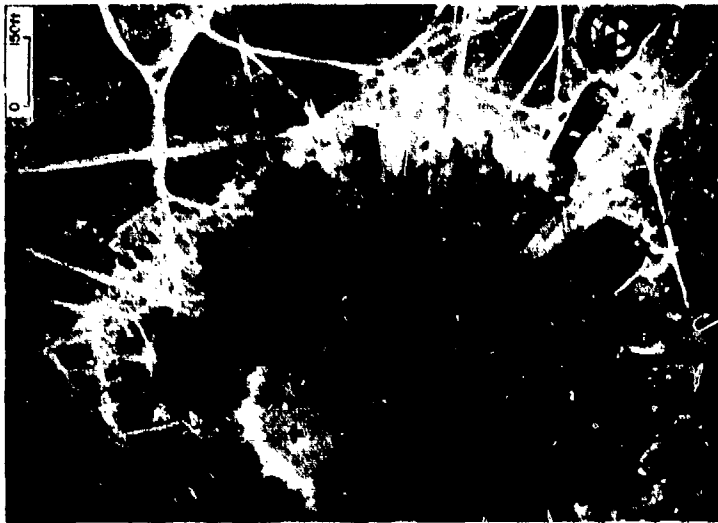
Figure 6a, b U.S. Geological Survey aerial stereophotographic pair of DIAL PACK crater taken 1.75 hours after detonation. (Difference in contrast between 6a and 6b is due to reflectivity change caused by slightly different sun angles. Central uplift and radial ridges on crater floor are surrounded by lake that formed from water flow from fractures in crater floor. White patches on crater walls are deformed alluvium exposed by slump of fallback. Blocky unit surrounding crater is mainly deeper clay beds that broke up during overturning of flap. Long, irregular darker to very bright patches in outer rim are water and deposits of alluvium brought to surface by water along fractures. See Figure 9 for description of units in overturned flap and locations of major topographic features.)
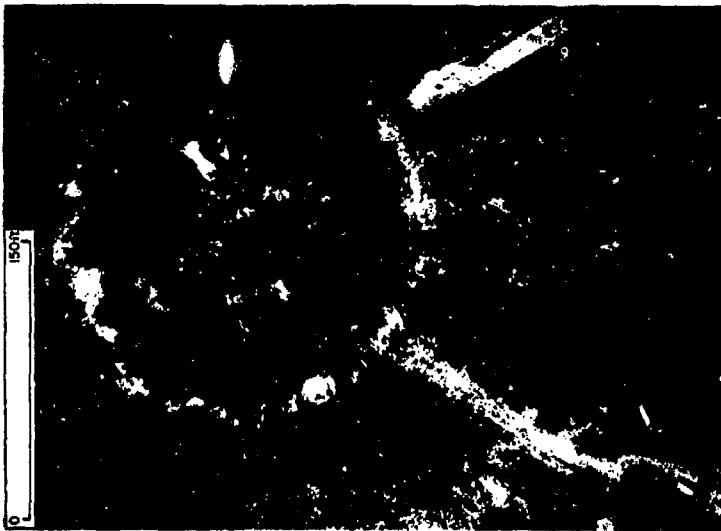
Figure 6c, d   U.S. Geological Survey aerial stereophotographic pair of DIAL PACK crater taken two days after detonation. (High-resolution flight pass at 150-foot altitude. Note central uplift, radial and concentric ridges on crater floor, and blocky overturned flap. Carbon-coating removed by walking on path in lower left corner of Figure 6c.)

Figure 6e   U.S. Geological Survey aerial stereophotograph of DIAL
PACK crater 2 days after detonation. (Representative high-
resolution photograph (flight altitude 150 feet) of car and
tree blast debris west of crater. White trailer and near-by
sedan were not present at detonation time. White concrete
crosses are 250 feet apart.)

116

Pre- and post-shot aerial mosaics have been completed at different scales using the aerial photography and a detailed topographic map (fig. 7) has been made by the Geological Survey, Flagstaff, Arizona, for the Waterways Experiment Station (LN301). The topographic map was completed at a scale of 1:500 with a contour interval of one foot and is being used by LN301 for crater volume and ejecta studies and by LN303 as the base for the geologic and structural maps.

Over fifteen hundred 35 mm and 4 x 5 documentary photographs were completed of the crater, its ejecta, and the crater excavations and are available in the U. S. Geological Survey files at Flagstaff, Arizona. These photographs are being used in preparing the geologic map and describing the details of the ground deformation exposed during different stages of the excavations.

Crater Morphology and Structure

Detonation of the Dial Pack sphere formed a broad, flat crater with a central uplift, radial and concentric ridges in the crater floor formed by uplifted folds, an inward-dipping faulted and folded rim, a large overturned flap overlying the rim, and surrounding discontinuous ejecta overlying a scorched prairie surface (figs. 8a, 8b, 8c, 8d, 8e). Geologic studies have shown that the crater is very similar in morphology and structure to the Prairie Flat crater (Roddy, 1969, 1970a) and to many large terrestrial and lunar craters which have been attributed to the

117
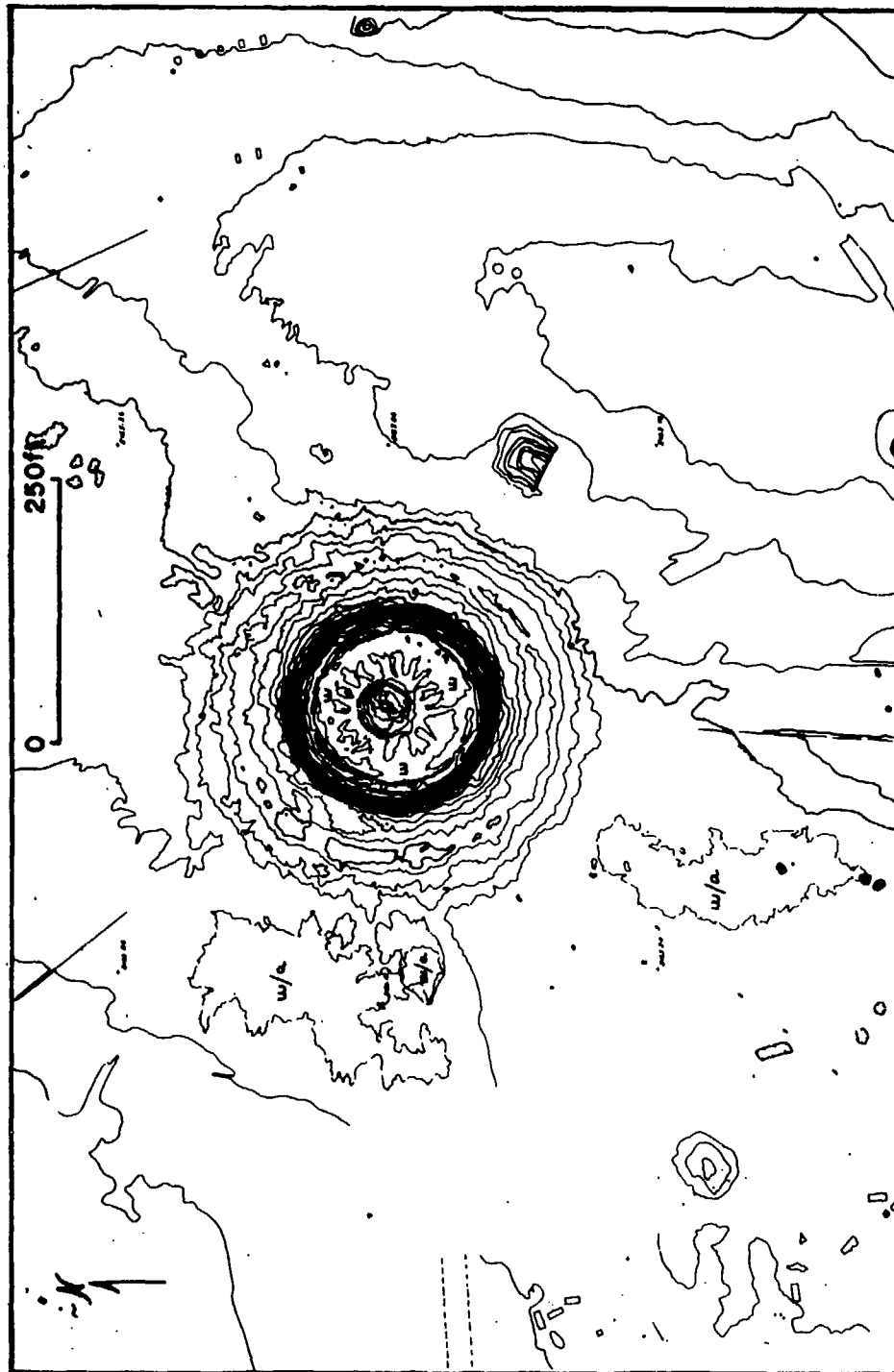
Figure 7 Topographic map of the DIAL PACK crater completed by the U.S. Geological Survey. (Contour interval is 1 foot. Symbol w/a indicates area of water/alluvium deposition from rim fracture; w indicates lake in crater.)

Figure 8a   Central uplift, radial ridges, and lake in DIAL PACK crater 1 day
             after detonation. (Central uplift is about 50 feet across and aver-
             ages 5.5 feet in height above crater floor. White zc·· :s on crater
             wall are deformed alluvium exposed by slump of fai:.oack.)

Figure 8b   Concentric ridge, about 1 meter high, formed by ring anticline at
             base of DIAL PACK crater wall. (Cubic blocks are from breakup
             of clay beds that originally lay between 15 and 24 feet below the
             ground surface.)

Figure 8c   Cubic blocks on the southwest rim of the DIAL PACK crater are formed by the breakup of clay beds that originally lay between 15 and 24 feet below the ground surface. (Blocks form the highest unit of the overturned flap. Deformed alluvium is exposed by slump of fallback on crater wall on left side of photograph.)

120
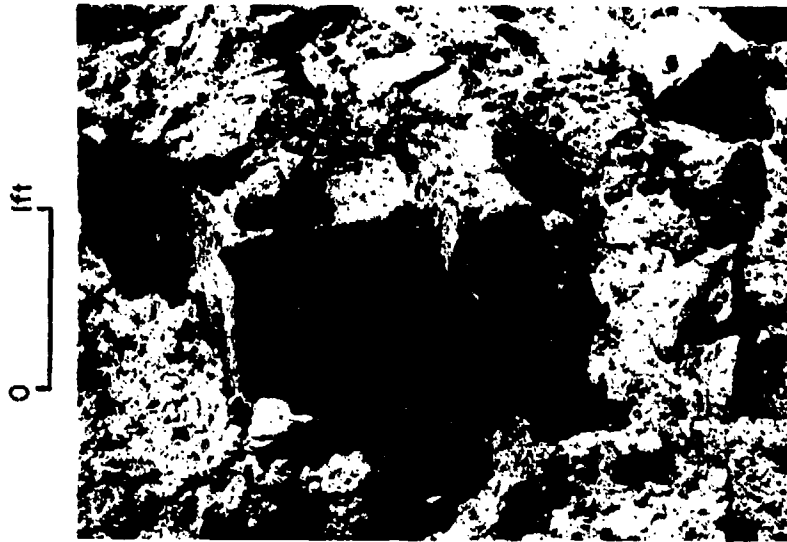
Figure 8d   Close-up view of cubic blocks of clay that formed by
             breakup of clay beds that originally lay between 15
             and 24 feet below the ground surface.

Figure 8e   Linear fracture near edge of overturned flap on west
             outer rim of DIAL PACK crater. (Light-colored
             material is fine-grained alluvium deposited by water/
             alluvial flow from fracture immediately after detonation.)

impact of comets (Roddy, 1968, 1969, 1970b). A generalized geologic map showing the distribution of major topographic features, the overturned flap and ejecta is shown in figure 9. Detailed geologic structure cross sections are shown in figures 10a, 10b, and general apparent crater dimensions are given as averaged values in the following table:

	Dial Pack Crater	Prairie Flat Crater
Diameter (rim to rim)	280 ft. (85.5 m)	270 ft. (82.5 m)
Diameter (ground level)	200 ft. (61 m)	210 ft. (64 m)
Depth (rim)	16 ft. (4.9 m)	15 ft. (4.6 m)
Depth (ground level)	12 ft. (3.7 m)	12 ft. (3.7 m)

Structural deformation in the central part of the crater consists of a low dome covered by large clay blocks of fallback (fig. 8a). The dome, about 50 feet across and averaging 5.5 feet in height, was formed by interbedded sand, silt and clay units uplifted 12 to 15 feet. Radial ridges and troughs extend out from the flanks of the central uplift and are formed by anticlinal (up) and synclinal (down) folds. An inner, discontinuous, concentric ring anticline locally forms a ridge beyond the radial ridges. Immediately beyond this inner ring lies a continuous ring anticline which forms a very prominent ridge at the base of the crater walls (fig. 8b). Excavations show both these rings are formed by anticlinal folding and uplift of a blue clay that originally lay at a depth of 24 to 26 feet below the ground surface (fig. 10a, 10b).

LEGEND

ob Overturned flap of carbon-coated, blocky clay fragments and fine-grained alluvium derived from 15 to 24 feet below ground surface. Wet, blocky clay locally dominant nearest crater. Very thin cover of carbon-coated fallout with fused alluvium and scattered high-angle ejecta.

oh Overturned flap with hummocky terrain of carbon-coated fine-grained fragments of alluvium derived from 5 to 15 feet below ground surface. Outer edge of unit is extensively fragmented and irregular and consists of blocky silty alluvium derived from upper 5 feet of soil. Very thin to discontinuous cover of carbon-coated fallout with fused alluvium and scattered high-angle ejecta.

de Discontinuous, carbon-coated ejecta, scattered, fragmented outer edge of overturned flap and fallout lying on carbon-coated, scorched prairie surface. Fine-grained alluvium from the turbulent dust jets locally forms thin, irregular carbon-coated ray deposits.

Al Alluvium, prairie surface with thin cover of range grass.

— · — Contact, gradational between units.

▓▓▓▓ Crater wall.

— · · — Local topographic ridge.

· · · · · Outer boundary of central uplift.

〜〜〜 Location of fracture in rim.

+ Ground zero.

Figure 9   Generalized geologic map of the DIAL PACK crater showing the distribution of the main units in the overturned flap and the locations of the major topographic features. (Photographic base is from aerial stereographic photograph taken 1 hour after detonation.)

Figure 10a, b   Generalized structure cross sections of the DIAL PACK crater. (Blue clay, raised 12 to 15 feet, forms central uplift and ridges on the crater floor. Blocky clay in overturned flap seen in Figure 8 is derived from breakup of thin clay beds that lay above the blue clay. Overturned flap overlies inward dipping inner rim.)

The result of the cratering processes was to crater to a depth of about 20 to 22 feet and complexly fold and raise lower units 10 to 15 feet. The entire crater floor is underlain by units that have moved, during the last sta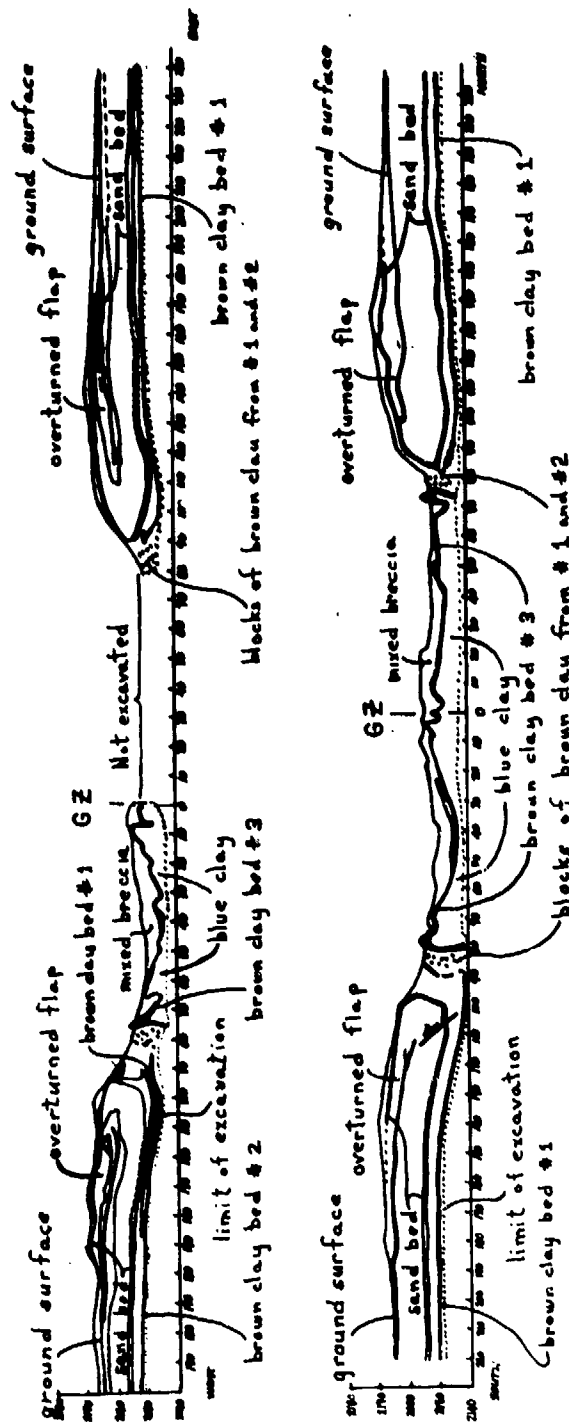ges of cratering, inward and upward; outward movement occurred locally on the anticlinal crests. Consequently, the topography observed on the crater floor is a prominent reflection of buried folds and uplift and is not merely a fallback pattern.

A thin veneer of white, fractured sandstone and sand is present on the flanks of the central dome and was locally also present at Prairie Flat. Previous studies (Roddy, 1970 a). considered a deep origin for this sand, but more recent excavations and field work by the writer at Prairie Flat and in this study show the sands are derived from a thin, lenticular sand that was initially about 20 feet below the ground surface.

Deformation in the rim consists of inward dipping strata overlain by a large, coherent overturned flap (fig. 10a, 10b). The inward dip, or downfold, is apparently caused by the massive inward movement of lower units towards the crater and the overturning of the flap. Many minor radial and concentric folds and faults are locally present in the rim strata. The ground surface near the crater wall exhibits small thrust faults with the upper blocks moved outward as at Prairie Flat. Geologic studies show that the region of plastic (folding) and brittle (faulting, fracturing) deformation in the upper rim extends out to about

125

200 feet from GZ, and that the overturned flap extends out to 300 to 350 feet from GZ. Individual stratigraphic units in the overturned flap are generally thinned and preserved in inverted order near the rim. Beyond about 300 feet from GZ local mixing of units is more common. Mass distribution is more symmetric at this crater than at Prairie Flat and the hummocky terrain in the overturned flap is less pronounced. Near the rim the overturned flap is as thick as 8 feet.

The final units to be involved in the overturned flap are several interbedded sandy silt and clay beds that originally lay between 15 and 25 feet. The clay beds broke into a series of large blocks that covered the crater walls and inner rim (fig. 8c). They are particularly pronounced in that the deeper clay beds were wet and appear as dark patches on the rim and walls (figs. 5a, 5b; 8c).

In terms of geologic mapping, the surface of the overturned flap can be divided into four units (fig. 9). The innermost and topographically highest unit consists mainly of coarse blocky clay with numerous wet patches of blocky clay that came from the deepest beds cratered. The next unit out has blocky clay but no wet patches, and it has a larger percentage of finer fragments of alluvium. The next unit out contains mostly finer fragments of alluvium and has a hummocky surface. The outermost and topographically lowest unit consists of fragments of the original upper 2 to 4 feet of soil. Each of these units represent continuous layers that form the inverted strata of the overturned flap (fig. 10a, 10b).

A high-angle ejecta and fallout blanket up to a few inches thick overlies the overturned flap and extends out to 450 to 550 feet from GZ as a thin discontinuous cover. Beyond this distance the ejecta consists of scattered carbon-coated and uncoated silty clay fragments; many fragments are shock-compressed.

Ray deposits identical to those at Prairie Flat were deposited on the ground in the outer ejecta blanket and appear to be related to the turbulent clouds of the dust jets. Photographs and field observations show that the part of the dust jets that extended outside the fireball deposited non-carbon coated soil fragments from these clouds. The fragments in the rays, however, are carbon coated, indicating that they either originated within the fireball or were engulfed by it. The dust jets and the carbon-coated rays were generated as part of the same region of outward, turbulent movement and this turbulent region extended back into the fireball. The curved patterns in the ray deposits on the ground are related to very late-stage turbulent motions at the time of particle deposition.

Within thirty minutes after detonation a water/alluvium mixture flowed rapidly from fractures in the central uplift and surrounding crater floor. The lower parts of the crater floor were finally covered by 2 to 4 feet of sand/clay deposited by the water and a temporary lake was formed (figs. 5a, 5b; 8a). Several fractures opened in the outer rim at about 300 feet from GZ and had an extensive flow of water/alluvium mixture carried up from

depths of at least 25 feet. Other natural changes which occurred included compaction of the ejecta and foldback by rain, subsidence during water flow from fractures, and surface erosion by rain and wind.

Fused Alluvium

Fused soil fragments identical to those formed at Prairie Flat were formed during the shock compression and heating of the silty clay below the charge (fig. 11a). The thermal effects range from slight baking of the outer surface of soil fragments to complete melting, accompanied by extreme vesiculation. The more intensely heated fragments develop hollow bubbles up to 0.5 inches across, many of which separated from the parent rock fragments. The fused material fell on top of the ejecta and fallback, and was the last material to be deposited.

Chemical analyses and disequilibrium thermal experiments were conducted on the fused material from both this experiment and similar fused material from Prairie Flat (Roddy, 1970a). X-ray fluorescence analysis of the Dial Pack fused material and of the local silty clay below GZ establishes the silty clay as the parent material. Disequilibrium thermal fusion experiments and petrographic studies of the glasses in the fused material indicate that fusion occurred at temperatures in excess of 1,100° C. and probably on the order of at least 1,500° C. The same temperatures were determined from similar experiments on the Prairie Flat material.
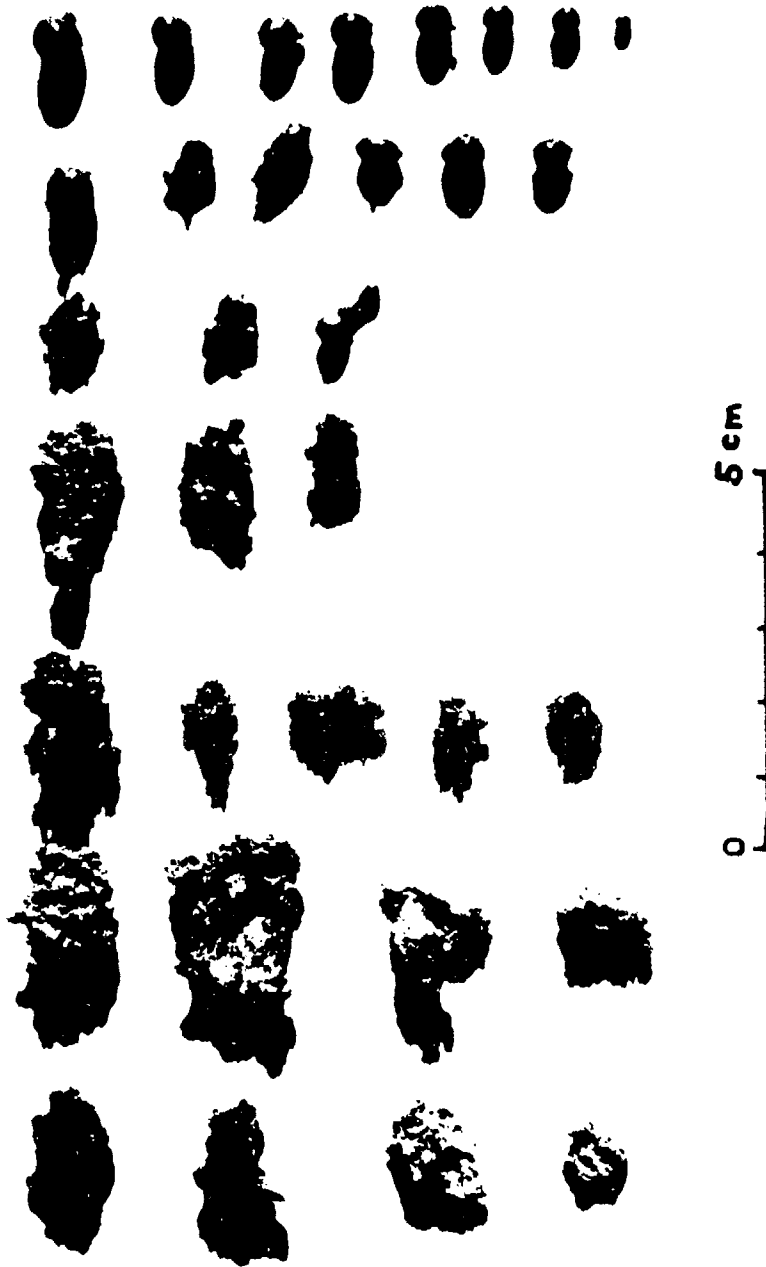
128

Figure 11a Fused and shock-metamorphosed alluvium from DIAL PACK crater. (This type of material fell as part of the final fallout for at least 15 minutes after detonation and was as widespread as 10,000 feet from the crater. The fragments in 11a are arranged in order of increasing thermal fusion effects. Fragments on the left side are baked with hard crusts; fusion and vesiculation increases to the right. The glass spheres on the extreme right are the final products of rapid melting, intense vesiculation, and final separation from parent fragment.

The fused material from these experiments has many morphological, shock and thermal metamorphic similarities with the fused lunar material returned in the Apollo 11 and 12 samples (fig. 11b).

B) Lunar Applications

Astronaut Training

Thirteen astronauts participated as part of the U.S. Geological Survey project in the Dial Pack experiment (figs. 12a, 12b). They included: G. P. Carr, C. M. Duke, Jr., R. F. Gordon, Jr., J. B. Irwin, W. R. Pogue, D. R. Scott, A. M. Worden, J. W. Young, J. P. Allen, V. D. Brand, A. W. England, F. W. Haise, Jr., and H. H. Schmitt. The writer and Dr. G. H. S. Jones (Defence Research Board, Canada) gave a pre-shot technical briefing to the astronauts and conducted the field examinations of the crater.

The field observations by the astronauts immediately after the explosion provided them an unusually good opportunity to observe the entire formational history of a large "fresh crater" that has many of the surface characteristics of the lunar craters at the Apollo landing sites. They were taken to the crater within five minutes after detonation and were able to construct a relatively complete sequence of cratering events from direct field observations. Numerous lunar analogs such as the blocky overturned flap, central uplift, fused material, concentric ridges and fractures, and raised rim were correctly described and placed in their proper cratering sequence of formation.
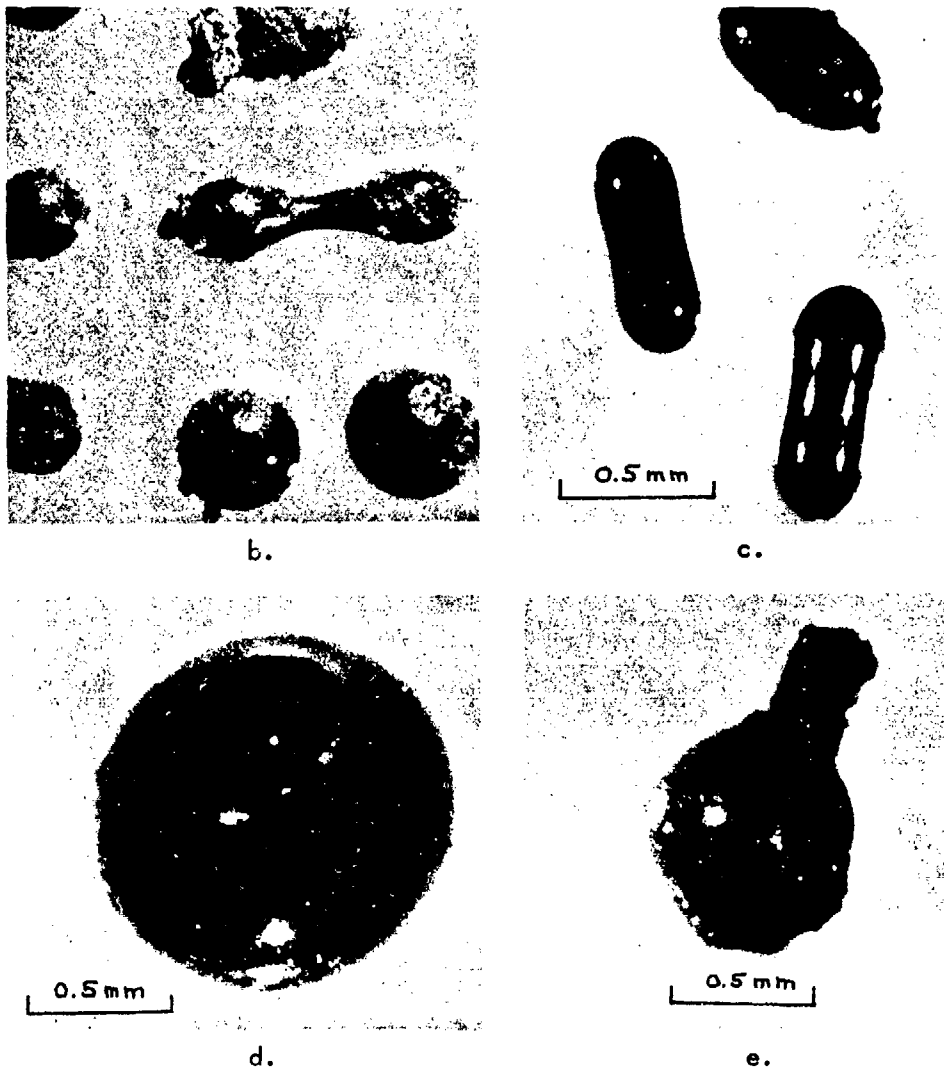
Figure 11b   Apollo lunar sample 10084-79 showing glass spheres and dumb-
             bell-shaped glass (see Figure 11a, row 5 for dumbbell shape) from
             500 to 1000 μm fraction. (Adhering surface material and internal
             vesicules are common to both lunar and DIAL PACK samples. Photo-
             graph courtesy of Duke, et al., 1970.)

Figure 11c, d, e   Apollo 11 lunar glass spherules and dumbbells. (Adhering
             surface material and internal vesicules are common to both
             lunar and DIAL PACK samples. Photograph courtesy of
             Frondel, et al., 1970.)

131

Figure 12a   Dr. G.H.S. Jones (right foreground) conducting the field examination of the DIAL PACK crater for 13 of the Apollo astronauts.

132

Figure 12b Dr. D.J. Roddy conducting the field examination of the DIAL PACK crater for the Apollo astronauts.

133

Lunar sampling and surface exploration techniques were
discussed in terms of the known stratigraphy for the Dial Pack
crater. The blocky overturned flap and knowledge of the original
stratigraphic positions of the various units were particularly
useful in demonstrating a crater as a "drill hole" for lunar
collecting techniques.

The success of this field trip by such an unusually large
number of astronauts was made possible by the excellent
cooperation and assistance from the U.S. Defense Atomic Support
Agency and the Canadian Defence Research Establishment Suffield.

Comparisons with Terrestrial and Lunar Impact Craters

Geologic studies of the 100- and 500-ton explosion craters
produced at the Defence Research Establishment Suffield show
remarkable similarities to many large, natural lunar and
terrestrial craters for which an impact origin has been proposed
(Roddy, 1968, 1969, 1970b; Wilshire and Howard, 1969). Similarities
with terrestrial structures include in part or in total: (1) central
uplifts, (2) thin breccia lenses below the crater floor, (3)
concentric ridges on the crater floor, (4) uplifted floor,
(5) concentric rim fractures, faults and folds occurring at
similar scaled distances, (6) overturned flaps with inverted
stratigraphy, (7) ejecta blankets and ray systems, and (8) fused
target material. Ratios of diameter/shear strength,
diameter/distances to concentric fracture zones, and
diameter/depths to deepest horizons exposed in the central

134

uplifts, are nearly identical, for example, for the Flynn Creek crater (figs. 13a, 13b) (3.6 km in diameter) in Tennessee and the Snowball (figs. 14a, 14b) and Prairie Flat craters (fig. 15a, 15b) (Roddy, 1968, 1969, 1970b). Jones and Diehl (1965) have also indicated structural similarities between the Snowball crater and the Ashanti Crater (Ghana, Africa, 11 km in diameter)(fig. 16).

Similarities between the explosion craters and lunar craters include: (1) bowl-shapes (100-ton and smaller explosions) (fig. 17a, 17b), (2) raised rims and hummocky, blocky overturned flaps (fig. 17a, 17b), (3) flat-floored with central uplifts (500-ton explosions) (fig. 5a, 5b, 14a, 15a, 18, 19), (4) terraced crater walls (fig. 14a, 18, 19), (5) concentric ridges on crater floor (fig. 5a, 5b, 15b, 20), (6) extensive ray and secondary impact systems (fig. 17a, 18). Other similarities include the shock and thermally metamorphosed target material.

C) Discussion

The Dial Pack crater is remarkably similar to the Prairie Flat (500-ton surface sphere) crater formed by a 500-ton surface sphere. Topographic and structural analogs include: same size, central uplift, amount of uplift, radial and concentric ridges and their positions, uplift of crater floor, thin breccia lens on floor, concentric fractures, faults and folds in the rim, overturned flap with inverted stratigraphy, ejecta and secondary craters, and fused alluvium. The Dial Pack crater differs from Prairie Flat only in having a more symmetric distribution of the overturned flap and ejecta.

135

0 _____ 5000 ft

Figure 13a   Model of the Flynn Creek crater, constructed from the structure
contour map, showing the crater shortly before deposition of the
Chattanooga shale in early late Devonian time. (The large hills
near the outer parts of the crater are underlain by megabreccia
blocks derived from the crater walls. The dotted line indicates
the position of the top of the crater wall in areas where large
volumes of ejecta have been washed back into the crater, modify-
ing the original crater shape. No vertical exaggeration. Lighting
is from south.)

Figure 13b   Generalized geologic cross sections of the Flynn Creek crater, showing the structure shortly before deposition of the Chattanooga shale in early late Devonian time. (Cross section C–C' shows positions of well cores projected into the plane of the cross section. Locations of the cross sections are shown in Roddy, 1968. The symbol * indicates rocks which strike nearly parallel to the plane of the cross section; k=Knox Group; s=Stones River Group; h=Hermitage Formation; c=Cannon Limestone; C=Catheys Limestone; L=Leipers Limtstone.)
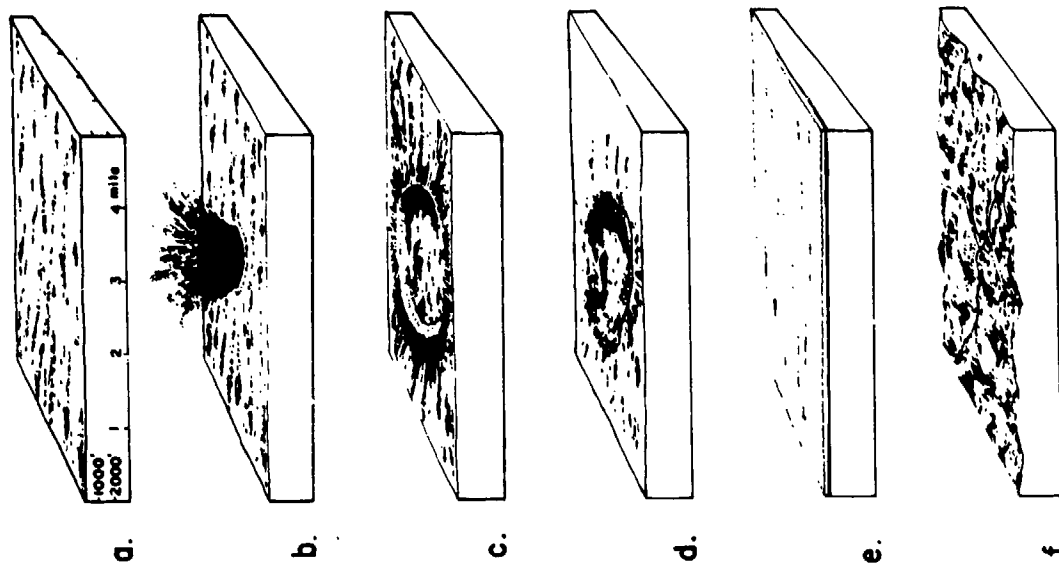
137

Figure 13c. Diagrammatic sequence of events during formation and subsequent history of the Flynn Creek crater.

(a) The Flynn Creek area, shortly before formation of the crater, about 360 million years ago, was apparently a rolling lowland or coastal plain exposing rocks of Leipers (Upper Ordovician) age. (b) Formation of the Flynn Creek crater by a comet impact about 360 million years ago, as interpreted by the writer. The area may have been inundated by the first shallow waters of the Chattanooga Sea. (c) The final crater, immediately after formation, was 3.6 km in diameter and about 150 m in depth; it contained a central hill that stood about 120 m above the crater floor. Rocks in the central hill were uplifted as much as 350 m from their original position; brecciated Knox dolomite contains shatter cones. An ejecta blanket surrounded the crater and overlay the highly deformed strata in the crater rim. The large rim thrust blocks and rim faulting and folding occurred when the crater was formed. (d) A period of erosion followed formation of the crater; many small valleys were formed on the crater rim. The ejecta blanket was removed, much of the ejecta being washed back into the crater. Subaqueous erosion and marine deposition of bedded breccias and bedded dolomite occurred in the crater during early Late Devonian time, in the first shallow waters of the Chattanooga Sea. (e) The Chattanooga Sea filled the crater with black muds in early Late Devonian time; the Flynn Creek area remained under water through at least Early Mississippian time, when the Fort Payne sediments were deposited. (f) Uplift and erosion during Quaternary (and probably Tertiary) time has produced a highly dissected region of steep-sided hills and valleys with an average relief of 150 m. The structure of the Flynn Creek crater is now well-exposed along the valley floors and walls.
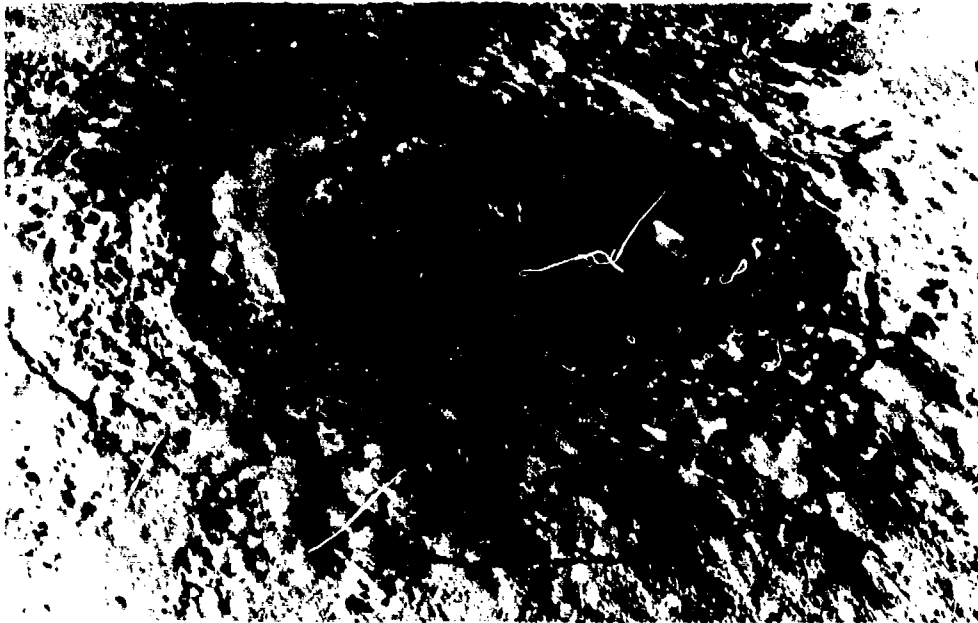
138

Figure 14a   Aerial oblique view of the Snowball, 500-ton TNT surface hemi-
sphere crater 1 day after formation, showing the central uplift,
structural terraces on the crater walls, depressed inner rim over-
lain by blocky overturned flap, hummocky terrain in outer part of
overturned flap and concentric fractures in the rim. (Photograph
courtesy of Dr. G.H.S. Jones, Defence Research Establishment
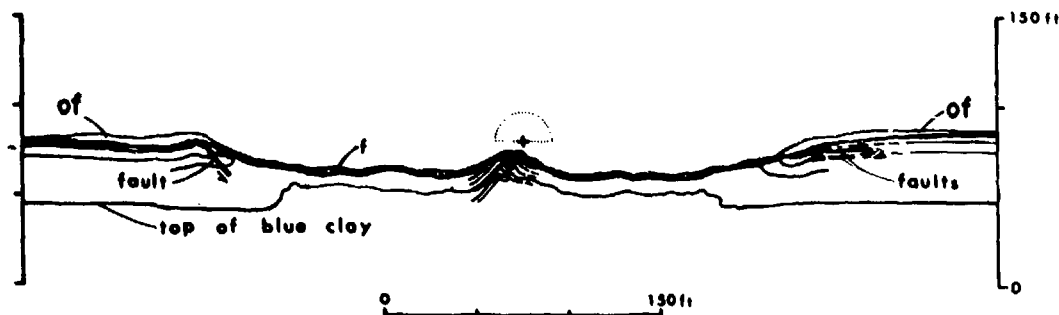Suffield, Alberta, Canada.)

Figure 14b   Structural cross section of the Snowball crater showing central
uplift caused by clay beds raised on the order of 25 feet and an
inward dipping, faulted and folded rim overlain by an overturned
flap (of). (Crater floor overlain by fallback (f) 1 to 4 feet thick,
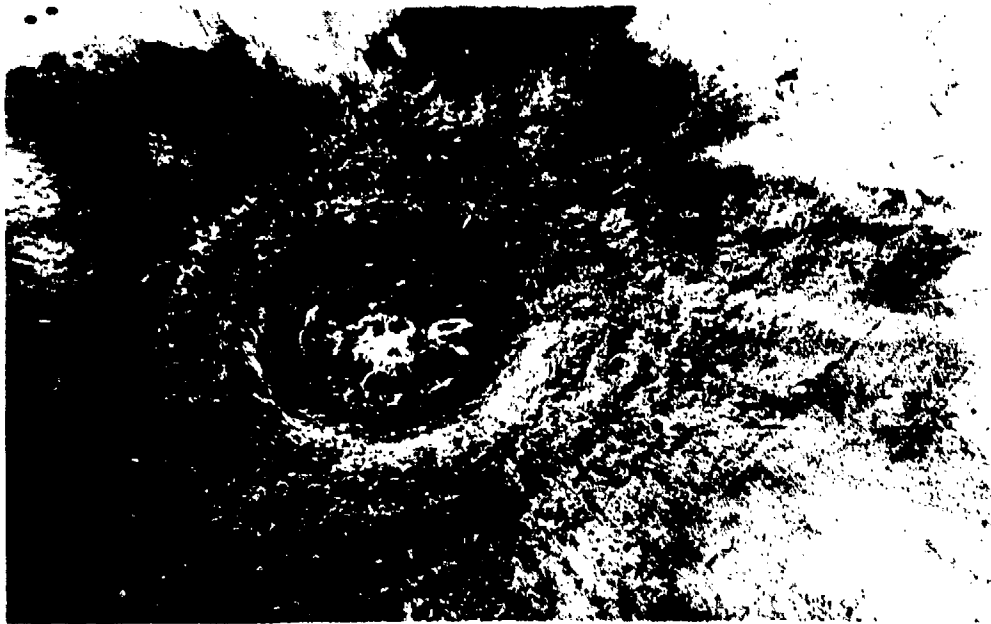composed of shock compressed alluvium.

139

Figure 15a   Aerial oblique view of the PRAIRIE FLAT 500-ton TNT surface
sphere crater, one-half hour after formation, showing water flow
from central uplift, radial and concentric ridges on crater floor
and on inner rim, depressed inner rim overlain by blocky over-
turned flap, hummocky terrain in outer part of overturned flap and
outer ray pattern. (Crater is approximately 215 feet across at the
locations where people can be seen standing at the top of the
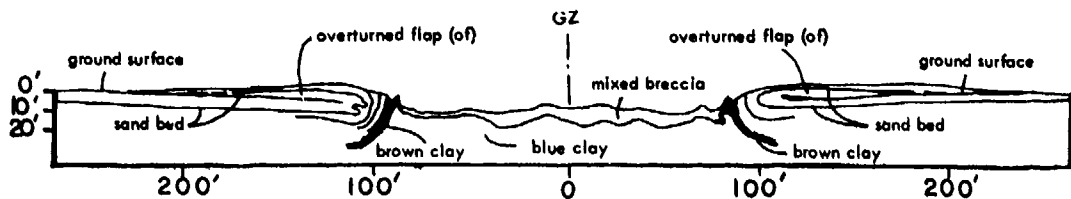crater walls.)

Figure 15b   Structure cross section of the PRAIRIE FLAT crater showing initial
uplift caused by clay beds raised on the order of 15 feet and an
inward dipping, faulted and folded rim overlain by a blocky over-
turned flap (of). (Concentric ridges and troughs on crater floor are
formed by clay beds uplifted and folded into concentric anticlines
and synclines.)

Figure 16   Lake Bosomtwe (Ashanti Crater, Ghana, Africa) and drainage system
with superimposed concentric and radial rim fractures scaled from the
Snowball crater. (Note that Snowball concentric fractures have good
scaled distances to either natural drainage divides (concentric ridges)
or drainage channels; both drainage divides and channels mark major
natural structural elements at Bosomtwe (Jones and Diehl, 1965).)

Figure 17a   Aerial oblique view of the AN/FO 100-ton hemisphere crater
showing bowl-shaped depression, terraced walls, blocky over-
turned flap, and ray pattern.

Figure 17b.   Vertical view of a 200-meter-diameter lunar crater showing bowl-
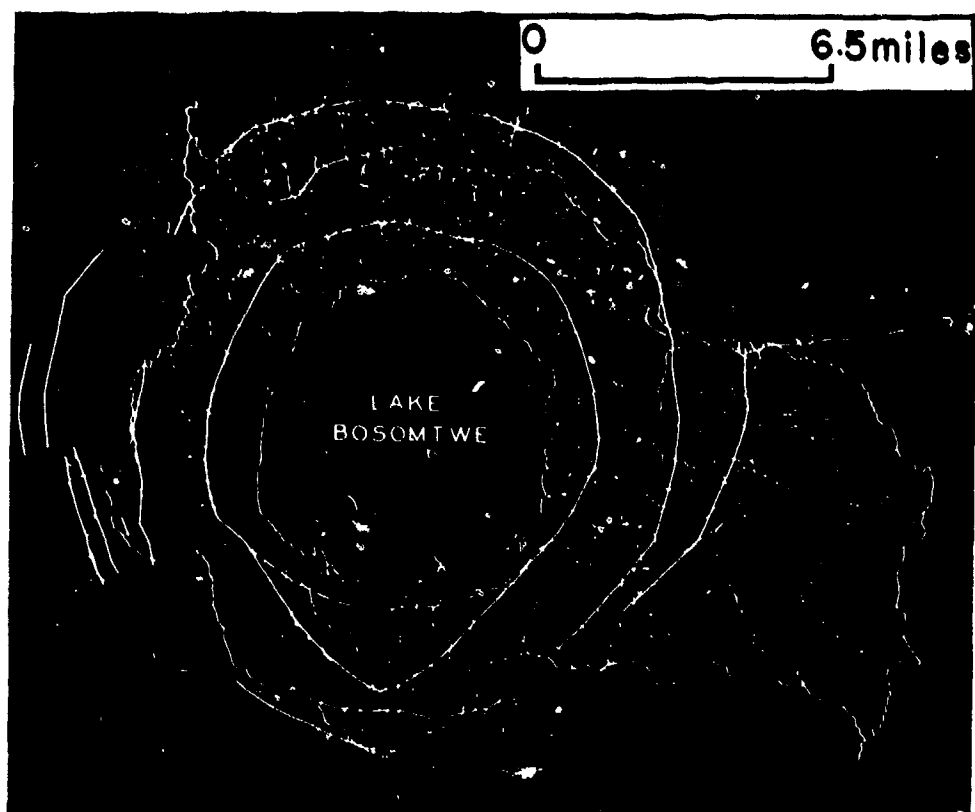shaped depression, terraced walls, blocky flap, and ray pattern.

Figure 16   Lake Bosomtwe (Ashanti Crater, Ghana, Africa) and drainage system
with superimposed concentric and radial rim fractures scaled from the
Snowball crater. (Note that Snowball concentric fractures have good
scaled distances to either natural drainage divides (concentric ridges)
or drainage channels; both drainage divides and channels mark major
natural structural elements at Bosomtwe (Jones and Diehl, 1965).)

Figure 17a   Aerial oblique view of the AN/FO 100-ton hemisphere crater showing bowl-shaped depression, terraced walls, blocky overturned flap, and ray pattern.
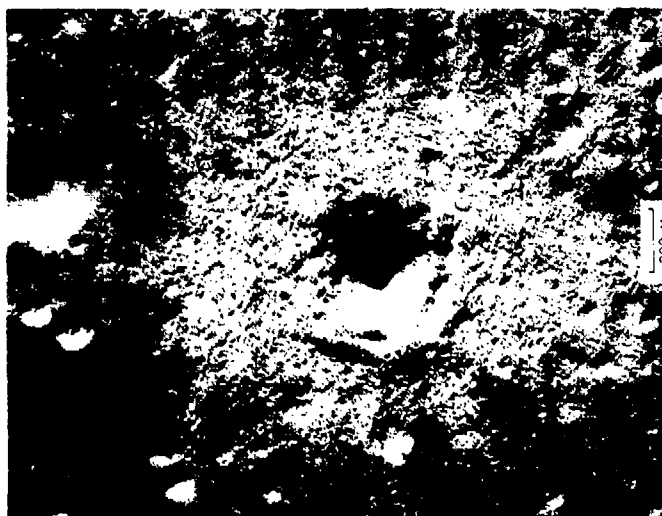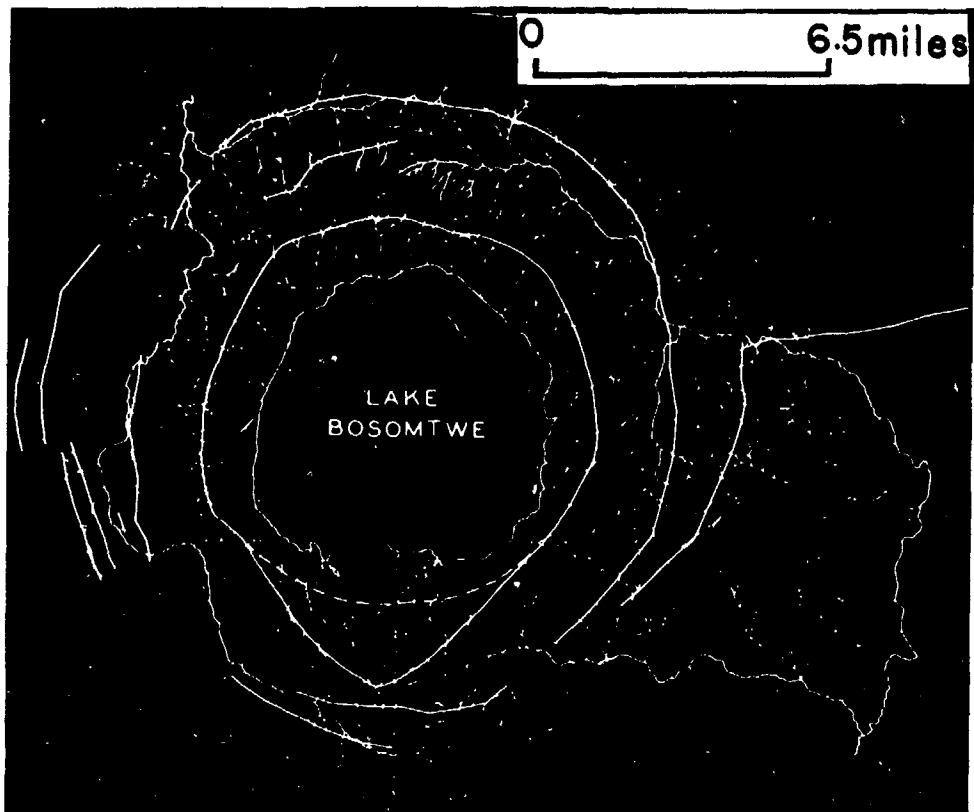

Figure 17b.   Vertical view of a 200-meter-diameter lunar crater showing bowl-shaped depression, terraced walls, blocky flap, and ray pattern.

Figure 18a   Copernicus, a large recent lunar crater 55 miles (95 km) in diameter, with central mountains, flat crater floor, terraced walls, hummocky flap, ray pattern and secondary impact crater fields. (Compare with Figures 5, 13, 14, and 15. Photograph from Lunar Orbiter series.)

143

b.

c.
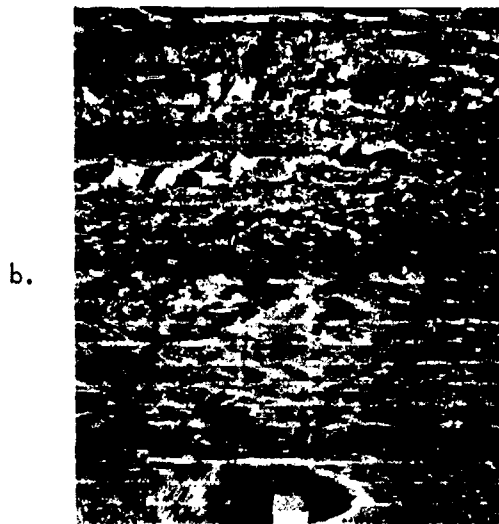
Figure 18b, c   Medium-resolution (18b) and high-resolution (18c) Orbiter photo-
graphs of the central mountains and terraced walls of the fresh lunar
crater Copernicus. (Central mountains with dipping bands rise about
1300 feet (400 m) above crater floor. Far, terraced crater walls rise
about 12,500 feet (3800 m) above crater floor. Hummocky flap in
foreground with crater Fauth in bottom of 18b (see 18a for location
of Fauth).)
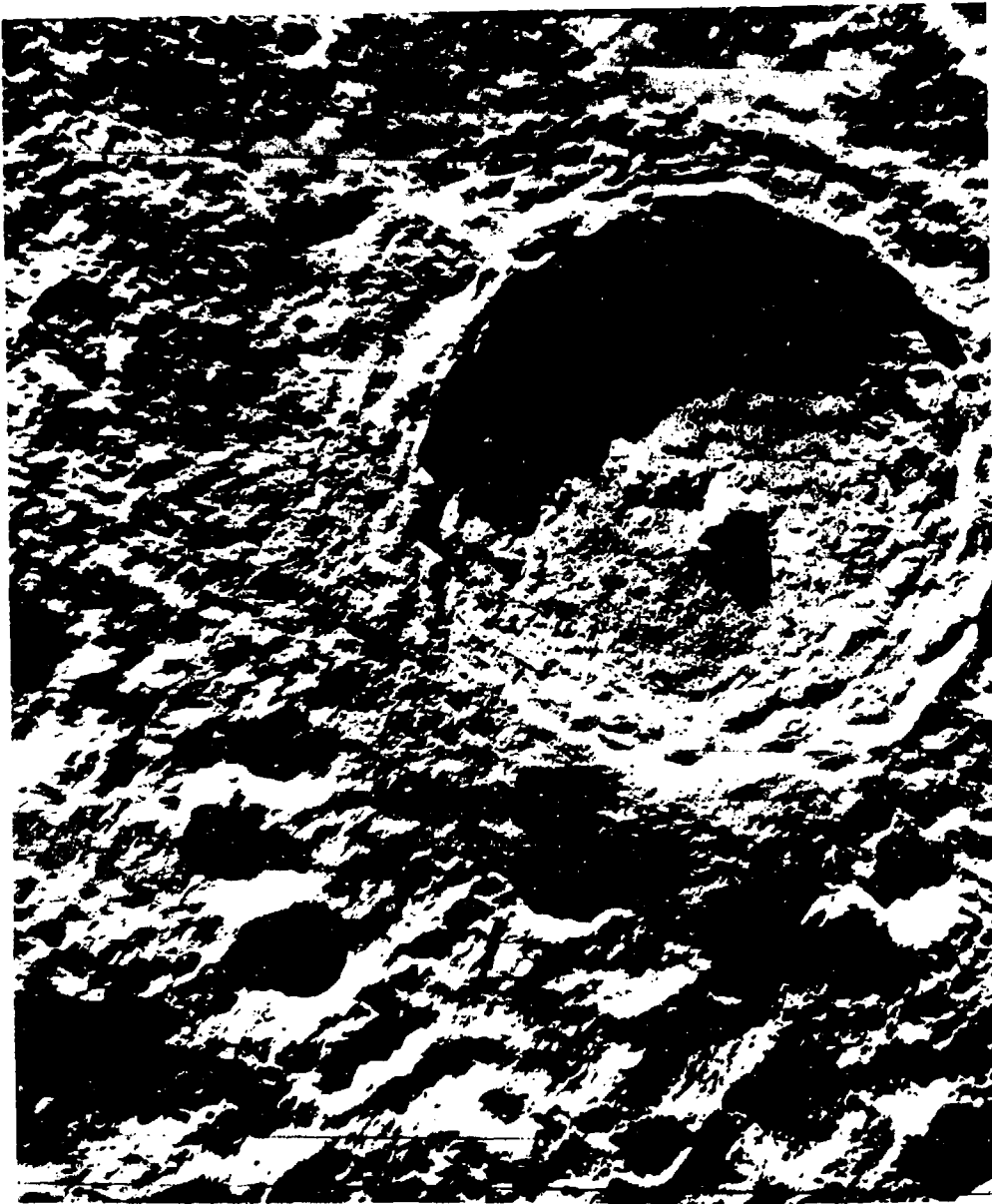
Figure 19   Tycho, a large young, fresh lunar crater 50 miles (86 km) in diameter
and 14,500 feet (4500 m) deep, with large, central mountains, rough
crater floor, terraced walls and hummocky flap overlying original, rough
cratered surface. (Secondary, probable impact-produced volcanic
fractures and mounds on crater floor.)

145

Figure 20   Mare Orientale, the largest, youngest lunar basin, with well defined con-
            centric ridges (from Orbiter IV, moderate-resolution camera, framelet
            width about 90 km). (The innermost concentric ridge is about 210 miles
            (360 km) across. Successively larger concentric ridges have diameters of
            280 miles (480 km), 350 miles (610 km), 540 miles (930 km), and 840 miles
            (1460 km) (McCauley, 1968). An enormous flap or ejecta blanket with a
            radial hummocky pattern can be seen beyond the fourth ring. Compare the
            concentric ring structure and hummocky terrain with the PRAIRIE FLAT and
            DIAL PACK craters (Figures 5 and 15).)

146

Comparisons of the airblast photography show similar luminous and dust jets for both events, except that luminous jets and fireball extensions are less pronounced on Dial Pack. This is consistent with the symmetry exhibited in the mass distribution of overturned flap. The stereo photography has superior resolution compared with previous events because of special low-altitude camera and film processing techniques. This has allowed extremely precise ejecta definition and location of fragments as small as one inch across. The high quality of the stereo photography also made it possible to produce a very accurate topographic map with a one-foot contour interval. This has provided a reliable base for a detailed geologic map and a material type and mass distribution interpretation of the various units in the overturned flap.

The Dial Pack crater also has had lunar applications in Apollo astronaut training and in the formation of fused and shock metamorphosed material similar in certain ways to fused lunar material returned in Apollo 11 and 12 samples. The topographic and structural similarities of Dial Pack and earlier surface-explosion craters with terrestrial and lunar craters has been of major importance in identifying impact-formed craters and in understanding impact cratering processes.

The sequence of cratering events determined from the Prairie Flat and previous high explosion surface experiments and

147

comparisons of calculations on hypervelocity and high explosion

shock wave processes is interpreted to be analogous to the effects

following the shock vaporization of an impacting comet which

experiences little or no penetration, and produces a

surface-developed, very high-energy shock wave (Roddy, 1968,

1970b). The numerous structural similarities between these

TNT-formed craters and certain very large terrestrial craters

up to tens of kilometers across suggest that this analogy can be

extended to include the largest of the natural sites. For example,

an unusually good morphological comparison can be made

between the ringed lunar structure, Mare Orientale (over 1,000 km

across) and the Prairie Flat and Dial Pack craters. Continued

detailed geologic and theoretical studies of the large natural impact

sites should extend our understanding of large impact and experimen-

tal surface cratering processes at energy levels which are beyond

those now acceptable in surface testing.

148

References

1. Duke, M. B., C. C. Woo, G. A. Sellers, M. L. Bird, and R. B. Finkelman, "Genesis of lunar soil at Tranquility Base," Proceedings of the Apollo 11 Lunar Science Conference, vol. 1, p. 347-361.

2. Frondel, C., C. Klein, Jr., Jun Ito, and J. C. Drake, "Mineralogical and chemical studies of Apollo 11 lunar fines and selected rocks," Proceedings of the Apollo 11 Lunar Science Conference, vol. 1, p. 445-474, 1970.

3. Jones, G. H. S. and C. H. H. Diehl, "Bosumtwi: an African meteorite crater," Sky and Telescope, vol. 30, no. 1, p. 15, 1965.

4. McCauley, J. F., "Geologic Results from the Lunar Precursor Probes," AIAA Journal, v. 6, no. 10, p. 1994.

5. Milton, D. J., and P. R. Brett, "Gosses Bluff astrobleme, Australia--the central uplift," Program of 64th Ann. Mtg. of Geol. Soc. America, Cordilleran Sec. at Tucson, Ariz., p. 82, 1968.

6. Roddy, D. J., "The Flynn Creek crater, Tennessee," in French, B., and Short, N., eds., Shock metamorphism of natural materials, p. 291-322, Mono Book Corp., Baltimore, Maryland, 1968.

7. _____, "LN303 Geologic Studies," in M. J. Dudash, ed., Operation Prairie Flat Symposium Report, vol. 1, pt. 1, p. 210-215, Defense Atomic Support Agency DASA 2377-1, DASIAC SR 92, January 1970a.

149

8. Roddy, D. J., "Large scale experimental cratering mechanics and impact cratering," Meteorite Impact and Volcanism Symposium, Lunar Science Institute, Houston, Texas, October, 1970b.

9. Roddy, D. J., G. H. S. Jones, and C. H. H. Diehl, Similarities of 100- and 500-ton TNT explosion craters and proposed impact craters," (abs.), American Geophysical Union Transactions, vol. 50, no. 4, p. 220, 1969.

10. Wilshire, H. G. and K. A. Howard, "Structural pattern in central uplifts of cryptoexplosion structures as typified by Sierra Madera," Science, vol. 162, no. 3850, p. 258-261, 1968.

R. J. Odello, Project Officer
Naval Civil Engineering Laboratory

C. R. Smith
Aerospace Corporation

PROJECT LN312
SILO CONFIGURATION AND EVALUATION TEST

INTRODUCTION

Objectives

The primary objective of this project was to obtain information on the response of a full-sized idealized silo sited in a layered soil media to high airblast overpressures and large direct induced ground motions. Specific objectives were:

a. To determine the body motions and the structural response of the silo including the character of the stress wave propagation down the launch tube.

b. To obtain data that will serve as reference checks in extending media-structure response codes to include non-linear and large deformation effects.

c. To obtain emperical data that can be used in future design efforts.

Background

The military requirements for this experiment are many. It will directly benefit existing and future Air Force weapon systems as well as those of the other services.

The test provided fundamental technology data in a previously untested section and provided survivability information in terms of emperical response data from direct induced motions. This includes the response of an idealized structure that is directly applicable for code verification.

In the early 1960's when the hardened structure design community became involved with designs for advanced missile systems having greatly increased survivability, concepts of utilizing composite structures in rock sites became more and more attractive. The first serious work in this direction was accomplished in project Pile Driver where sections CR7 and BL10 represented composite designs intended to mobilize the confined strength and ductility of concrete encased in a steel liner. Based on these results and other empirical data, preliminary designs for subsequent systems began to emphasize to a greater degree the application of composite sections based in a rock media.

Two milestone studies of the 1966-67 time period included rigorous trade off analyses to quantify the benefits of composite sections and rock siting in comparison with reinforced concrete and solid steel walls sited in a variety of media ranging from soft soils to very hard rock. The results of these studies were reflected in the prototype designs of the launch control and launch facility structures proposed for the WS 120A Advanced Missile System. This system and its design concepts were transposed into the Hard Rock Silo Program.

In 1969 the Alternatives for Strategic Missile Force Improvements
was conducted for the Air Force. One system included in this program
was the Nemesis ICBM system which utilized a very small, highly
proliferated missile system as an advanced facet of the U. S. strategic
forces. Systems analysis indicated a possibility that portions of this
missile system would have to be sited in a soil area due to the large
area requirements of the missile system and the stringent criteria
associated with the siting processes. Accordingly, the designs were
analyzed as reinforced concrete structures to affirm the suitability
of soil sited composite structure launch facilities.

A sandwich type structure with a section of concrete placed
between two pieces of steel plate is an economical and efficient
technique for achieving high strength reinforced concrete designs.
In the case of the DIAL PACK test article the one-half inch steel
inner liner represents the equivalent of 4 percent steel in the form of
reinforcing bar acting in both directions. In addition, there is the
advantage that the rebar in both directions is coupled and offers
100 percent of the steel strength in all directions in the plane of
the plate. The quarter inch outer steel linear (equivalent to tensile
rebars) represents 2 percent reinforcement in both directions. The
same advantage that accrued to the inner liner accrued to the outer
liner. From a construction standpoint the liners also doubled as the
construction forms. With the elimination of shear steel and rein-
forcing bars in the design, emplacement processes are greatly simplified
while quality assurance of the structure is enhanced.

153

The Air Force has further expended considerable effort in acquiring response and survivability information on full-size and large-scale launch facilities in HEST tests[1,2] and in Operation PRAIRIE FLAT.[3] Tests on small models for correlation with the field results have been performed at the U. S. Army Engineer Waterways Experiment Station. The experiment outlined in this report will extend present knowledge to the realm of higher overpressures and more extreme ground motions.

In summary, the DIAL PACK silo structural design represents a logical extension of the technology development program initiated and vigorously pursued by the Air Force over the past ten years. The structural concept has demonstrated its performance, efficiency, economies, and other major advantages that could also accrue to a large missile system.

The data gained from this experiment will be directly applicable to potential modifications to the Minuteman force. It should correlate with and extend knowledge gained in previous tests to a high pressure region that contains a significant direct induced ground motion pulse. Further, it can be used to examine the response of a composite construction technique that could be of interest if new launch equipment rooms should become desirable. The data obtained in this experiment may also be applicable to other future systems such as Advanced Mobile Systems (hardened garages), Anti-Ballistic Missile Defense Systems (interceptor silos) and other highly survivable hardened facilities.

Theory

An analysis of the airblast induced silo behavior was made using a finite element program known as WINDAX, which was developed under the direction of E. L. Wilson of the University of California at Berkeley.[4] The program solves problems of plane strain and axisymmetric solids subjected to transient loads. Although the code contains options which allow for non-linear, non-elastic material properties, and large displacement, only the linear elastic formulation was used in the analysis. A discussion of the finite element idealization, the code results and a comparison with the measured silo response is presented in a later section.

PROCEDURE

Test Article

The test structure for this experiment was an idealized but otherwise full-size Nemesis missile silo which was located at the 135 foot range from the DIAL PACK ground zero (Figure 1). Predicted peak overpressure was approximately 900 psi, but the intent of this test was to get a mixture of high overpressure and large direct induced motions.

Figure 2 shows a cross-section of the silo. It was 43 feet deep with its top surface at ground level. The top 10 foot section was 11 ft-8 in. outside diameter. Below that was a 6 foot conical section which tapered to a 7 ft-8in. outside diameter, and the lower 27 foot section was 7 ft-8 in. outside diameter. The structure was of composite

construction with a 1/4 inch thick outer steel liner and a 1/2 inch
thick inner steel liner. The annular space between these liners was
filled with unreinforced concrete with an average compressive strength
of 4,180 psi. The silo closure was of similar construction with a 1/2
inch thick steel liner. Construction operations are described in
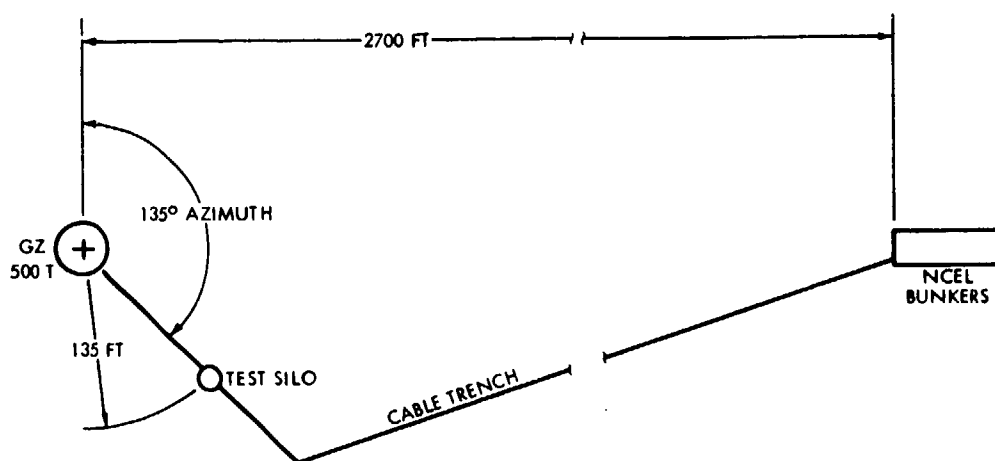detail in the Project Officers' Preliminary Report.[5]
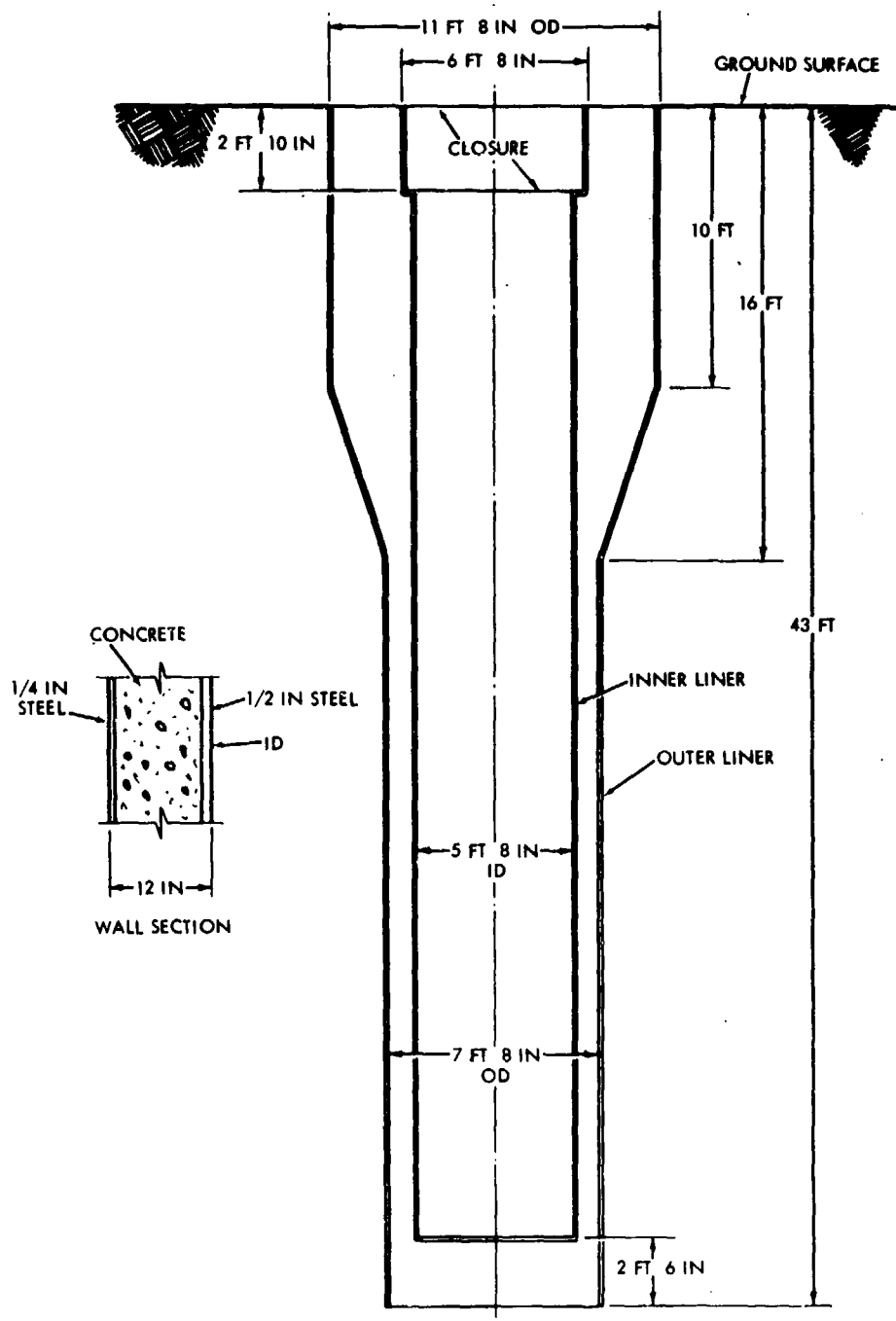

Figure 1 (U) Test layout (U).

Figure 2 (U)   Silo configuration (U).

Instrumentation

Gages used in this test are shown in Figure 3. There were a total of 31 gages used; these included 2 overpressure gages, 7 velocity gages located within the structure, 6 velocity gages in canisters in the soil, 9 strain gages and 4 slip gages.

These last gages were used to measure the relative motion or slip at the soil-structure interface. Two of them were located at the 4-foot depth, and two were located at the 18-foot depth on the outside of the silo. Each gage consists of a Bournes linear motion potentiometer, which was rigidly attached to the structure, and a 5 inch diameter steel plate, which was attached to the steel shaft of the potentiometer. The plate protruded into the soil and moved with the soil while the base moved with the structure. This was the first time such measurements have been made on a large scale test structure, and they are expected to provide useful information for the development of computer codes and design analyses.

RESULTS AND DISCUSSION

All magnetic tape recorders ran, and all channels were operating at shot time. The gages appeared to have functioned satisfactorily and all channels contained useful data. An electronic disturbance at about $z + 0.6$ seconds and a brief power failure at about $z + 5$ seconds had little effect on the results. This section contains a discussion of the post-shot silo condition and the results of the data analysis.
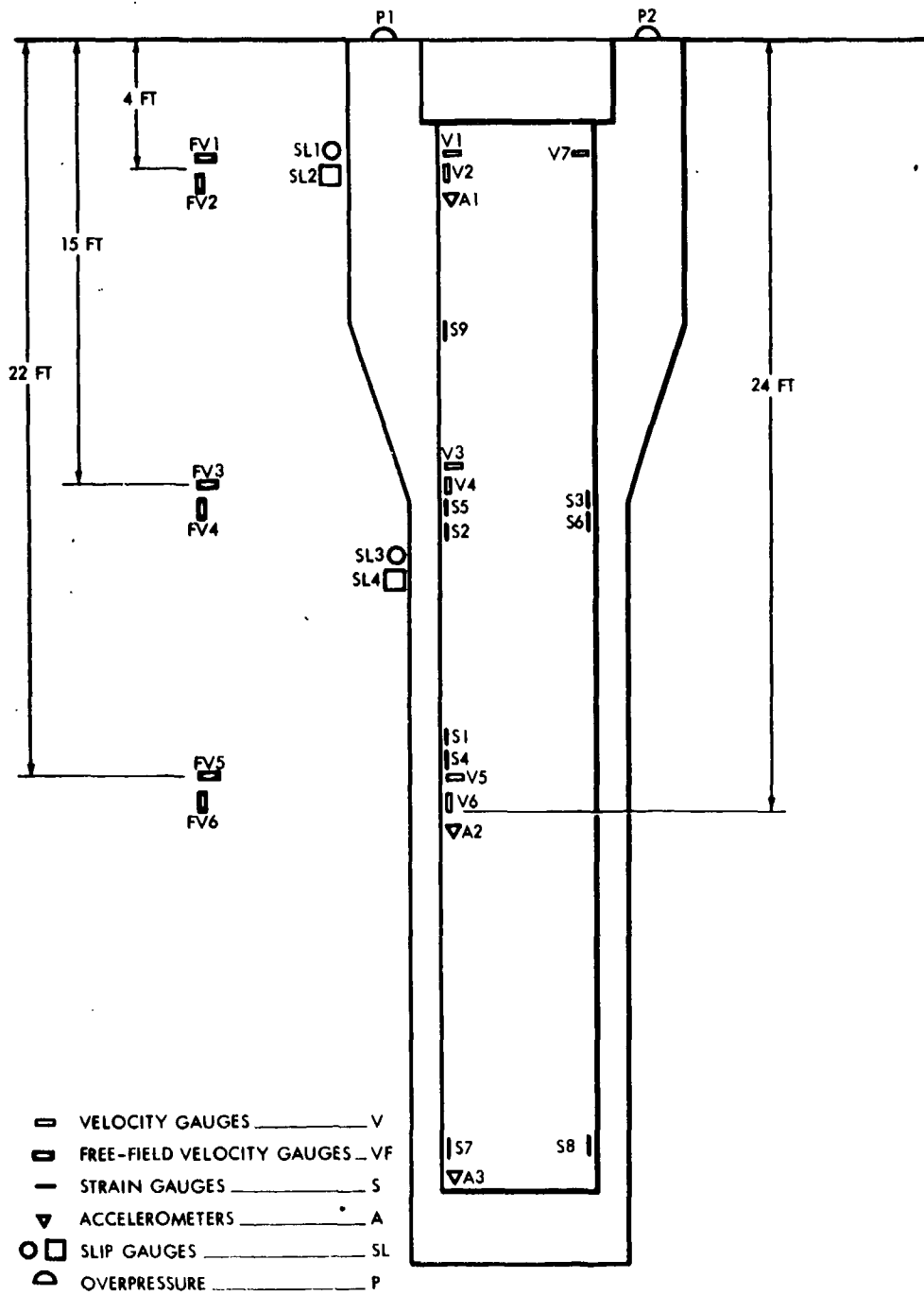
Figure 3 (U)   Gage location (U).

Survivability

A post-shot examination of the silo showed that it was near the lip of the crater and was covered by 6 to 8 feet of ejecta. When the ejecta was removed, no evidence of concrete cracking or separation from the steel liners could be seen. The interior of the silo showed no evidence of damage or permanent deflection.

Survey data showed that the structure was displaced 0.15 feet outward from Ground Zero and 1.5 feet downward from its pre-shot position. The top of the structure was tilted less than 1/2 degree toward Ground Zero with respect to the bottom. Tangental tilting of the structure was negligible.

Overpressure

Both pressure gages showed the same type of overpressure record with approximately the same peak overpressure. Gage P1 on the south side of the silo showed a peak pressure of 900 psi and Gage P2 on the north side showed a peak pressure of 800 psi. The overpressure record for gage P1 is shown in Figure 4.

Silo Velocity and Displacement

The initial movement was almost straight downward due to airblast, but was followed by much larger and longer duration direct induced motions. Airblast induced motions predominated for less than 100 msec, but the direct-induced motions continued for more than 2 seconds.
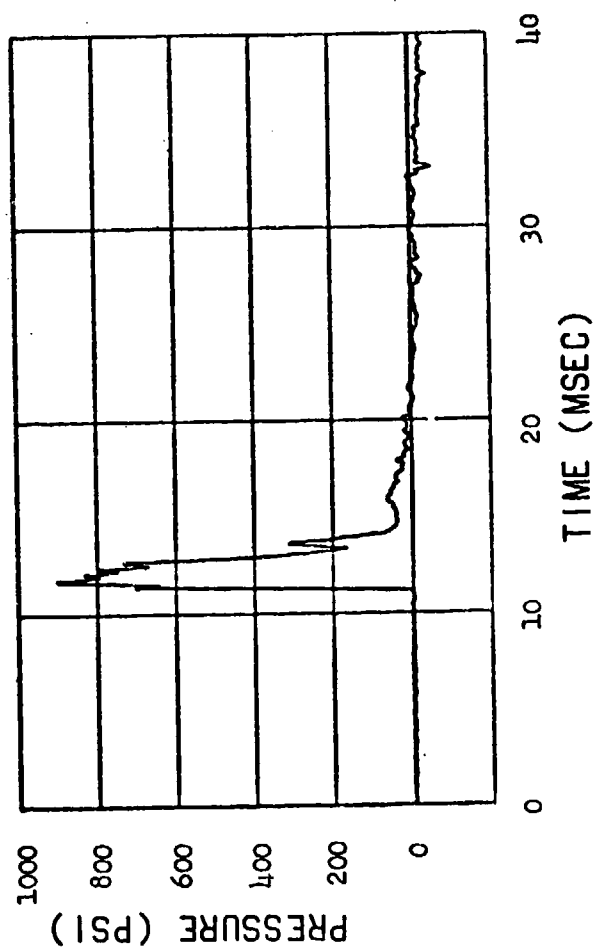
160

Figure 4 (U)   Overpressure from gage P1 (U).

161

Vertical silo velocities for the first 100 msec are shown in Figure 5. Maximum downward velocity occurred at about 25 msec after detonation zero, and was between 20 and 35 ips (inches per second). By integrating these curves the maximum airblast induced displacement was determined to be about 0.5 inches downward.

Longer time histories of the silos vertical and horizontal velocities are shown in Figures 6 and 7. These records show the large upward and outward movements of the silo during direct induced motions. Data from all gages were in close agreement and showed maximum upward and outward velocities of 100 ips.

Data from adjacent horizontal and vertical gages were integrated to provide a record of the absolute cartesian displacement of the structure. Figure 8 shows the displacement for the gages at the 4-foot depth. On this figure, time reference is given by symbols at 100 msec intervals. The maximum displacement was about 40 inches upward and 50 inches outward. The gages also indicate that the structure returned to near its original position.

Soil-Silo Interaction

The free-field soil velocity gages and the slip gages mounted on the silo provided data on effects of silo motion on the response of the structure. This section presents the results of those measurements.

Free-field velocity gages showed motions very similar to the silo motions during cratering induced motions. The early time response of
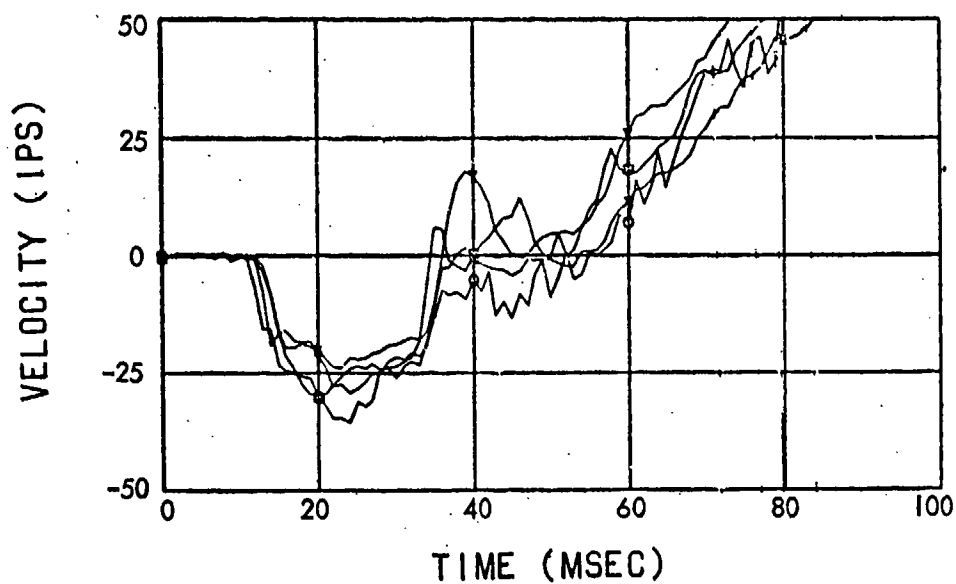
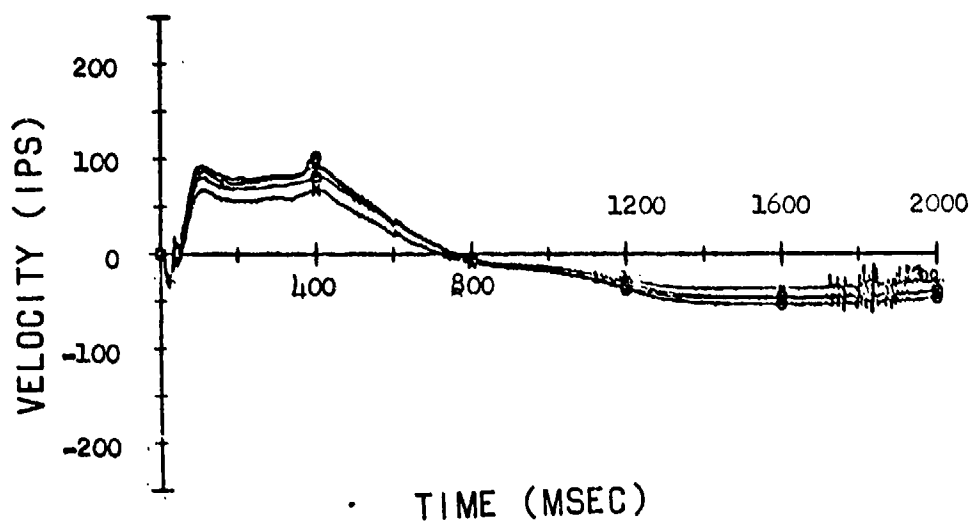Figure 5 (U)   Airblast induced vertical silo velocities (U).
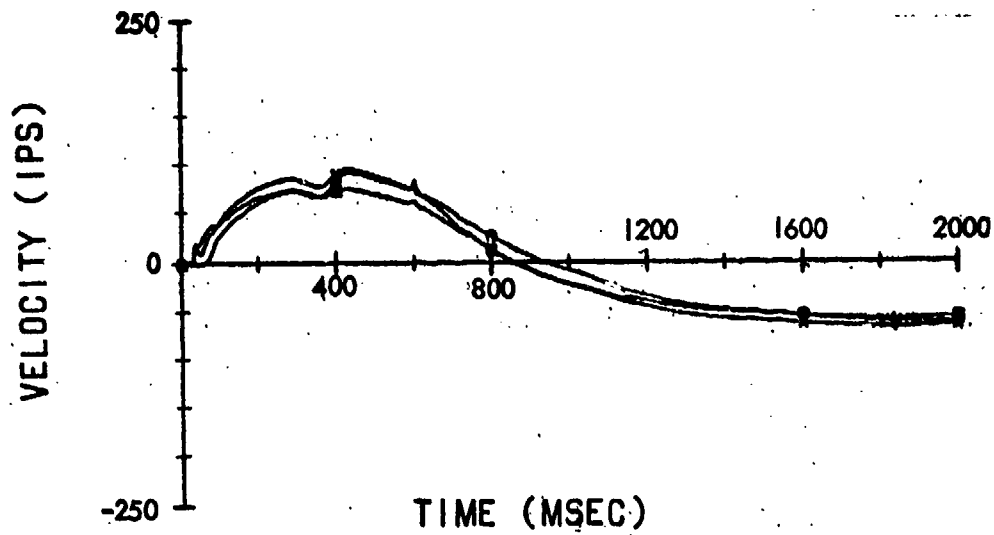

Figure 6 (U)   Vertical silo velocities (U).

163

Figure 7 (U)   Horizontal silo velocities (U).

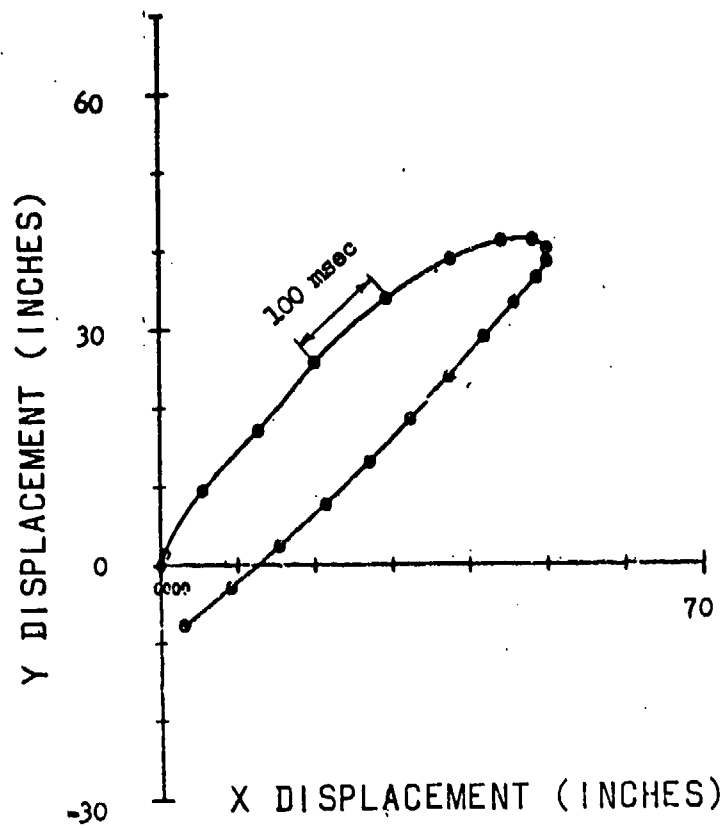Figure 8 (U)   Silo displacement at 4-foot depth (U).

the vertical gages was different at each depth of soil. Vertical velocity gage data are shown in Figure 9. The gage at the 4 foot depth shows an initial downward velocity of about 170 ips before, the upward motions predominate. The gage at 16 feet showed a downward velocity of about 50 ips before the cratering induced velocities, which were of much lower magnitude than for the shallower gage, predominated. At 22 feet, however, the initial velocity was upward at about 100 ips, and later time response is very similar to the velocities at the 16 foot depth. It is believed that the initial upward motion at the 22 foot depth was caused by the direct induced wave arriving before the airblast wave from the surface.

Horizontal free-field velocity gages showed motions very similar to the structure motions except that at late times the records are suspect because of gage tilting and resultant zero shifts.

The slip gages provided much valuable data on the relative motions at the soil-structure interface. Data from the vertical slip gage at the 4 foot depth is shown in Figure 10. The sign convention is that a positive value indicates the silo is moving down with respect to the soil. Also plotted on this figure is the relative displacement calculated by integrating the free-field and structure velocity gage data at the corresponding depth and subtracting the results. The first 250 msec of the slip data appear to be valid and to agree in shape with the velocity gage data. However, beyond that time the shaft of the potentiometer was apparently jammed and did not move freely. It is also
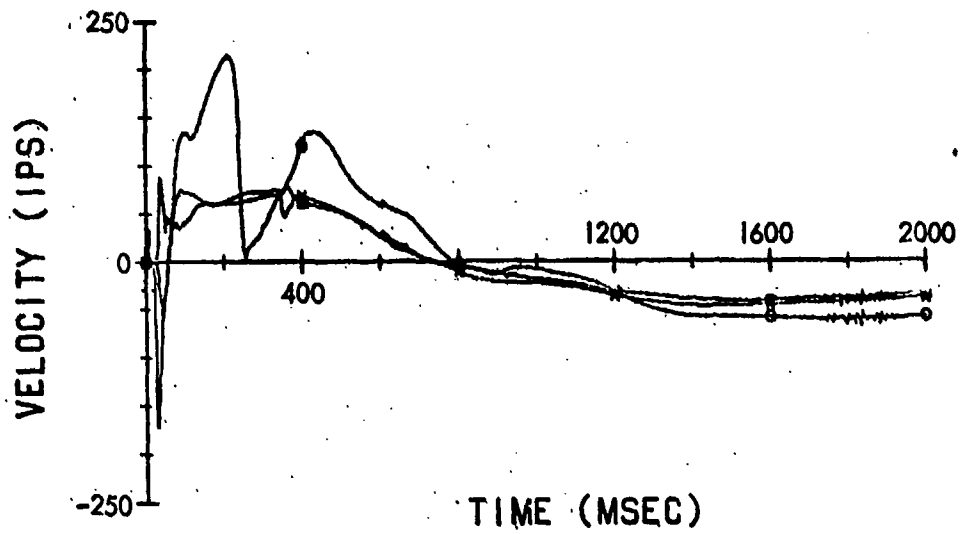
165

Figure 9 (U)   Vertical soil velocities (U).

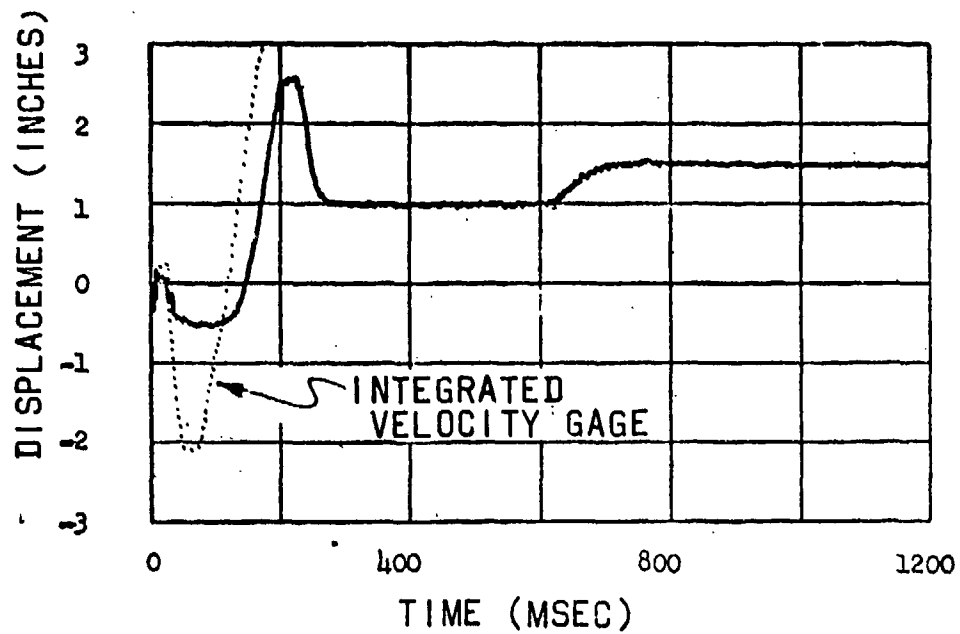Figure 10 (U)   Vertical slip at 4-foot depth (U).

possible that the flat parts of the curve indicate times when there was no relative motion at the interface. In general these gages performed satisfactorily and provided much useful information on the soil-silo interaction phenomenum.

Accelerations

Data from one of the vertical accelerometers located in the structure are shown in Figure 11. The plot shows the structure response during the first 110 msec only, but no significant accelerations were recorded after that time. Peak vertical accelerations were 200 to 300 g's. These accelerations indicate the nature and magnitude of the shock wave propagation in the walls of the structure. The body accelerations of the structure, which were obtained by differentiating the velocity gage data, were of much lower frequency and amplitude. The peak body accelerations resulting from air blast were 22 g's down and 10 g's upward. Direct-induced motions resulted in peak accelerations of approximately 0.5 g's horizontally and vertically.

Strains

In general, the strain gage data provided good information on the arrival times and indicated that the structure experienced no strains large enough to indicate yielding of the inner liner. A typical example of the data obtained from the vertical strain gages is shown in Figure 12. The normal sequence of events is an initial compressive peak followed by a tension peak which may be greater than the initial
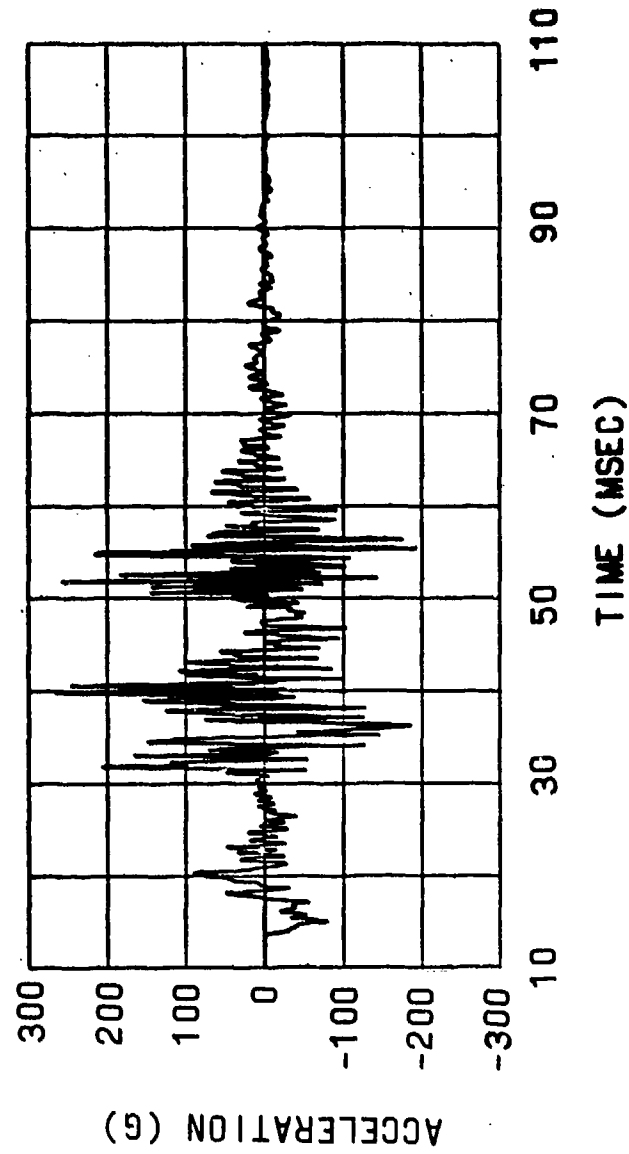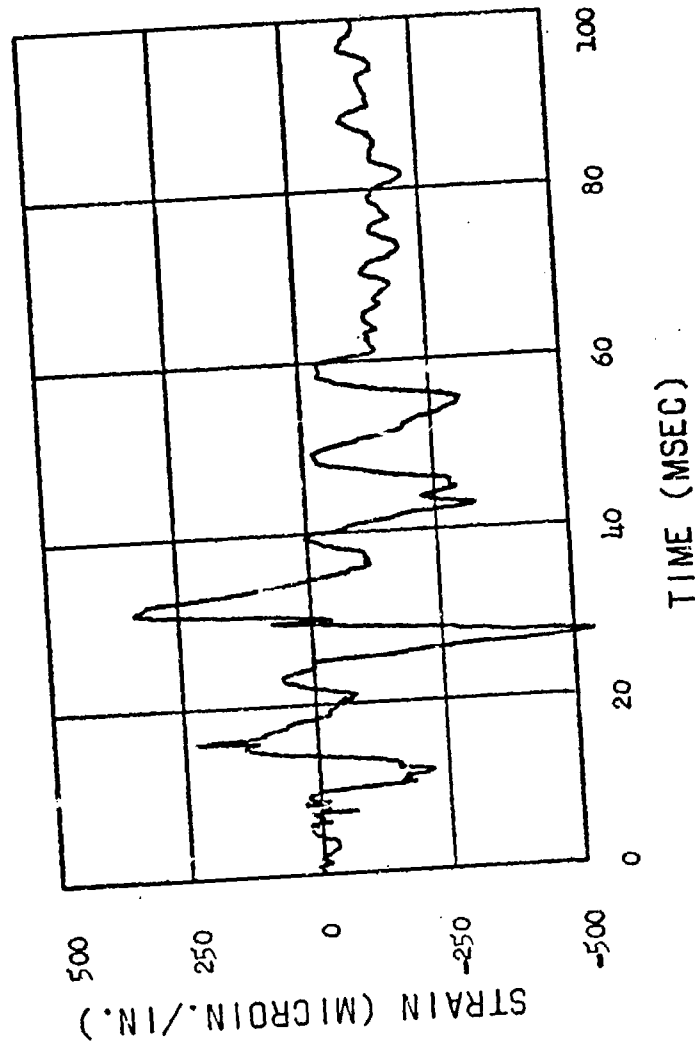
167

Figure 11 (U) Vertical structure acceleration (U).

168

Figure 12 (U; Vertical strain from gage SG6 (U).

169

peak. After a few oscillations, the structure appears to vibrate freely with a natural period of about 12 msec. All of the vertical strain gages showed this same trend with similar magnitudes for the first compression peaks. Few gages showed significant strain after the first 100 msec. Of those that showed strain at late times, two vertical gages on opposite sides of the silo indicated that some bending moment of the gross silo cross-section may have occurred at the bottom of the conical section. However, these bending strains and all other measured strains were far below levels which would cause distress in the structure.

Computer Analysis

One of the objectives of this test was to acquire data which would provide checks on computer code calculations of dynamic soil-structure interaction. This section contains some comparisons of measured data with results of calculations using a linear elastic finite element code. This analysis is limited to axisymmetric airblast loading effects, but, even in the linear-elastic formulation presented here, the comparison with measured data is good.

The finite element idealization used is shown in Figure 13. Boundaries between different soil layers were determined from the silo construction records, and different material properties were assigned based on previously published data on DRES soils. The applied load was a multi-linear idealization of the measured overpressure.

170
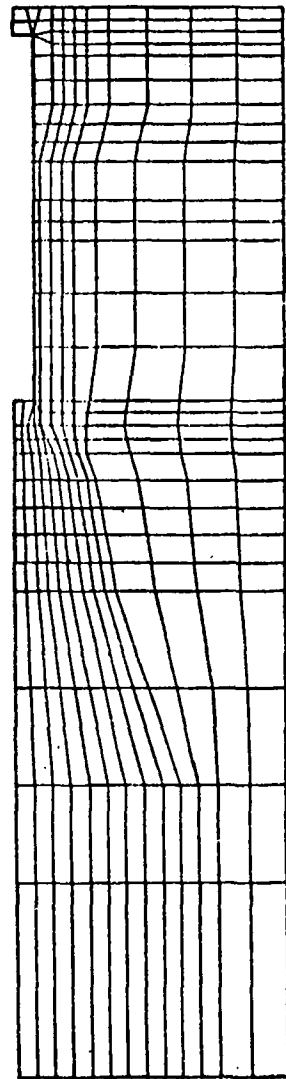
337 ELEMENTS

380 NODES

10 MATERIALS

Figure 13 (U)   Finite element idealization (U).

171

Figure 14 shows the comparison between the measured vertical velocity data traces and the code predicted response (heave line). The magnitudes of the peak velocities are very similar as are the shapes of the curves. The computer results show more oscillations than might be expected, but previous analyses indicate that these are a result of the assumption of linear elastic material properties rather than an instability in the numerical solution. The comparison between the measured and calculated vertical strain at the location of gage SG2 also indicates a good correlation (Figure 15). This close correlation is to be expected, however, because the steel was not strained beyond the elastic limit.

It must be emphasized that the input for this computer analysis was based almost entirely on pre-shot data. Soil conditions and locations of various strata were based on information obtained while the silo was being constructed. The only post-shot modification of the data was to use the idealization of the measured overpressure data. The close agreement of post-shot results with pre-shot calculations demonstrates that this code provides a reasonable basis for predicting the air blast induced behavior of structures.

TEST RESULTS AND SYSTEMS IMPLICATIONS

The test provided valuable information on the survivability, body motions and structural response of an idealized full size missile silo at the 135 foot range from the DIAL PACK ground zero. Some of the more significant results are as follows:

1. The silo received an average peak overpressure of 850 psi.

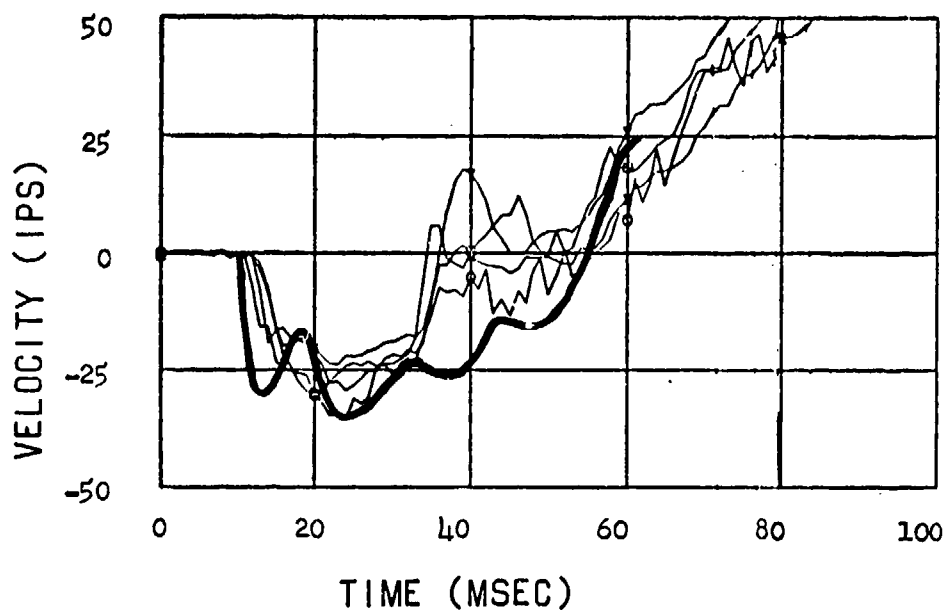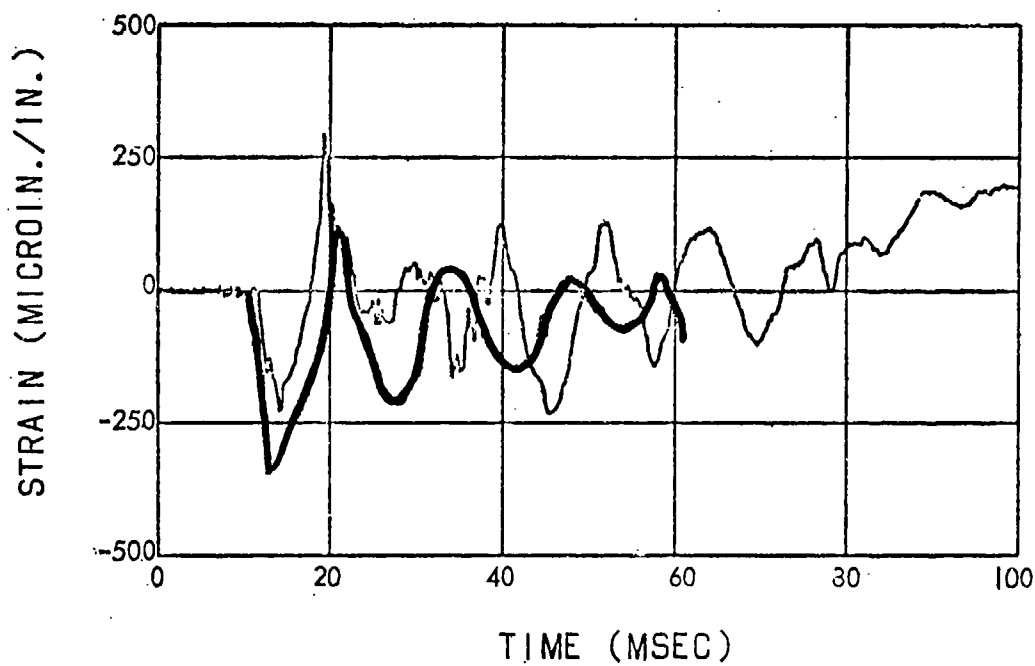Figure 14 (U)   Measured and computer code predicted velocities (U).

Figure 15 (U)   Measured and computer code predicted strains (U).

173

2. The structure sustained no noticable damage.

3. Residual displacement was 1.5 feet down and 0.15 feet outward from Ground Zero, with a residual tilt of less than 1/2 degree.

4. Air blast induced displacements were small compared to crater-induced displacements which were 40 to 50 inches upward and outward.

5. Maximum vertical slip at the 4-foot depth was 2 1/2 inches and other slip gages provided useful data on the slip at the soil-silo interface.

6. Maximum airblast induced accelerations in the silo walls were 200 to 300 g's, but the maximum body accelerations were about 22 g's.

7. Strain gage data indicated that the inner steel liner was not strained beyond the yield point.

8. Results of the computer analysis based on linear elastic material properties compare well with measured silo velocities and strains.

9. Sufficient data were obtained to provide checks for existing and future analyses for cratering-induced and non-linear effects.

In assessing the implication of the design of advanced weapon systems, it must be reviewed against the background of its design strength. It consisted of minimal wall and steel thicknesses as well as low steel and concrete strengths. By increasing one or more of the above parameters, designs can be developed for much more severe environments.

174

The test article survived the test environment without evidence of yielding in any portion of the facility. Indeed, the data indicate that it could probably have been located in a much more severe environment--up to the crater's edge or within the outer reaches of the crater-- without exceeding its structural strength capability.

The data show that the air blast induced accelerations experienced within the walls were sufficiently large so that operating ground support equipment should be mounted on a shock isolated platform. Body accelerations during this time were quite moderate. The direct induced structure motion included peak accelerations of approximately one-half g. Large displacements were experienced during the direct-induced motion, but the transient tilt of the structure is believed to have been small--less than 2 degrees from the vertical. Depending on the fragility level of the protected systems which will to a large extent dictate the shock isolation system criteria, it is believed that these ground motion characteristics can be dealt with within the state of the existing art.

The amount of differential motion between the test structure and the free field appears to be high. Peak differences in displacements obtained from free field and structure mounted gages was approximately 22 inches at the 4-foot depth while that indicated by the slip gages was only 2-1/2 inches. The above indicated values are believed to represent an upper and lower boundary to differential motions. It is believed that the slip gages did not measure the total differential

175

displacement between the structure and the media. However, both of these values when scaled to a credible nuclear threat would be excessive. The implication of these motions are that it would be exceedingly difficult for a penetration through a silo wall to survive for service, communication, or air conditioning.

The test structure encountered the most severe debris environment produced by the 500 ton explosion. A similar relative position to the crater's edge in a nuclear environment would impose excessively deep amounts of debris overlying the weapon system structure. In a launch facility system considerations must be provided for protecting the interior of the facility from debris cave-ins during door openings and launch sequence operations. In both launch facility and manned applications, serious consideration should be given to closed cycle life support and environment control systems. It is questionable whether an open cycle system could provide access to the free atmosphere.

176

REFERENCES

1. Boeing Company Report D2-31679-1: HEST Test III, Weapons Systems Impact Report, (U), 1967. SECRET

2. Boeing Company Report D2-31853-2: HEST Test V, Final Report (U), 1969. SECRET.

3. Naval Civil Engineering Laboratory. Technical Report R-646: Body motions of model silos (U), by J. R. Allgood and T. K. Lew. Port Hueneme, California. Oct 1969. SECRET.

4. Farhoomand, I. Non-linear Dynamic Stress Analysis of Two-Dimensional Solids, PhD Dissertation, University of California, Berkeley, California. June 1970.

5. Defense Atomic Support Agency. Information and Analysis Center. Special Report DASIAC SR-   : Event DIAL PACK, preliminary report, edited by M. J. Dudash. Santa Barbara, California.

J. M. Watt, Jr., Project Officer
Waterways Experiment Station

PROJECT LN314B
EVALUATION OF PROTECTIVE MILITARY
PERSONNEL SHELTERS, BRITISH MARK II DESIGN (U)

CHAPTER 1

INTRODUCTION (U)

(U)1.1 Background. The United States, United Kingdom, Canada, and
Australia in a quadripartite agreement are currently attempting to
standardize the development of field fortifications and to optimize the
combat soldiers protection against the effects of nuclear weapons. The
British Mark II shelter tested in Event DIAL PACK is an outstanding
example of the international cooperation existing between the scientific
and engineering staffs of these countries. The Mark II shelter was
designed and supplied by the British, tested in a Canadian field trial,
with the United States installing the shelter, instrumenting and
compiling a final report. In addition to the international effort,
cooperation from various agencies within the United States contributed
significantly to the success of the Mark II shelter test. The Ballistic
Research Laboratories provided pressure measurements inside and outside
the shelters, the Naval Civil Engineering Laboratories provided and
installed deflection gages for measuring deflection of a roof arch-rib in
each shelter, and the Lovelace Foundation placed the anthropomorphic
dummies and installed movie cameras to record their response. It was the
responsibility of the Waterways Experiment Station to install the shelters

and recover all data for inclusion in a final report.

(C)1.2 Objective. The general objective of this investigation was to collect data for the purpose of determining the habitability and hardness of the Bristish Mark II command post shelter when subjected to ground surface airblast effects from a 500-ton TNT detonation. The specific objectives of the investigation were as follows: (1) to record the centerline deflection of a roof arch-rib, (2) to record the airblast pressure inside and outside the shelter, and (3) to record photographically the displacement-time history of the dummies placed in each shelter. In addition, preshot and postshot measurements of the cross-sectional geometry of the shelter were made along with complete documentary photographic coverage.

(C)1.3 Scope. Two prototype British Mark II field shelters of the command post configuration were tested in Event DIAL PACK. Shelter 1 was located at the predicted 30-psi range (645 feet from ground zero GZ) and Shelter 2 was located at the predicted 20-psi range (750 feet from GZ). The general site layout is shown in Figure 1.1.

(C) During the test, 6 channels of data were recorded along with two movie cameras recording the motions of the dummies (Figure 1.2). The measurements in each shelter included midpoint deflection of a center arch-rib and internal pressure at two locations. Pressure measurements outside the shelter were taken from the basic blast-line study.

179

Figure 1.1 (C) Site plan (U).

ENTRANCE

GZ

1/11 2/10

C1

30 PSI
645 FEET

MISSILE
TRAP

a. SHELTER 1

LEGEND

○ PRESSURE GAGE

△ DEFLECTION GAGE

⬡ ANTHROPOMORPHIC DUMMIE

▭◀ MOVIE CAMERA

◗ CAMERA LIGHTING

ENTRANCE

GZ

3/11 4/11

C2

20 PSI
750 FEET

MISSILE
TRAP
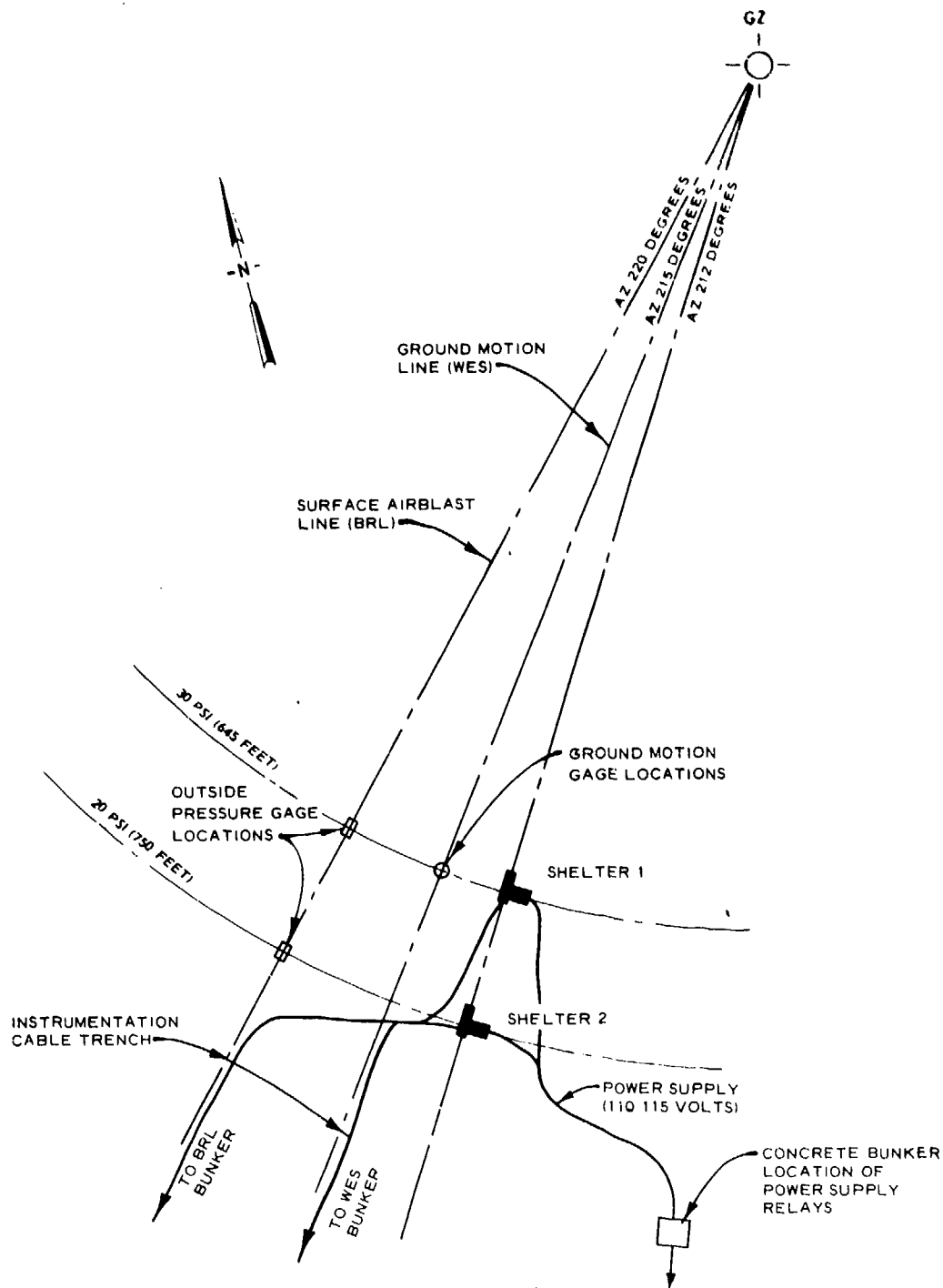
b. SHELTER 2

Figure 1.2 (C)   Instrumentation layout (U).

181

CHAPTER 2

SHELTER DESCRIPTION AND INSTALLATION (U)

(C) The shelter consisted of a steel frame covered with a flexible
fabric (Figure 2.1) and was assembled in a 4-foot 6-inch deep excavation
having a main chamber approximately 6 by 10 feet. The shelter design
consisted of four basic components, i.e., pickets, arches, spacers,
and flexible fabric. The excavation was made with a back hoe. Spacers
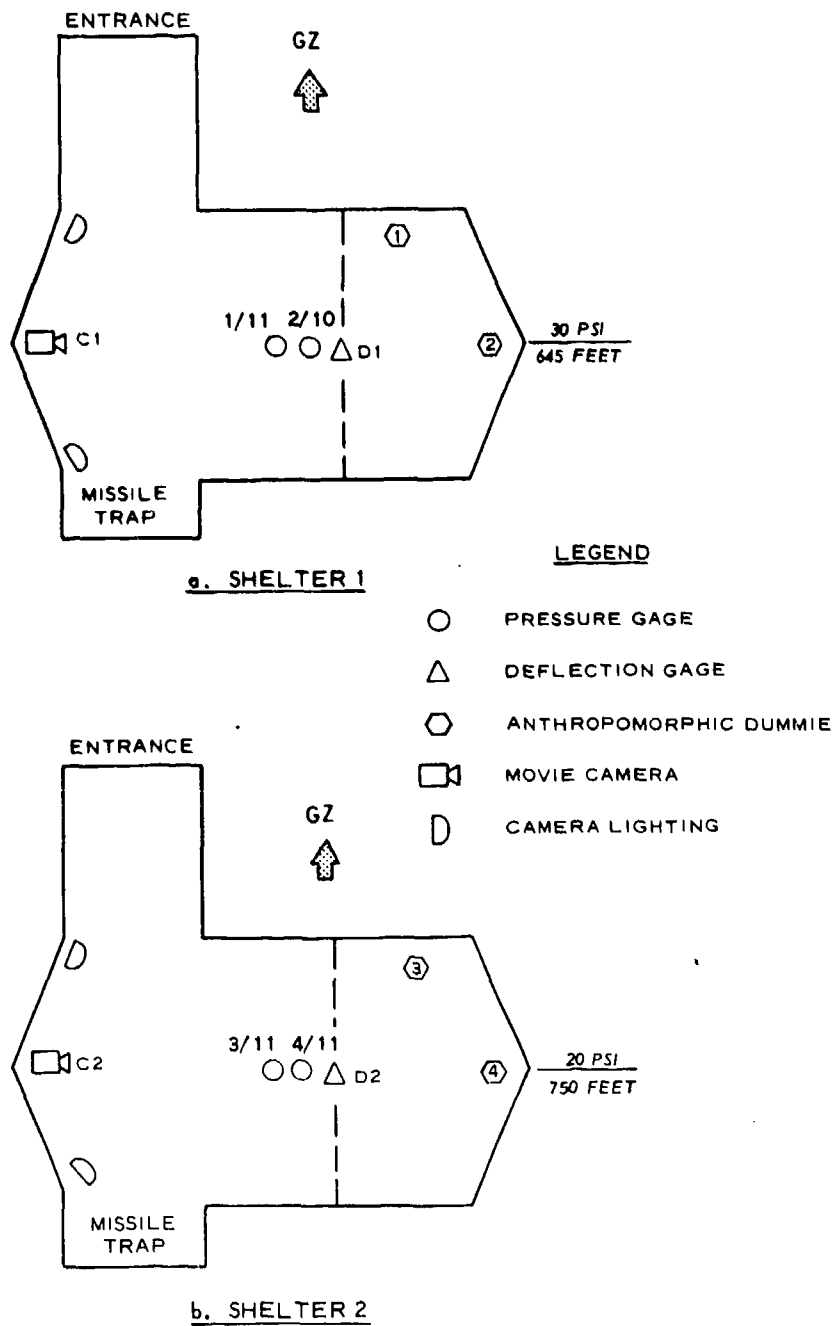were then used as a templet and the pickets were driven into the ground with
a sledge hammer (Figure 2.2). The spacers and arches were placed and all
joints were tied with wire. The flexible fabric was placed around the
sides of the shelter and backfill placement was begun. A 9 by 15 foot sheet
of fabric was placed over the main chamber (Figure 2.3) and the shelter
was covered with backfill material. Backfill was placed to a depth of
18-inches over the main chamber, 9-inches over the entrance tunnel and
was sloped at a 30-degree angle to the horizontal. The entrance into the
shelter remained open during the test. Shown in Figure 2.4 is the completed
shelter.

(C) The interior of the shelter was painted white with a black grid placed
on the back wall opposite the cameras to provide a reference for interpretation
of the dummie movements. Deflection and pressure gage installations and
a view down the entrance tunnel are shown in Figure 2.5.

Figure 2.1 (C) MARK II shelter assembly plan (U).
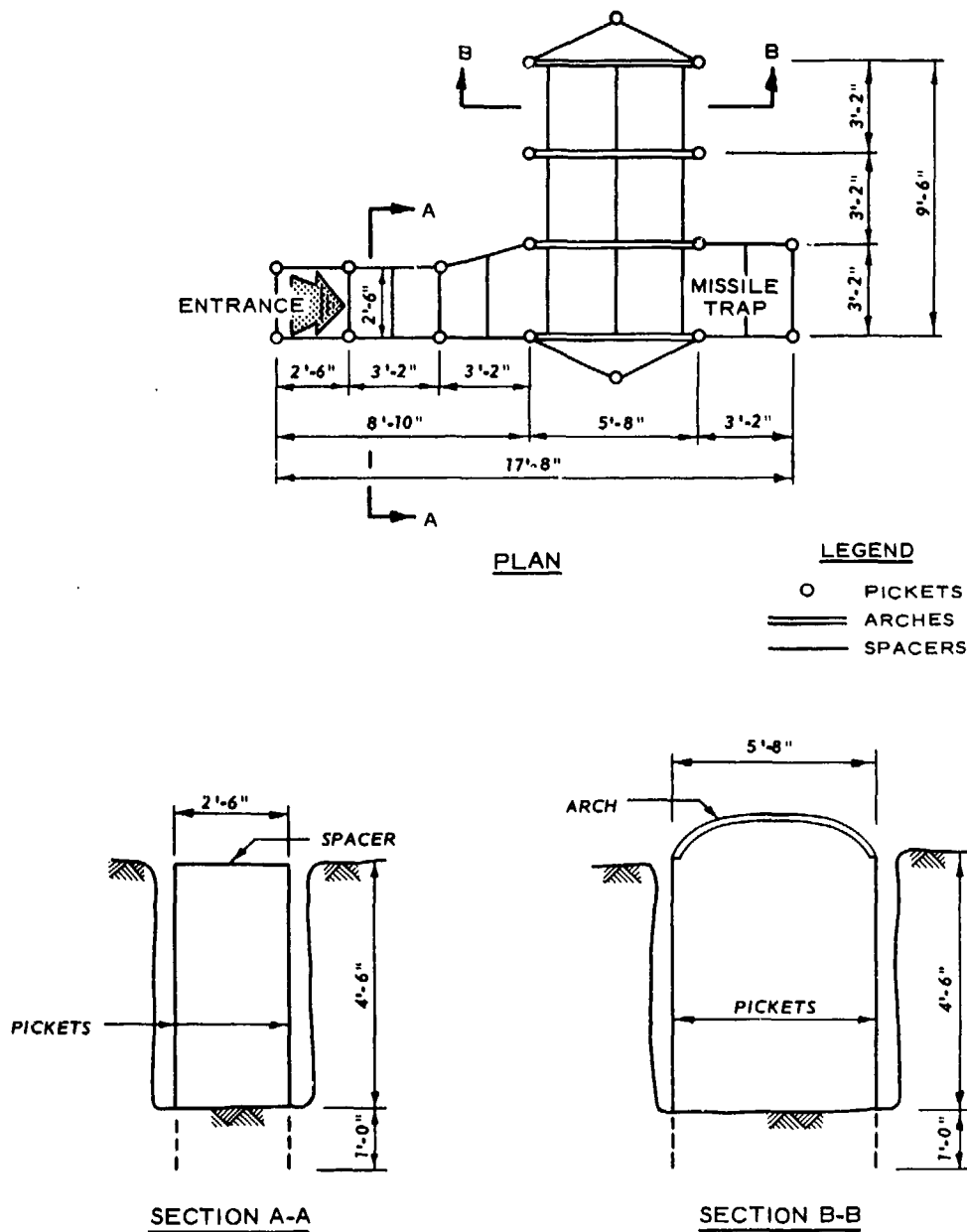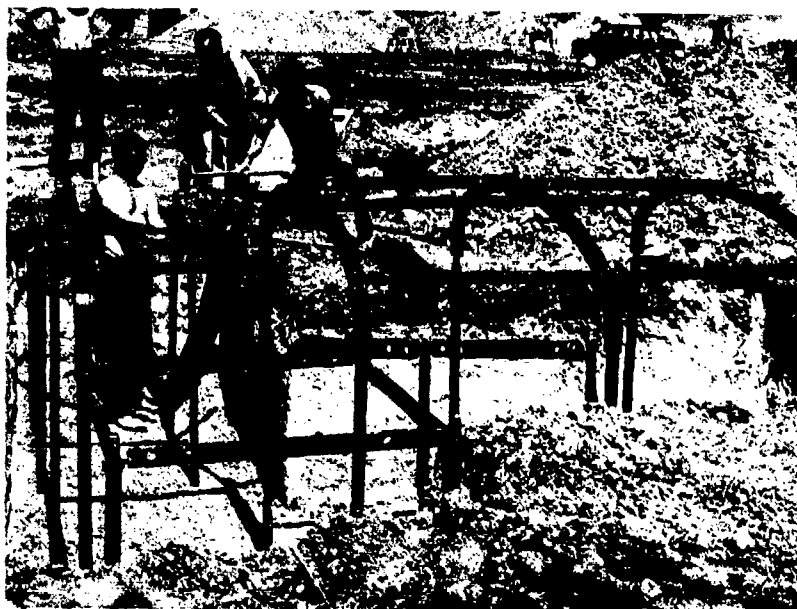
Figure 2.2 (C)   Erection of steel frame (U).

Figure 2.3 (C)   Placement of fabric on main chamber (U).

184

Figure 2.4 (C)　Preshot view of completed shelter (U).

Figure 2.5 (C)　Preshot view of shelter interior (U).

CHAPTER 3

RESULTS AND DISCUSSION (U)

(C) Since Shelter 1 at the 30-psi overpressure level was subjected to the severest environment of the two shelters, and the damage to both varied only in intensity, the results and discussion will be confined to Shelter 1. The overpressure at both locations was essentially that predicted, i.e., 30- and 20-psi.

(C) The outside pressure at Shelter 1 was recorded as having a peak of 30-psi. Pressure inside the shelter had an average initial peak of 8-psi and then a rise to a peak of 12 psi in approximately 36 msec. The shaded area in the graph of Figure 3.1 indicates the actual load the shelter experienced. However, it should be remembered that the flexible fabric was not attached to the steel frame and thus, the steel frame could not respond to the reverse loading caused by the overshot of the pressure inside the shelter. As shown by the deflection curve the steel frame continued to deflect in the presence of the load reversal.

(C) The major structural damage caused by the airblast occurred at the entrance (Figure 3.2) and along the entrance tunnel. Pickets and spacers were bent and the flexible fabric within the entrance tunnel was torn. Some soil spillage (approximately 6 cy yds) occurred at the entrance; however, entrance into the shelter was possible by sliding through the restricted opening. There were no tares or soil spillage anywhere else in the shelter.

186

SHELTER NO. 1
30-PSI OVERPRESSURE
645-FEET FROM GZ
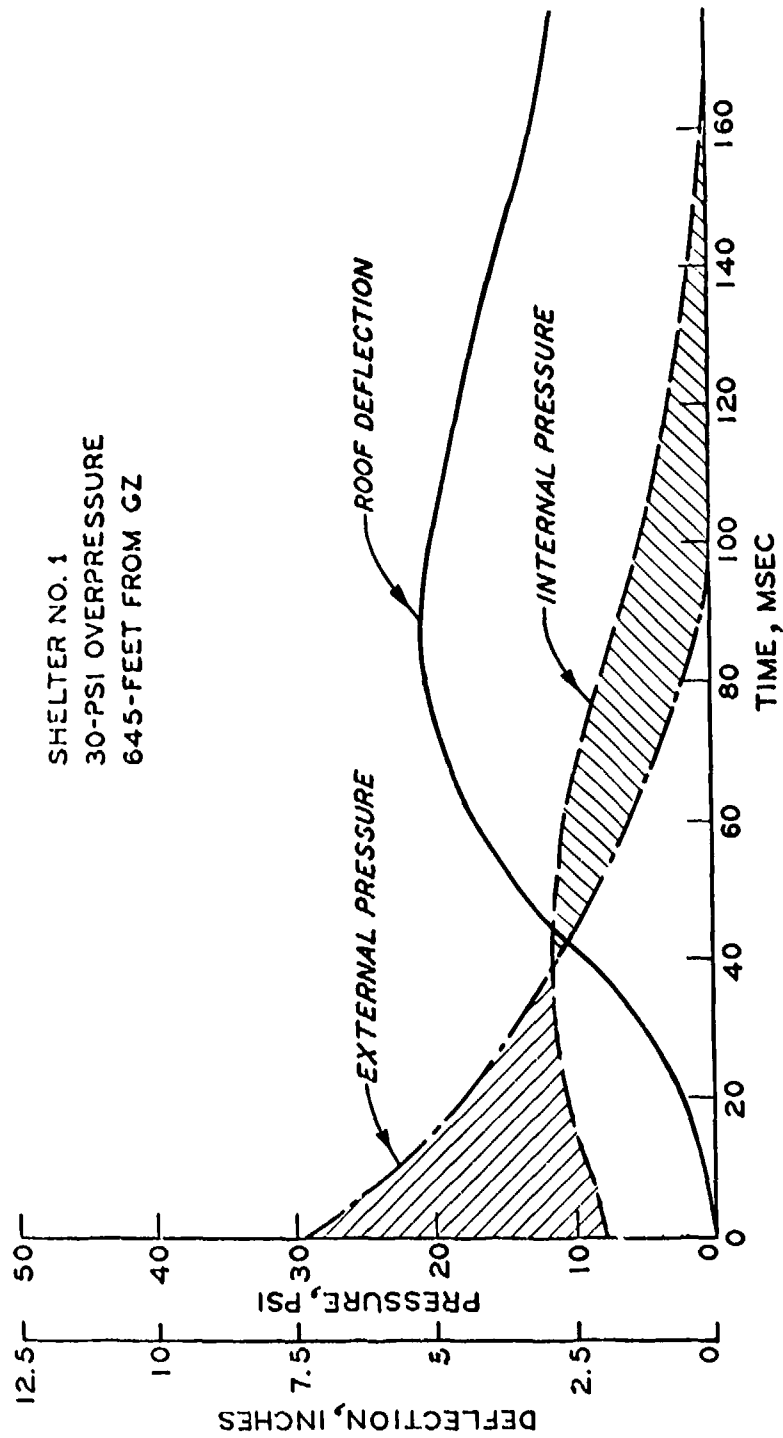
Figure 3.1 (C)   Shelter loading and response curves (U).

Figure 3.2 (C)   Postshot view of entrance damage, shelter 1 (U).

Figure 3.3 (C)   Postshot view of dummies, shelter 1 (U).

188

(C) The dummies appeared to have experienced very little movement

(Figure 3.3).   They were in their original position and posture.   There

was only slight movement of the head and shoulders.

(C) The camera and lights ran; however, the filaments in the lights were

broken by the shock from the explosion and only a few milliseconds of

movie time were recorded.   Air movement into the shelter and fluttering

of the dummies' clothing were observed on the film.

CHAPTER 4 (U)

CONCLUSIONS

(C) The general structural performance of the two Mark II shelters was good and the shelters would provide considerable protection from blast and debris for personnel. The entrance tunnel is the weakest element of the shelter and it is believed that it can be hardened with a minimal effort.

(C) The results indicate that there would be little or no hazard to individuals from blast displacement in the main chamber of the shelters under conditions of this test. Except for the probability of eardrum rupture, personnel would not be injured from the direct blast effects (overpressure).

DISTRIBUTION LIST

CHAIRMAN
ARMED SERVICES EXPLOSIVES SAFETY BOARD
DEPARTMENT OF DEFENSE
RM GB-270, FORRESTAL BUILDING
WASHINGTON, D. C. 20314

(01) MR. RUSSEL G. PERKINS

DEFENSE DOCUMENTATION CENTER
CAMERON STATION
ALEXANDRIA, VIRGINIA 22314

(02) TC

DIRECTOR
DEFENSE INTELLIGENCE AGENCY
WASHINGTON, D.C. 20301

(01) DI-7B, PHYS, VUL, DIV., MR, FRANK DEEDS

DIRECTOR
DEFENSE NUCLEAR AGENCY
WASHINGTON, D.C. 20305

(15) SPLN, MAJ WILLIAM J, SHEPARD

(01) DDST

(02) APTL (TECHNICAL LIBRARY)

(01) APSI (ARCHIVES)

(01) SPLN, MR. JACK R. KELSO

(01) STMD, MAJ HAL F, STOLZ

(01) SPSS

(01) SPAS

COMMANDER
FIELD COMMAND
DEFENSE NUCLEAR AGENCY
KIRTLAND AFB, NEW MEXICO 87115

(01) TECHNICAL LIBRARY, FCWS-SC

CHIEF
LIVERMORE DIVISION, FIELD COMMAND DNA
LAWRENCE LIVERMORE LABORATORY
P.O. BOX 808
LIVERMORE, CALIFORNIA 94550

(01) FCWD-D

COMMANDER
TEST COMMAND
DEFENSE NUCLEAR AGENCY
KIRTLAND AFB, NEW MEXICO 87115

(01) TCDT-B

(01) LTC W. J. DAVIS

DIRECTOR
WEAPONS SYSTEMS EVALUATION GROUP, ODDR+E
OFFICE, SECRETARY OF DEFENSE
400 ARMY-NAVY DRIVE
WASHINGTON, D.C. 20305

(01) CAPT DONALD E. MCCOY, USN

COMMANDING OFFICER
ABERDEEN PROVING GROUND
ABERDEEN PROVING GROUND, MARYLAND 21005

(01) TECHNICAL LIBRARY

DIRECTOR
ADVANCED BALLISTIC MISSILE DEFENSE AGENCY
COMMONWEALTH BLDG.
1320 WILSON BLVD.
ARLINGTON, VIRGINIA 22209

(01) DR. JACOB B. GILSTEIN

COMMANDING OFFICER
ARMY COLD REGION RESEARCH ENGINEERING LAB
P.O. BOX 282
HANOVER, NEW HAMPSHIRE 03755

(01) DOCUMENT CONTROL

COMMANDING OFFICER
ARMY ENGINEER EXPLOSIVE EXCAVATION RESEARCH OFFI
LAWRENCE LIVERMORE LABORATORY
LIVERMORE, CALIFORNIA 94550

(01) DOCUMENT CONTROL

DIRECTOR
ARMY ENGINEER WATERWAYS EXPERIMENT STATION
BOX 631
VICKSBURG, MISSISSIPPI 39180

(01) WESNV

(01) G. E. ALBRITTON

(01) G. L. ARBUTHNOT

(01) T. E. KENNEDY

(01) J. GATZ

(01) D. W. MURRELL

(01) J. M. PINKSTON

(01) A. D. ROOKE

(01) J. N. STRANGE

COMMANDING OFFICER
ARMY MOBILITY EQUIPMENT R AND D CENTER
FORT BELVOIR, VIRGINIA 22060

(01) SMEFB-EAX, D. B. DINGER

CHIEF
ARMY SATELLITE COMMUNICATIONS AGENCY
FORT MONMOUTH, NEW JERSEY 07703

(01) LTC MCGIVERN

D-3

COMMANDING OFFICER
ARMY TERRESTRIAL SCIENCES CENTER
P.O. BOX 282
HANOVER, NEW HAMPSHIRE 03755

(01) DOCUMENT CONTROL

ASSISTANT CHIEF OF STAFF FOR FORCE DEVELOPMENT
DEPARTMENT OF THE ARMY
WASHINGTON, D.C. 20310

(01) DIRECTOR OF CHEMICAL AND NUCLEAR OPERATIONS

DIRECTOR
BALLISTIC RESEARCH LABORATORIES
ABERDEEN PROVING GROUND, MARYLAND 21005

(01) DR. N. J. HUFFINGTON

(01) AMXBR-TB, MR. JULIUS J. MESZAROS

(01) N. H. ETHRIDGE

(01) L. GIGLIO TOS

(01) J. H. KEEFER

(01) R. P. LONG

(01) R. E. REISLER

(01) R. N. SCHUMACHER

CHIEF OF ENGINEERS
DEPARTMENT OF THE ARMY
WASHINGTON, D. C. 20314

(01) MAJ G. CHASE

(01) ENGME-RD

DIRECTOR OF CIVIL DEFENSE
DEPARTMENT OF THE ARMY
WASHINGTON, D.C. 20310

(01) STAFF DIRECTOR, RE(SR), MR. GEORGE N. SISSON

COMMANDING OFFICER
FRANKFORD ARSENAL
BRIDGE AND TACONY STREETS
PHILADELPHIA, PENNSYLVANIA 19137

(01) B. SCHEIN

DEPARTMENT OF THE ARMY
HARRY DIAMOND LABORATORIES
WASHINGTON, D.C. 20438

(01) AMXDO-NP

COMMANDING OFFICER
PICATINNY ARSENAL
DOVER, NEW JERSEY 07801

(01) A. FLUGER

COMMANDING GENERAL
SAFEGUARD SYSTEM COMMAND
P.O. BOX 1500
HUNTSVILLE, ALABAMA 35807

(01) SSC-DH, COL ROBERT A. PURPLE

SAFEGUARD SYSTEM MANAGER
SAFEGUARD SYSTEM OFFICE
1320 WILSON BLVD.
ARLINGTON, VIRGINIA 22209

(01) CSSSO

DIRECTOR
U S ARMY ADVANCED BALLISTIC MISSILE DEFENSE AGEN
HUNTSVILLE OFFICE
P.O. BOX 1500
HUNTSVILLE, ALABAMA 35807

(02) CRDABH-S, MR. MELVIN T. CAPPS

U.S. ARMY COMBAT DEVELOPMENTS COMMAND
NUCLEAR AGENCY
FORT BLISS, TEXAS 79916

(02) CDINS-E

CHIEF
U.S. ARMY COMBAT DEVELOPMENTS COMMAND

COMMUNICATIONS-ELECTRONICS AGENCY
FORT MONMOUTH, NEW JERSEY 07703

(01) CSG-CE-M

COMMANDING GENERAL
U.S. ARMY COMPUTER SYSTEMS COMMAND
FORT BELVOIR, VIRGINIA 22060

(01) CSC-EN

COMMANDING GENERAL
U.S. ARMY ELECTRONICS COMMAND
FORT MONMOUTH, NEW JERSEY 07703

(01) AMSEL-GG-EI

(01) AMSEL-KL-I

COMMANDING GENERAL
U.S. ARMY MATERIEL COMMAND
WASHINGTON, D.C. 20315

(01) AMCRD-B

(01) AMCRD-BN-RE-2, MR. JOHN J. F. CORRIGAN

(01) B. H. STOUT

COMMANDING GENERAL
U.S. ARMY MISSILE COMMAND
REDSTONE ARSENAL
HUNTSVILLE, ALABAMA 35809

(01) AMSMI-PLD, MR. BOUNDS

COMMANDING GENERAL
U.S. ARMY TANK AUTOMOTIVE COMMAND
WARREN, MICHIGAN 48089

(01) C. HENNE

D-6

COMMANDING GENERAL
U.S. ARMY TEST AND EVALUATION COMMAND
ABERDEEN PROVING GROUND, MARYLAND 21005

(01) AMSTE-NB

DEPARTMENT OF THE ARMY
U.S. ARMY WEAPONS COMMAND HEADQUARTERS
ROCK ISLAND, ILLINOIS 61201

(01) MR. R. O. BORDEN

COMMANDING GENERAL
WHITE SANDS MISSILE RANGE, NEW MEXICO 88002

(01) TE-N MR. MARVIN P. SQUIRES

CHIEF OF NAVAL MATERIAL
NAVY DEPARTMENT
WASHINGTON, D.C. 20360

(01) MAT 0323, MR. IRVING JAFFE

CHIEF OF NAVAL OPERATIONS
NAVY DEPARTMENT
WASHINGTON, D.C. 20350

(01) OP-752, CAPT REX GYGAX

CHIEF OF NAVAL RESEARCH
DEPARTMENT OF THE NAVY
ARLINGTON, VIRGINIA 22217

(01) CODE 418, DR. THOMAS P. QUINN

(01) TECHNICAL INFORMATION SERVICES

COMMANDING OFFICER
NAVAL CIVIL ENGINEERING LABORATORY
PORT HUENEME, CALIFORNIA 93041

(01) DR. WARREN A. SHAW

(01) J. R. ALLGOOD

(01) R. S. CHAPLER

D-7

(01) J. A. NORBUTAS

(01) R. H. SEABOLD

(01) S. K. TAKAHASHI

(01) D. E. WILLIAMS

COMMANDER
NAVAL ELECTRONIC SYSTEMS COMMAND
HEADQUARTERS
WASHINGTON, D.C. 20360

(01) PME 117-21

COMMANDER
NAVAL FACILITIES ENGINEERING COMMAND
COMMAND HEADQUARTERS
WASHINGTON, D.C. 20390

(01) CODE 03A, MR. STANLEY ROCKEFELLER

COMMANDER
NAVAL ORDNANCE LABORATORY
SILVER SPRING, MARYLAND 20910

(01) CODE 121, NAVY NUCLEAR PROGRAMS OFFICE

(01) CODE 241, MR. JOSEPH PETES

COMMANDER
NAVAL ORDNANCE SYSTEMS COMMAND
HEADQUARTERS
WASHINGTON, D.C. 20360

(01) ORD-035D, MR. WILLIAM W. BLAINE

DIRECTOR
NAVAL RESEARCH LABORATORY
WASHINGTON, D.C. 20390

(01) DOCUMENT CONTROL

COMMANDER
NAVAL SHIP RESEARCH AND DEVELOPMENT CENTER
WASHINGTON, D.C. 20034

(01) CODE 745, MR. EDWARD T. HABIB

(01) W. R. CONLEY

COMMANDER
NAVAL SHIP SYSTEMS COMMAND
NAVAL SHIP SYSTEMS COMMAND HEADQUARTERS
WASHINGTON, D.C. 20360

(01) SHIPS 03541, MR. WILLIAM S. BROWN

COMMANDER
NAVAL WEAPONS CENTER
CHINA LAKE, CALIFORNIA 93555

(01) DOCUMENT CONTROL

COMMANDER
NAVAL WEAPONS LABORATORY
DAHLGREN, VIRGINIA 22448

(01) TIEC

COMMANDER
AF SPECIAL WEAPONS CENTER, AFSC
KIRTLAND AFB, NEW MEXICO 87117

(01) MAJ W. WHITTAKER

(01) LT J. L. BRETTON

(01) MR. R. CLARK

AF WEAPONS LABORATORY, AFSC
KIRTLAND AFB, NEW MEXICO 87117

(01) DEV, DR. HENRY COOPER

(01) C. E. NEEDHAM

(01) DOGL, TECHNICAL LIBRARY

(01) MAJ LEIGH

CHIEF
AIR FORCE AUDIO-VISUAL CENTER
NORTON AFB, CALIFORNIA 92409

(01) K. HACKMAN

(01) G. PRATT

HEADQUARTERS
AIR FORCE SYSTEMS COMMAND
ANDREWS AFB
WASHINGTON, D.C. 20331

(01) SDR

CHIEF OF STAFF
U.S. AIR FORCE
WASHINGTON, D. C. 20330

(02) RD (DCS, RESEARCH + DEVELOPMENT)

SPACE AND MISSILE SYSTEMS ORGANIZATION, AFSC
NORTON AFB, CALIFORNIA 92409

(01) LTC J. CAHOON

(01) CPT M. R. PIERCE

ASSISTANT GENERAL MANAGER FOR MILITARY APPLICATI
U.S. ATOMIC ENERGY COMMISSION
WASHINGTON, D.C. 2.545

(01) DOCUMENT CONTROL FOR RES. + DEV. BRANCH

SANDIA LABORATORIES
P.O. BOX 5800
ALBUQUERQUE, NEW MEXICO 87115

(01) DOCUMENT CONTROL FOR J. W. REED

DEPARTMENT OF THE INTERIOR
U.S. GEOLOGICAL SURVEY
601 E. CEDAR STREET
FLAGSTAFF, ARIZONA 86001

(01) DR. DAVID J. RODDY, ASTROGEOLOGIC STUDIES

D-10

AEROSPACE CORP.
P.O. BOX 5866
SAN BERNARDINO, CALIFORNIA 92408

(01) C. R. SMITH

BELL TELEPHONE LABORATORIES, INC.
MOUNTAIN AVENUE
MURRAY HILL, NEW JERSEY 07971

(01) DR. E. F. WITT

(01) MR. MEAD F. STEVENS

(01) R. W. MAYO

GENERAL AMERICAN TRANSPORTATION CORPORATION
GENERAL AMERICAN RESEARCH DIVISION
7449 N. NATCHEZ AVENUE
NILES, ILLINOIS 60648

(01) MR. M. R. JOHNSON

GENERAL ELECTRIC COMPANY
TEMPO-CENTER FOR ADVANCED STUDIES
816 STATE STREET (P.O. DRAWER QQ)
SANTA BARBARA, CALIFORNIA 93102

(01) DASIAC

LOVELACE FOUNDATION FOR MEDICAL EDUCATION AND RE
5200 GIBSON BLVD., S.E.
ALBUQUERQUE, NEW MEXICO 87108

(01) PRESIDENT-DIRECTOR, DR. CLAYTON S. WHITE

(01) ASSOCIATE SCIENTIST, DR. E. ROYCE FLETCHER

(01) DR. D. R. RICHMOND

NEW MEXICO, UNIVERSITY OF
DEPT. OF CAMPUS SECURITY
CARLISLE GYMNASIUM
ALBUERQUERQUE, NEW MEXICO 87106

(01) ERIC H. WANG, CIVIL ENG. RESEARCH FACILITY

D-11

PHYSICS INTERNATIONAL COMPANY

2700 MERCED STREET
SAN LEANDRO, CALIFORNIA 94577

(01) MR. C. T. VINCENT

(01) MR. FRED M. SAUER

TRW SYSTEMS GROUP
ONE SPACE PARK
REDONDO BEACH, CALIFORNIA 90278

(01) MR. F. A. FEIPER

URS RESEARCH COMPANY
155 BOVET ROAD
SAN MATEO, CALIFORNIA 94402

(01) J. V. ZACCOR

(01) C. WILTON

WEIDLINGER, PAUL, CONSULTING ENGINEER
110 EAST 59TH STREET
NEW YORK, NEW YORK 10022

(01) DR. MELVIN L. BARON

CANADIAN GENERAL ELECTRIC
3603 8TH STREET, S.E.
CALGARY, ALBERTA, CANADA

(01) MR. D. J. DALTON

CHIEF SUPERINTENDENT
DEFENCE RESEARCH ESTABLISHMENT, SUFFIELD
RALSTON, ALBERTA, CANADA

(01) MR. D. LITTLE ·

(01) MR. W. HART

(01) MR. A. P. R. LAMBERT

(01) MR. A. M. PATTERSON

(01) MR. R. C. WYLD

(01) MR. F. DAVEY

(01) MR. R. B. HARVEY

INTERNATIONAL TELEPHONE AND TELEGRAPH CORP.
500 WASHINGTON AVENUE
NUTLEY, NEW JERSEY 07110

(01) MR. FRANK JOHNSON (DEFENSE SPACE GROUP)

DOCUMENT CONTROL DATA - R & D

(Security classification of title, body of abstract and indexing annotation must be entered when the overall report is classified)

1. ORIGINATING ACTIVITY *(Corporate author)*	2a. REPORT SECURITY CLASSIFICATION
General Electric-TEMPO	CONFIDENTIAL
816 State Street	2b. GROUP
DASIAC, Santa Barbara, California 93102	1

3. REPORT TITLE

EVENT DIAL PACK SYMPOSIUM REPORT - VOLUME III (U)

4. DESCRIPTIVE NOTES *(Type of report and inclusive dates)*

5. AUTHOR(S) *(First name, middle initial, last name)*

6. REPORT DATE	7a. TOTAL NO. OF PAGES	7b. NO. OF REFS
November 1971		

8a. CONTRACT OR GRANT NO.	9a. ORIGINATOR'S REPORT NUMBER(S)
DASA 01-69-C-0147	DNA 2722T
b. PROJECT NO. NWER XAXN	
c. Task and Subtask A007	9b. OTHER REPORT NO(S) *(Any other numbers that may be assigned this report)*
d. Work Unit 14	DASIAC SR 127

10. DISTRIBUTION STATEMENT

11. SUPPLEMENTARY NOTES	12. SPONSORING MILITARY ACTIVITY
	Director
	Defense Nuclear Agency
	Washington, D.C. 20305

13. ABSTRACT

Event DIAL PACK is the nickname for the 500-ton TNT blast and shock trial carried out at the Canadian Defence Research Establishment Suffield on 23 July 1970 under the auspices of The Technical Cooperation Program. This event and the PRAIRIE FLAT Event are part of the MIDDLE NORTH Series.

This volume contains the U.S. Project Officer's classified papers, and those selected to be published with the classified papers, which were presented at the DIAL PACK Symposium held in Ottawa, Canada 30 March through 1 April 1971. The other papers presented at the symposium have been published by the Defence Research Board of Canada in Volumes I and II.

The information contained herein describes the objectives of the projects, test setup procedures, the instrumentation used to gather and analyze the data obtained, and an analysis of the results.

DD FORM **1473** REPLACES DD FORM 1473, 1 JAN 64, WHICH IS OBSOLETE FOR ARMY USE.

14. KEY WORDS	LINK A		LINK B		LINK C	
	ROLE	WT	ROLE	WT	ROLE	WT
DIAL PACK						
PRAIRIE FLAT						
The Technical Cooperation Program						
Blast and Shock						
Simulation						

Defense Threat Reduction Agency
45045 Aviation Drive
Dulles, VA 20166-7517

CPWC/TRC

May 6, 1999

MEMORANDUM FOR DEFENSE TECHNICAL INFORMATION CENTER
ATTN: OCQ/MR WILLIAM BUSH

SUBJECT: DOCUMENT REVIEW

The Defense Threat Reduction Agency's Security Office has reviewed and declassified or assigned a new distribution statement: *Waiting for reply*

- AFSWP-1069, **AD-341090**, STATEMENT A
- DASA-1151, AD-227900, STATEMENT A
- DASA-1355-1, **AD-336440**, STATEMENT A OK
- DASA-1298, AD-285252, STATEMENT A
- DASA-1290, AD-444208, STATEMENT A
- DASA-1271, AD-276892, STATEMENT A
- DASA-1279, AD-281597, STATEMENT A
- DASA-1237, AD-272653, STATEMENT A
- DASA-1246, AD-279670, STATEMENT A
- DASA-1245, AD-419911, STATEMENT A
- DASA-1242, AD-279671, STATEMENT A
- DASA-1256, AD-280809, STATEMENT A
- DASA-1221, AD-243886, STATEMENT A
- DASA-1390, **AD-340311**, STATEMENT A
- DASA-1283, AD-717097, STATEMENT A OK
- DASA-1285-5, AD-443589, STATEMENT A
- DASA-1714, AD-473132, STATEMENT A
- DASA-2214, AD-854912, STATEMENT A
- DASA-2627, AD-514934, STATEMENT A
- DASA-2651, AD-514615, STATEMENT A
- DASA-2536, AD-876697, STATEMENT A
- DASA-2722T-V3, AD-518506, STATEMENT A
- DNA-3042F, AD-525631, STATEMENT A
- DNA-2821Z-1, AD-522555, STATEMENT A

If you have any questions, please call me at 703-325-1034.

Ardith Jarrett

ARDITH JARRETT
Chief, Technical Resource Center